© 2015 Yannick Degeilh

STOCHASTIC SIMULATION OF POWER SYSTEMS WITH INTEGRATED RENEWABLE AND UTILITY-SCALE STORAGE RESOURCES

BY

YANNICK DEGEILH

DISSERTATION

Submitted in partial fulfillment of the requirements
for the degree of Doctor of Philosophy in Electrical and Computer Engineering
in the Graduate College of the
University of Illinois at Urbana-Champaign, 2015

Urbana, Illinois

Doctoral Committee:

Professor George Gross, Chair
Professor Peter W. Sauer
Assistant Professor Alejandro D. Domínguez-García
Assistant Professor Enlu Zhou, Georgia Institute of Technology

ABSTRACT

The push for a more sustainable electric supply has led various countries to adopt policies advocating the integration of renewable yet variable energy resources, such as wind and solar, into the grid. The challenges of integrating such time-varying, intermittent resources has in turn sparked a growing interest in the implementation of utility-scale energy storage resources (*ESR*s), with *MWweek* storage capability. Indeed, storage devices provide flexibility to facilitate the management of power system operations in the presence of uncertain, highly time-varying and intermittent renewable resources. The ability to exploit the potential synergies between renewable and *ESR*s hinges on developing appropriate models, methodologies, tools and policy initiatives. We report on the development of a comprehensive simulation methodology that provides the capability to quantify the impacts of integrated renewable and *ESR*s on the economics, reliability and emission variable effects of power systems operating in a market environment. We model the uncertainty in the demands, the available capacity of conventional generation resources and the time-varying, intermittent renewable resources, with their temporal and spatial correlations, as discrete-time random processes. We deploy models of the *ESR*s to emulate their scheduling and operations in the transmission-constrained hourly day-ahead markets. To this end, we formulate a scheduling optimization problem (*SOP*) whose solutions determine the operational schedule of the controllable *ESR*s in coordination

with the demands and the conventional/renewable resources. As such, the *SOP* serves the dual purpose of emulating the clearing of the transmission-constrained day-ahead markets (*DAM*s) and scheduling the energy storage resource operations. We also represent the need for system operators to impose stricter ramping requirements on the conventional generating units so as to maintain the system capability to perform "load following", i.e., respond to quick variations in the loads and renewable resource outputs in a manner that maintains the power balance, by incorporating appropriate ramping requirement constraints in the formulation of the *SOP*. The simulation approach makes use of Monte Carlo simulation techniques to represent the impacts of the sources of uncertainty on the side-by-side power system and market operations. As such, we systematically sample the "input" random processes – namely the buyer demands, renewable resource outputs and conventional generation resource available capacities – to generate the realizations, or sample paths, that we use in the emulation of the transmission-constrained day-ahead markets via *SOP*. As a result, we obtain realizations of the market outcomes and storage resource operations that we can use to approximate their statistics. The approach not only has the capability to emulate the side-by-side power system and energy market operations with the explicit representation of the chronology of time-dependent phenomena – including storage cycles of charge/discharge – and constraints imposed by the transmission network in terms of deliverability of the energy, but also to provide the figures of merit for all metrics to assess the economics, reliability and the environmental impacts of the performance of those operations. Our efforts to address the implementational aspects of the methodology so as to ensure computational tractability for large-scale systems over longer periods include relaxing the *SOP*, the use of a "warm-start" technique as well

as representative simulation periods, parallelization and variance reduction techniques. Our simulation approach is useful in power system planning, operations and investment analysis. There is a broad range of applications of the simulation methodology to resource planning studies, production costing issues, investment analysis, transmission utilization, reliability analysis, environmental assessments, policy formulation and to answer quantitatively various what-if questions.

We demonstrate the capabilities of the simulation approach by carrying out various studies on modified *IEEE* 118- and *WECC* 240-bus systems. The results of our representative case studies effectively illustrate the synergies among wind and *ESR*s. Our investigations clearly indicate that energy storage and wind resources tend to complement each other in the reduction of wholesale purchase payments in the *DAM*s and the improvement of system reliability. In addition, we observe that CO_2 emission impacts with energy storage depend on the resource mix characteristics. An important finding is that storage seems to attenuate the "diminishing returns" associated with increased penetration of wind generation. Our studies also evidence the limited ability of integrated *ESR*s to enhance the wind resource capability to replace conventional resources from purely a system reliability perspective. Some useful insights into the siting of *ESR*s are obtained and they indicate the potentially significant impacts of such decisions on the network congestion patterns and, consequently, on the *LMP*s. Simulation results further indicate that the explicit representation of ramping requirements on the conventional units at the *DAM* level causes the expected total wholesale purchase payments to increase, thereby mitigating the benefits of wind integration. The stricter ramping requirements are also shown to impact the revenues of generators that do not even provide any ramp capability services.

ACKNOWLEDGMENTS

I would like to thank my advisor, Prof. George Gross, for the guidance, dedication and support he provided throughout the course of my studies at UIUC. His unwavering attention to detail and high standards have sharpened my critical eye and made me a better professional. I am also thankful for having had the opportunity to attend his comprehensive and well thought-out classes.

I would also like to express my gratitude to Raj, Dimitra, Kai, Siming, Matt, Christine and all the other students in the power group for all those wonderful moments spent together, from the laughs to the intellectually stimulating discussions we have had. You all have certainly contributed to sweetening my overall experience. I am also grateful to my committee members as well as the faculty and staff for their kindness, willingness to help and openness, and for making the Power and Energy Systems Group a great place to study and thrive.

Finally, a great many thanks to my wife, Diana, for her unconditional love and faith, and for keeping me on track during all those years. Thanks to my parents as well for being understanding and always supportive of my life choices, even if they sometimes put us a few thousand miles apart.

TABLE OF CONTENTS

LIST OF FIGURES viii

CHAPTER 1 INTRODUCTION 1

CHAPTER 2 MODELS OF STORAGE RESOURCES AND RAMPING REQUIREMENTS FOR THE SIMULATION APPROACH . . 11
2.1 Stochastic Models of the Simulation Inputs 12
2.2 *ESR* Modeling and *SOP* Formulation 27
2.3 Explicit Representation of the Ramping Requirements on Conventional Generators 35
2.4 Summary 40

CHAPTER 3 SIMULATION METHODOLOGY 41
3.1 Time Frame of the Stochastic Simulation 41
3.2 The Proposed Monte Carlo Simulation Procedure 43
3.3 Simulation Run Mechanics 47
3.4 Implementational Aspects of the Simulation Approach 54
3.5 Summary 59

CHAPTER 4 ILLUSTRATIVE CASE STUDIES 61
4.1 Overview of the Test Systems and Case Studies 61
4.2 The Economic, Reliability and Emission Impacts of Deepening Wind Penetration in Power Systems with/without Integrated *ESRs* 64
4.3 Ability of a Combination of Wind and Storage Resources to Replace Conventional Resources from a Pure System Reliability Perspective 67
4.4 Impacts of *ESR* Siting on Transmission Utilization and Economics at a Load Center 70
4.5 Explicit Ramping Requirements Impacts on Conventional Generation Resources 74
4.6 Summary 78

CHAPTER 5 CONCLUDING REMARKS 81
5.1 Summary 81
5.2 Possible Directions for Future Research 84

APPENDIX A NOTATION 86
A.1 General Notation 86
A.2 Time in the Simulation 86
A.3 Random Processes 87
A.4 Transmission Network (DC Power Flow Assumptions) 89
A.5 *SOP* 89
A.6 Ramping Requirements 91

APPENDIX B A COMPARISON OF STOCHASTIC MODELING TECHNIQUES: THE KERNEL DENSITY ESTIMATION APPROACH VS. THE MARKOV CHAIN MODEL 92
B.1 The Markov Chain Model 93
B.2 Assessing the Distance Between Two Random Processes . . . 96
B.3 Results of the Comparison 99
B.4 Concluding Remarks 102

REFERENCES 104

LIST OF FIGURES

1.1 Misalignment of the aggregated wind power and load 2
1.2 Effects of deeper wind penetration on the variability of the controllable load 4

2.1 Historical sample path collection from the time-series data of 4 midwestern wind farms 16
2.2 Historical wind speeds at two Midwestern sites in the same hour h and the resulting Kernel density estimation (Gaussian Kernel functions and smoothing parameters equal to 1) 21

3.1 The time dimension in the simulation approach 42
3.2 Conceptual structure of the stochastic simulation approach . . 45
3.3 Monte Carlo simulation: conceptual flow chart 46
3.4 Role of the SOP in the emulation of the DAMs of a simulation period 51
3.5 Simulation of a day as part of a simulation run 52

4.1 Expected hourly storage operations 65
4.2 Expected hourly SMPs 66
4.3 Average hourly total wholesale purchase payments; all values are averages over the hours of the year 67
4.4 Expected hourly total CO_2 emissions; all values are averages over the hours of the year 68
4.5 Annual LOLP 69
4.6 Annual EUE 70
4.7 Annual $LOLP$ versus system reserves margins 71
4.8 Annual EUE versus system reserves margins 72
4.9 ESR locations in the $IEEE$ 118-bus test system network for each subcase: each letter "S" represents an ESR while the sub-index denotes the remoteness in terms of nodes removed from bus 59 73
4.10 Expected hourly total congestion rents and system load 74
4.11 Section of the 118-bus system near the load center with the identified congested path in bold line 75

4.12 Expected hourly LMP at bus 59 before doubling the transmission capacity of the path 76
4.13 Expected hourly LMP at bus 59 after doubling the transmission capacity of the path 77
4.14 Expected hourly total wholesale purchase payment duration curves 78
4.15 Expected total wholesale purchase payment 79
4.16 Expected hourly payments duration curve to generator 36 . . 80
4.17 Expected hourly generator 36 LMP duration curve 80

B.1 Definition of the system state space 95
B.2 An 8 state Markov chain with hourly subperiods 96

CHAPTER 1

INTRODUCTION

There is a growing worldwide interest in integrating renewable resources into the grid to achieve a range of sustainability objectives, including the reduction of greenhouse gas emissions, limiting one's exposure to the fluctuating prices of fossil fuels, the creation of supply paths less reliant on the dwindling fossil fuel resources and the pursuit of a nation's energy independence [1, 2, 3]. Renewable resources such as wind can be harnessed locally and, not withstanding their construction and maintenance, have no associated fuel cost nor emissions. As such, they are widely expected to displace costly and polluting fossil-fuel fired conventional units, thereby reducing greenhouse gas emissions, driving energy prices down and alleviating the dependence on foreign fuels. However, the deepening penetration of intermittent renewable resources presents major challenges in power system planning and operations in light of their highly time-varying nature and their associated geographical and climatological sources of uncertainty. Indeed, unlike conventional resource outputs, wind and solar resource outputs cannot be controlled by the operator except to be curtailed. The high variability in wind speeds and insolation patterns, both temporal and spatial, results at times in intermittent wind and solar resource outputs [1]. A consequence is that the wind and solar outputs do not necessarily track the load pattern and thus cannot always contribute to serve the peak loads, as illustrated in Fig. 1.1.

There are also concerns about "spilling" of wind energy at night due to

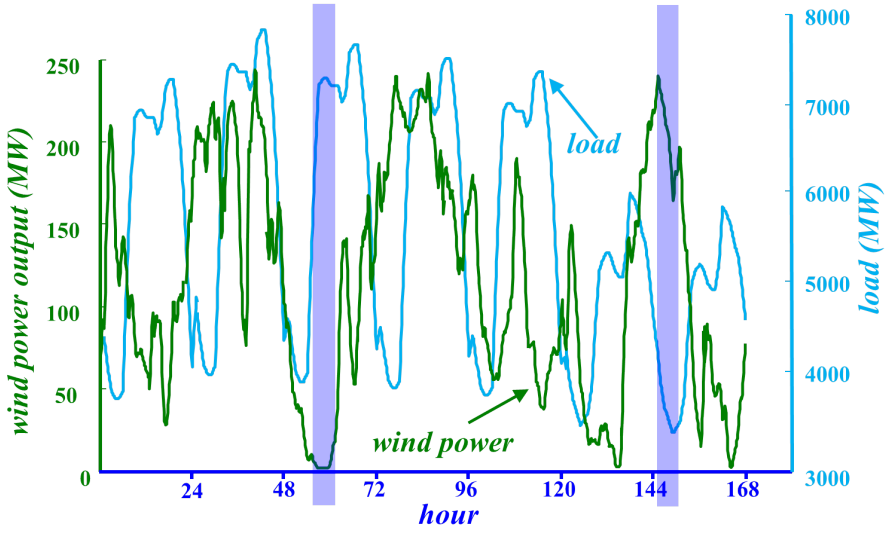

Figure 1.1: Misalignment of the aggregated wind power and load

the insufficient load demand and the physical impossibility to shut down the base-loaded conventional units for short periods. While morning and mid-day solar power outputs are aligned with the loads, their quick decline after sunset occurs when the loads are still high. Both wind and solar resources therefore impose additional requirements on the conventional units to effectively manage the variability/intermittency and uncertainty effects. Further issues arise from the fact that the wind speed and insolation patterns show various degrees of spatial correlation, resulting in highly variable nodal power injections which may lead, at times, to congestion. These complications illustrate the critical need to appropriately represent the temporal and spatial correlations of the wind and solar resource outputs in the assessment of the power system performance.

Situations involving the "spillage" of wind energy create excellent applications for utility-scale storage resources, with *MWweek* storage capability, to improve the utilization of the wind resources. *ESR*s may take advantage of arbitrage opportunities by storing energy during low-load hours –

or when high wind power outputs contribute to reduce the electricity prices for example – and discharging during peak-load hours so as to displace the costly energy from polluting generating units. While *ESR*s are very costly investments, their effective management – charge-discharge schedule and operations – impacts considerably the variable portion of the total costs [4]–[7]. Effective storage deployment can, moreover, obviate or defer the need for specific transmission improvements and/or addition of new generation resources.

As the wind penetration deepens, there are also concerns that wind generation will result in larger ramping requirements on an hourly basis [8, 9]. Wind resources tend to put an additional burden on the controllable units that are required to adjust their power outputs in response to a variation of the so-called controllable load, that is, the net difference between the total system load and the total time-varying resource power outputs (including the net scheduled interchanges). Under such circumstances, the grid operator is led to enforce stricter ramping requirements on the controllable units to maintain the power system capability to perform load following. Figure 1.2 illustrates situations when the aggregated wind power output pattern exacerbates the variability of the controllable load.

In light of these observations, there is an acute need for a practical simulation tool that can reproduce with good fidelity the expected variable effects – in terms of economics, reliability and emissions – of systems with renewable and storage resources, as well as the impacts of the renewable resource outputs on the ramping requirements. In this work, we seek to quantify the impacts of integrated renewable resources on the power system variable economic, reliability and emission variable effects. We also seek to investigate to what extent *ESR*s can extend the benefits and rein in the costs of deepening

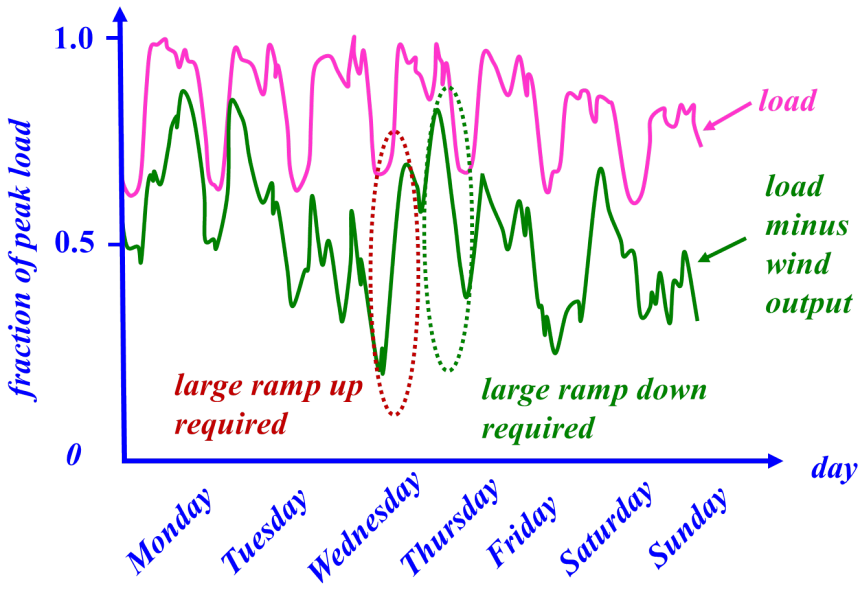

Figure 1.2: Effects of deeper wind penetration on the variability of the controllable load

penetrations of integrated renewable resources into the power systems. Concerns over the economic impacts of enforcing stricter ramping requirements on controllable resources due to the highly time-varying renewable resources are another facet of our research. We aim at a computationally effective simulation tool capable of performing comprehensive renewable and storage integration studies on large scale systems over longer-term periods. Our approach must notably be able to represent all the salient features of power system operations. In line with today's power industry, we require the explicit representation of the side-by-side power system and market operations, along with the capability to represent the associated policies and regulations that impact them. We also require a detailed representation of the resources, with the need to explicitly represent the demand and supply-side resource time-varying nature together with their associated uncertainty, as well as the grid transmission constraints. We emphasize the need to represent the spatial

and temporal correlations among the demands and the renewable power outputs at the various sites, so as to faithfully represent the congestion patterns as well as the potential misalignments between the variations of the loads and renewable power outputs. We also require the ability to schedule *ESR* operations in coordination with the demands and conventional/renewable resources so as to take advantage of arbitrage opportunities over multiple periods, and the appropriate representation of ramping requirements in the market clearing mechanism.

The conventional probabilistic simulation approach [10] and its extensions [11], [12] cannot adequately provide the needed level of detail due to its inability to represent chronological phenomena such as the grid operations and their impacts on the *DAM* outcomes, as well as the time-dependent nature and temporal correlations of the demands and supply resources, particularly the renewable resources. A distinctly different approach, which may be used to represent the uncertain *DAM* outcomes with the capability to explicitly represent the grid constraints, is the probabilistic optimal power flow (*P-OPF*), [13]. One drawback of the *P-OPF* approach, however, is that it requires a number of significant simplifying assumptions to render the problem into a solvable form. For instance, the representation of the power system evolution over time, including the temporal correlations among the system variables, requires the formulation of a *multi-period P-OPF*, whose tractability is questionable even for a small number of periods. Many renewable integration studies in the literature report the use of the Monte Carlo simulation to represent the power system and its sources of uncertainty. Morales et al. [14], for example, introduce a Monte Carlo simulation framework to study the impacts on locational marginal prices (*LMPs*) of multi-site wind production. The authors focus on the evaluation of the *LMP*s in a given

time period, without providing the explicit description of the extension to multiple periods. Many of the Monte Carlo simulation papers in the power system literature also focus exclusively on the probabilistic modeling of a single renewable resource, generally, wind [15], [16]. We are not aware of a comprehensive approach which integrates under a single umbrella the various sources of uncertainty that impact power system operations across time. We propose to go even further by also representing the operations of *MWweek*-scale *ESR*s that are, typically, scheduled over horizons ranging from a few days to a week. Examples of such utility-scale *ESR*s include pumped-hydro storage, compressed-air energy storage (*CAES*) and some types of battery technologies, such as sodium sulfur (*NaS*) and flow batteries [4], p.39. In this work, we assume that the *ESR*s are deployed as a system resource by the Independent System Operator (*ISO*). As such, the *ESR*s are scheduled and operated in such a way as to bring maximum economic benefits to the side-by-side power system and *DAM* operations. While there is a large body of literature that investigates the operations and impacts of hybrid wind-storage systems [17]–[20] and the participation of *ESR*s in the markets as speculative sellers [21]–[23], we view our work as the first to focus on the evaluation of the impacts on the variable effects of *MWweek*-scale *ESR*s deployed as system resources [1] in power systems with integrated renewable resources. A salient characteristic of our approach is the explicit representation of the *ESR* operations and their interactions with the transmission-constrained dispatch of the demands and supply resource outputs in a competitive electricity market environment.

[1]We note that the proposed framework is sufficiently flexible to incorporate, if desired, *ESR*s that participate in the *DAM*s as speculative sellers. Their modeling is no different from a bidding/offering entity once the *ESR* status, i.e., charge/discharge/idle, has been determined by their speculative sellers.

Specifically, the modeling of the buyer demands, renewable resource outputs and conventional generator available capacities is in terms of discrete-time random processes ($r.p.$s). Such models account for not only the uncertain and time-dependent behavior of the demands and supply-resource outputs, but also the spatial correlations among the various buyer demands/renewable resource sites (e.g. wind farms) as well as their temporal correlations. Our simulation methodology uses systematic sampling mechanisms based on Monte Carlo simulation techniques to generate the realizations – the so-called sample paths ($s.p.$s) – of the various "input" $r.p.$s that represent the uncertain and time-varying demands, renewable resource outputs and conventional generator available capacities. Based on such $s.p.$s, we formulate the offers and demands to be used as inputs into the emulation of the hourly DAMs for a one-week simulation period. Now, the incorporation of ESRs requires that we schedule their operations over multiple time periods so as to appropriately reflect their charge/discharge cycles. Thus, the representation of ESRs requires the development of a market clearing mechanism with the ability to represent their time-coupled operations. To this end, we develop the so-called *scheduling optimization problem* (SOP) and deploy its solution as the basic mechanism in the stochastic simulation framework to represent the impacts of ESR operations on the DAM outcomes over each hour of a simulation period. We formulate the SOP as a multi-period optimization able to take advantage of arbitrage opportunities in the coordinated operations of each ESR so as to meet, together with the set of conventional and renewable resources, the demand in a transmission-constrained system. The SOP is, in addition, amenable to the representation of interhourly ramping requirements that are defined based on the realizations of the demands and renewable power output $r.p.$s. Conceptually, absent the representation of the

*ESR*s and their operational intertemporal constraints, a *SOP* defined over the 168 hours of a weekly simulation period solves the identical problem as that solved by 168 separate *OPF*s that clear the hourly *DAM*s. For all intents and purposes, the *SOP* can be seen as the "time-coupled", generalized statement of the *DAM* clearing problem. In our simulation approach, the *SOP* solution serves two purposes: to emulate the *DAM* clearings and to schedule, concurrently, the *ESR* operations. More specifically, we solve the *SOP* for an optimization period spanning multiple days. We interpret the *SOP* solutions for the first 24 hours of the optimization period as the outcomes of the 24 *DAM*s for these hours. The other days must be considered so the *ESR*s are operated in such a way as to account for their continued utilization in the days beyond the first 24 hours. Such process is repeated for each day in the simulation period. As such, we actually solve a sequence of 7 *SOP*s to emulate the clearings of the 168 hourly *DAM*s and schedule, concurrently, the *ESR*s. The *DAM* outcomes obtained from the *SOP* solutions are then used in the assessment of various performance metrics of interest for the power system. Such metrics include the expected hourly *LMP*s, wholesale purchase payments, generator revenues, congestion rents, CO_2 emissions, *ESR* operations and contributions to the reliability indices *LOLP* and *EUE*. We note that in all these metrics, we implicitly account for the effects of the deliverability of the electricity, as well as those (when implemented) of the ramping requirements. From the hourly values, we then determine the values for the simulation periods, which are then used to determine the metric values for the study period. The methodology is able to capture the seasonal effects in demands and renewable power outputs, the impacts of maintenance scheduling and the ramifications of new policy initiatives. There is a broad range of applications of the simulation methodology

to planning, investment, transmission utilization and policy formulation and analysis studies for systems with integrated storage and renewable resources.

We also pay particular attention to the implementational aspects of the methodology so as to ensure computational tractability for large-scale systems over longer periods. Measures implemented to reduce the computational requirements include relaxing the *SOP* into a more tractable problem, the use of a "warm-start" technique as well as representative simulation periods, parallelization and variance reduction techniques. We also point out that, while our approach can easily be adapted to incorporate various stochastic models to represent the time-varying demands, renewable resource outputs and conventional generator available capacities, including models based on copulas, statistical transforms for multivariate dependence such as principal component analysis, time-series synthesis using many variants of *ARMA*-type schemes, numerical weather prediction methods, historical time-series re-sampling and hindcast [24]–[29], our objective is to construct a practical scheme based on models that require neither calibration nor the use of complex transforms, unlike the various models just mentioned. As such, we construct appropriate stochastic models to capture the time-varying and uncertain behavior of multi-site renewable power outputs, with the cross-correlations between the sites and time correlations explicitly accounted for and to incorporate into a comprehensive stochastic simulation framework. Our approach, while relatively easy to implement, can handle any type of renewable output probability distribution, including non-parametric distributions, as we require no assumptions on the shape of their joint cumulative distribution functions (*j.c.d.f.*s). Such implementation, in fact, contributes to ensure the computational tractability of the approach for power systems of realistic size.

This dissertation contains four additional chapters. For clarity in the presentation, the only renewable resource we consider in the rest of the thesis is wind. In chapter 2, we discuss the stochastic modeling of the buyer demands, multi-site wind speeds and conventional generator available capacities, develop models for the *ESR*s and formulate the mathematical statement of the *SOP* complete with ramping requirements. In chapter 3, we define the simulation time frame and delve into the mechanics of our stochastic simulation approach. We also discuss implementational aspects aimed at improving the simulation tractability. In chapter 4, we illustrate the broad capabilities of the approach with four sets of case studies performed on modified *IEEE* 118- and *WECC* 240-bus systems. The studies focus on the impacts of deepening wind penetration in a system with/without integrated *ESR*s, the ability of a combination of wind and storage resources to replace conventional resources from a pure system reliability perspective, the influence of *ESR* siting on transmission utilization and economics, and the economic impacts of ramping requirements in systems with deepening penetration of wind resources. We summarize in chapter 5 the main contributions and results of the thesis. We provide in Appendix A a summary of the notation used throughout the dissertation and in Appendix B a case study that compares two stochastic modeling technique in their representation of the aggregated wind power output.

CHAPTER 2

MODELS OF STORAGE RESOURCES AND RAMPING REQUIREMENTS FOR THE SIMULATION APPROACH

We devote this chapter to describing the models used in the analytical framework of our stochastic simulation approach. We start out with the stochastic modeling of the simulation "inputs", i.e., the uncertain and time-varying phenomena that drive the bids and offers made into the hourly *DAM*s. More specifically, we detail the construction of random process-based models for such simulation inputs as the demands, multi-site wind speeds (outputs) and conventional resource available capacities. We also discuss systematic sampling mechanisms to generate the "realizations" of such input *r.p.*s, the so-called (input) sample paths *s.p.*s. Within the framework of the proposed stochastic simulation approach, such *s.p.*s are meant to be inputs to the *DAM* clearing mechanism. We next discuss the modeling of the *ESR*s as system resources, which in turn highlights the need for an advanced scheduling tool – the so-called *scheduling optimization problem* (*SOP*) – to coordinate the clearing of the *DAM*s with the scheduling of the *ESR*s. Thus, we provide the formulation of the mathematical statement of the *SOP* that is solved to emulate the clearing of the *DAM*s and schedule, as part of the same procedure, the hourly *ESR* operations. The solution to the *SOP* are notably used to generate *s.p.*s of the market outcome and storage operation *r.p.*s. We finish by discussing the incorporation of ramping requirements into the *SOP* so as to represent their impacts on the *DAM* outcomes and *ESR* scheduling.

2.1 Stochastic Models of the Simulation Inputs

2.1.1 Buyer Demands

Let $\mathcal{B}$ the set of buyers in the hourly DAMs. For simplicity and clarity in the notation, we assume that each buyer $b \in \mathcal{B}$ submits a demand bid for a load located at one node and one node only. From the outset, we wish to capture the spatial and temporal correlations among the various buyer demands. Now, given that the cleared demands, as observed from historical load data, are seasonal and have a weekly cycle, we assume that, in each week of the same season, the buyer demands over a week period can be modeled by the discrete-time *r.p.* $\left\{\underset{\sim}{\underline{D}}[h] : h = 1, \ldots, 168\right\}$, where $\underset{\sim}{\underline{D}}[h] = \left[\underset{\sim}{D}^{1}[h], \ldots, \underset{\sim}{D}^{|\mathcal{B}|}[h]\right]^{\dagger}$ and † denotes the transpose. Such a *r.p.* is the collection of time-indexed random vectors $\underset{\sim}{\underline{D}}[h]$ for $h = 1, \ldots, 168$, with each random vector $\underset{\sim}{\underline{D}}[h]$ in hour h containing the ordered collection of the buyer demand *r.v.*s for each buyer $b \in \mathcal{B}$. Such representation explicitly accounts for the correlations across buyer and time that exist among the hourly demands $\underset{\sim}{D}^{b}[h]$ of each buyer $b \in \mathcal{B}$. For clarity, we may represent all the jointly distributed *r.v.*s $\underset{\sim}{D}^{b}[h]$, $\forall b \in \mathcal{B}$, $h = 1, \ldots, 168$ making up the buyer demand *r.p.* in the following array:

$$\begin{bmatrix} \underset{\sim}{D}^{1}[1] & \underset{\sim}{D}^{1}[2] & \ldots & \underset{\sim}{D}^{1}[168] \\ \underset{\sim}{D}^{2}[1] & \underset{\sim}{D}^{2}[2] & \ldots & \underset{\sim}{D}^{2}[168] \\ \vdots & \vdots & \ddots & \vdots \\ \underset{\sim}{D}^{|\mathcal{B}|}[1] & \underset{\sim}{D}^{|\mathcal{B}|}[2] & \ldots & \underset{\sim}{D}^{|\mathcal{B}|}[168] \end{bmatrix}.$$

We now describe how to construct and sample, in practice, the discrete-time *r.p.* of the (hourly) buyer demands over a week. We gather weeks of *simultaneously-measured* hourly buyer demands from a seasonally disag-

gregated historical database so as to capture the cross-dependencies among the buyer demands across multiple time periods. We use these data to construct their multi-dimensional histogram [30], p. 21, thus approximating the joint probability distribution of the buyer demands with a joint probability mass function (*j.p.m.f.*) More specifically, we construct the sample space $\Omega_{\left\{\underline{\underline{D}}[h]:h=1,\ldots,168\right\}}$ of the buyer demand *r.p.* Note that each weekly set of simultaneously-measured hourly buyer demands constitutes a *s.p.* of $\left\{\underline{\underline{D}}[h] \ : \ h = 1, \ \ldots \ , 168\right\}$ and as such, contains realizations of each *r.v.* $\underline{\underline{D}}^b[h]$, $h = 1, \ \ldots \ , 168, \ b \in \mathcal{B}$. We assume the equi-probability of each one of the *s.p.*s retrieved from the historical data to approximate the *j.p.m.f.* of $\left\{\underline{\underline{D}}[h] \ : \ h = 1, \ \ldots \ , 168\right\}$. We note that the obtained distribution is non-parametric.

We proceed to discuss the sampling procedure of such *j.p.m.f.* The method is the multidimensional case of the procedure described in [31], p. 139, to generate a realization from a (discrete) *r.v.* "empirical" *c.d.f.* The procedure entails drawing one of the historical *s.p.*s making up the sample space $\Omega_{\left\{\underline{\underline{D}}[h]:h=1,\ldots,168\right\}}$ with probability one over the total number of *s.p.*s making up said sample space. The selected sample-path contains hourly realizations $d^b[h]$, $h = 1, \ldots, 168$, $b \in \mathcal{B}$ that are consistent with the correlations existing among the $\underline{\underline{D}}^b[h]$, $b \in \mathcal{B}$, $h = 1, \ \ldots \ , 168$, *r.v.*s making up the buyer demand *r.p.* Another way to restate this statement is to say that, since every historical *s.p.* has the cross-dependency information relating the hourly buyer demands embedded in it, so does the selected *s.p.*

In practice, the time series data for the buyer demands may not be available. In such a case, we propose an alternative stochastic model for the buyer demands. The approach entails making use of some more readily available data, i.e., those of the *system* load, the sum of all loads in the system.

Throughout the discussion, we use the system load as a proxy for the system demand. We model the system load as a discrete-time *r.p.* denoted by $\left\{\underset{\sim}{D}[h] \,:\, h = 1, \ldots, 168\right\}$. Similarly as before, we gather weeks of hourly data within the same season to construct the sample space $\Omega_{\left\{\underset{\sim}{D}[h] \,:\, h=1,\ldots,168\right\}}$ of the weekly system load *r.p.* We approximate its *j.p.m.f.* by assuming that each week of hourly data used in the construction of $\Omega_{\left\{\underset{\sim}{D}[h] \,:\, h=1,\ldots,168\right\}}$ is equiprobable. We further assume that the load associated to each buyer $b \in \mathcal{B}$ is a specified, constant fraction δ^b of the system load in all $h = 1, \ldots, 168$. As such, we represent the load associated to buyer $b \in \mathcal{B}$, which translates into buyer b demand in the market, by discrete-time *r.p.* $\left\{\underset{\sim}{D}^b[h] \,:\, h = 1, \ldots, 168\right\}$, where $\underset{\sim}{D}^b[h] = \delta^b \times \underset{\sim}{D}[h]$, $\forall b \in \mathcal{B}$, $\forall h = 1, \ldots, 168$. With such construction, we capture the time-dependency of the demand for electricity, as well as its geographical pattern. However, by assuming that each buyer load is a constant fraction of the system load, we effectively make the more limiting assumption that the individual buyer loads are perfectly positively cross-correlated in each hour $h = 1, \ldots, 168$.

The sampling procedure of *r.p.* $\left\{\underset{\sim}{D}[h] \,:\, h = 1, \ldots, 168\right\}$, and by extension, that of *r.p.*s $\left\{\underset{\sim}{D}^b[h] \,:\, h = 1, \ldots, 168\right\}$, $\forall b \in \mathcal{B}$ makes use of the same approach as that used for the sampling of the buyer demand *r.p.* as described previously. Here, however, we sample the system load $\left\{\underset{\sim}{D}[h] \,:\, h = 1, \ldots, 168\right\}$ first, then deduce the sample paths of *r.p.*s $\left\{\underset{\sim}{D}^b[h] \,:\, h = 1, \ldots, 168\right\}$, $\forall b \in \mathcal{B}$ by multiplying the sample path obtained from the system load *j.p.m.f.* by the appropriate constant δ^b. Indeed, it follows that buyer b load (demand) associated sample path is given by $\left\{d^b[1], d^b[2], \ldots, d^b[168]\right\} = \delta^b \times \{d[1], d[2], \ldots, d[168]\}$.

2.1.2 Multi-Site Wind Speeds (Outputs)

We apply an analogous approach to the stochastic modeling of the multi-site hourly wind speeds. We denote a wind farm location by index $i \in \mathfrak{I}$. For simplicity in the notation, we assume that each wind farm is a distinct seller in the hourly *DAM*s. We define a one-to-one and onto mapping between each wind farm location i and its seller $s \in \mathcal{S}^w$ in the market, where $\mathcal{S}^w$ is the collection of the $|\mathcal{S}^w| = |\mathfrak{I}|$ sellers at the nodes where the farms are located. We assume that each wind speed at each farm location is uniform for the entire farm. Furthermore, we assume that the wind speeds are seasonal and have a daily cycle. In a similar manner as with the hourly buyer demands, we seek to capture the spatial and temporal correlations of the wind speed *r.v.*s $\underset{\sim}{V}_i[h]$ across locations $i \in \mathfrak{I}$ and hours of the day $h = 1, \ldots, 24$. Thus, we represent the multi-site hourly wind speeds by the discrete-time *r.p.* $\left\{\underline{\underset{\sim}{V}}[h] : h = 1, \ldots, 24\right\}$, where $\underline{\underset{\sim}{V}}[h] = \left[\underset{\sim}{V}_1[h], \ldots, \underset{\sim}{V}_{|\mathfrak{I}|}[h]\right]^\dagger$. We note that, similarly as for the buyer demand *r.p.*, the multi-site wind speed *r.p.* is the collection of time-indexed random vectors $\underline{\underset{\sim}{V}}[h]$ for $h = 1, \ldots, 24$, with each random vector $\underline{\underset{\sim}{V}}[h]$ in hour h containing the ordered collection of the wind speed *r.v.*s at the multiple sites represented in set $\mathfrak{I}$. For clarity, we may represent all the jointly distributed *r.v.*s $\underset{\sim}{V}_i[h]$, $\forall i \in \mathfrak{I}$, $h = 1, \ldots, 168$ making up the multi-site wind speed *r.p.* in the following array:

$$\begin{bmatrix} \underset{\sim}{V}_1[1] & \underset{\sim}{V}_1[2] & \ldots & \underset{\sim}{V}_1[24] \\ \underset{\sim}{V}_2[1] & \underset{\sim}{V}_2[2] & \ldots & \underset{\sim}{V}_2[24] \\ \vdots & \vdots & \ddots & \vdots \\ \underset{\sim}{V}_{|\mathfrak{I}|}[1] & \underset{\sim}{V}_{|\mathfrak{I}|}[2] & \ldots & \underset{\sim}{V}_{|\mathfrak{I}|}[24] \end{bmatrix}.$$

The construction and sampling procedures of such a discrete-time *r.p.* closely follow those of the buyer demand *r.p.* We use wind speed historical

data at multiple sites to construct the multi-dimensional histogram of the multi-site wind speeds, thus approximating the joint probability distribution of the multi-site wind speeds with a *j.p.m.f.* As such, a *s.p.* of the multi-site wind speed *r.p.* is a collection of hourly wind speed realizations at all the sites. We note that such a collection of hourly wind speeds is representative of the wind speed patterns at the multiple sites and so captures the existing cross dependencies. We illustrate in Fig. 2.1 how the historical *s.p.s* are extracted from the time-series data of 4 midwestern wind farms.

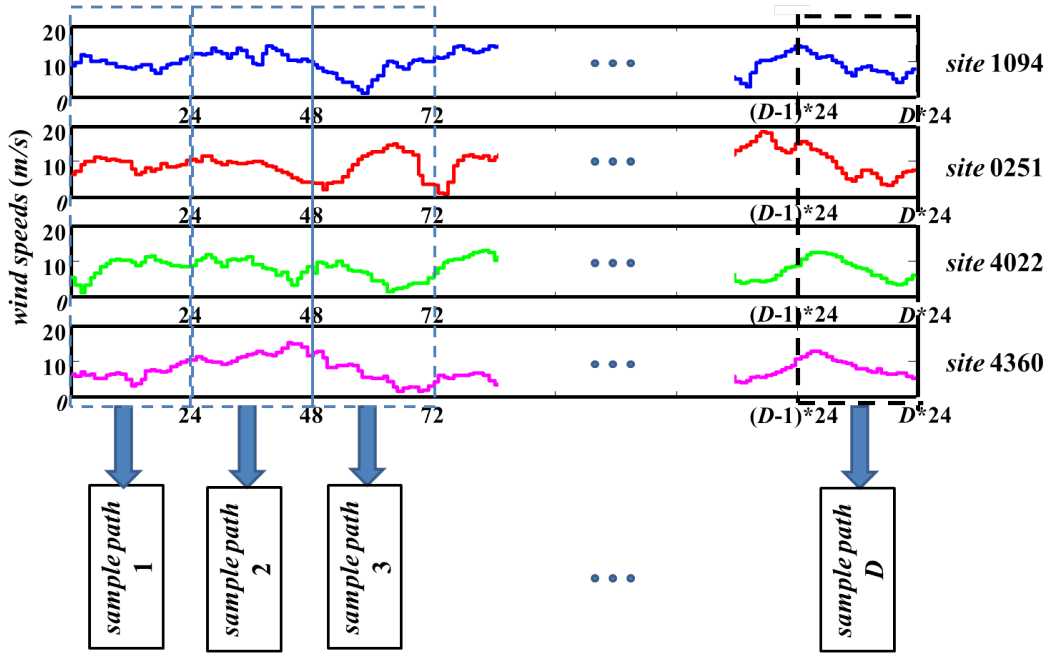

Figure 2.1: Historical sample path collection from the time-series data of 4 midwestern wind farms

In the specific case of the multi-site wind speed *r.p.*, however, we need to generate 7 daily *s.p.*s in order to construct the *s.p.* for the 7×24 hours in a week. Let us denote by $\underline{\underline{v}}^{(j)}$ the *jth s.p.* independently drawn from the *j.p.m.f.* of $\left\{\underline{\underline{V}}[h] \ : \ h = 1, \ \ldots \ , 24\right\}$. We sample and collect 7 independent *s.p.*s from the *j.p.m.f.* of $\left\{\underline{\underline{V}}[h] \ : \ h = 1, \ \ldots \ , 24\right\}$ to obtain the *s.p.* for the

week $\left\{ \underline{\underline{v}}^{(1)},\ \underline{\underline{v}}^{(2)},\ \ldots\ \underline{\underline{v}}^{(7)} \right\}$. Note that $\underline{\underline{v}}^{(j)}$ does not necessarily have to represent the multi-site wind speeds of day j; it can represent any arbitrary day in the week. However, for simplicity in the notation, we make it represent day j. Under this notation, $v_i^{(j)}[h]$ denotes the wind speed at wind farm $i \in \mathfrak{I}$ in hour h of day j.

At this stage, we may convert the *s.p.* wind speeds into their corresponding power outputs. To do so, we make use of the wind farm characteristic power curves, using the procedure described in appropriate detail in [12]. As such, the power output of a particular wind farm is a piece-wise polynomial function of its wind speed. Note that by converting all the *s.p.*s making up the sample space of $\left\{ \underline{\underline{V}}[h] \ :\ h = 1,\ \ldots\ , 24 \right\}$, we obtain the corresponding multi-site wind power output *r.p.* $\left\{ \underline{\underline{W}}[h] \ :\ h = 1,\ \ldots\ , 24 \right\}$ in a straightforward manner. Now, exploiting the one-to-one and onto mapping that relates a wind farm location $i \in \mathfrak{I}$ to its seller $s \in \mathcal{S}^w$, we may denote by $w_i^{(j)}[h] = (w^s)^{(j)}[h]$ the wind farm power output that is obtained from the conversion of $v_i^{(j)}[h]$. For convenience in the rest of the thesis however, and to reflect the fact that we have constructed a multi-site wind power output *s.p.* for the week, we drop the dependency on exponent j and express h in terms of a week hour, so that $w^s[h]$ denotes the wind power output of seller $s \in \mathcal{S}^w$ in hour h of the week.

2.1.3 Application of Kernel Density Estimation to the Modeling of the Buyer Demands and Multi-Site Wind Speeds Random Processes

A Kernel density estimation technique [30], p. 66, [32], p. 3, may also be used to "smooth out" the non-parametric distributions of the buyer demand and multi-site wind speed (output) *r.p.*s to effectively approximate their *j.c.d.f*s,

by contrast with the more conservative approach deployed in sections 2.1.1 and 2.1.2 that would only allow the construction of their multi-dimensional histograms from historical data, thus approximating their distributions with a *j.p.m.f.* [30], p. 21. We introduce the Kernel density estimation technique as an alternative to the methods discussed so far in 2.1.1 and 2.1.2, as it is thought to be preferable, in many respects, to the (multi-dimensional) histogram-based approach [32], p. 3, [30], p. 39. In the following discussion, we apply a Kernel density estimation technique to the approximation of the multi-site wind speed *j.c.d.f* and show how to sample such distribution for the purposes of the Monte Carlo simulation. [1] Wind speeds being highly variable, it is natural to assume that the joint probability distribution of the multi-site wind speed *r.p.* is rather a smooth one. Therefore, we may wish to "extrapolate" the *j.p.m.f.* constructed in section 2.1.2 so as to obtain a smooth, continuous joint probability distribution that can be characterized by a *j.c.d.f.* We denote by $\left\{\underline{\widehat{V}}[h] : h = 1, \ldots, 24\right\}$ the extrapolated multi-site wind speed *r.p.*, and by $\phi_{\left\{\underline{\widehat{V}}[h]:h=1,\ldots,24\right\}}(\cdot)$ its *j.p.d.f.* In effect, we want to give some probability density to points pertaining to the vicinities of the historical *s.p.*s in $\Omega_{\left\{\underline{V}[h]:h=1,\ldots,24\right\}}$, the sample space of the multi-site wind speed *r.p.* We do so by applying a Kernel density estimation technique to the historical data (in the form of the aforementioned *s.p.*s) collected. We select a Gaussian Kernel function for our purpose [2] and, by centering a multivariate Gaussian distribution on each historical *s.p.*, i.e., by having the mean value vector of the multivariate Gaussian distribution equal to the

[1] The technique is also applicable to the approximation of the buyer demand *j.c.d.f.*

[2] We note that the choice of the Kernel has, in fact, little impact on the efficiency of the density estimation, as discussed in [30], p. 61 and [32], p. 3. In the absence of further information on the true shape of the multi-site wind speed joint probability distribution, we select a radial-symmetric Kernel function such as the Gaussian.

historical *s.p.*, [3] we obtain a multivariate Gaussian mixture – a distribution characterized by a weighted sum of multivariate normal distributions. Let $\aleph$ denote the number of historical *s.p.s* in $\Omega_{\left\{\underline{\underline{V}}[h]:h=1,\ldots,24\right\}}$. The weight of each multivariate Gaussian in the mixture is simply $\frac{1}{\aleph}$. Let $\phi_{\mathcal{N}(\underline{\mu},\Sigma)}$ be the probability density function of a random vector indexed by j and normally distributed with mean value $\underline{\mu}$ and covariance matrix Σ and $\underline{\underline{v}}^{(j)}$ the jth historical *s.p.* in $\Omega_{\left\{\underline{\underline{V}}[h]:h=1,\ldots,24\right\}}$. Then, the probability density function of $\left\{\underline{\underline{\widehat{V}}}[h] : h = 1, \ldots, 24\right\}$ may be expressed as:

$$\phi_{\left\{\underline{\underline{\widehat{V}}}[h]:h=1,\ldots,24\right\}}\left(\underline{\underline{x}}\right) = \frac{1}{\aleph}\sum_{j=1}^{\aleph}\phi_{\mathcal{N}(\underline{\underline{v}}^{(j)},\Sigma^{(j)})}\left(\underline{\underline{x}}\right). \tag{2.1}$$

We further assume, for convenience and ease of implementation, that the components of each individual multivariate Gaussian distribution are statistically independent from one another [32], p. 7. Thus, the *j.p.d.f.* of a multivariate Gaussian distribution may be written as the product of the marginal *p.d.f.* of each component. Let $\phi_{\mathcal{N}(\mu,\sigma^2)}$ be the probability density function of a random variable normally distributed with mean value μ and variance σ^2. Then, the *p.d.f.* of $\left\{\underline{\underline{\widehat{V}}}[h] : h = 1, \ldots, 24\right\}$ may be expressed as:

$$\phi_{\left\{\underline{\underline{\widehat{V}}}[h]:h=1,\ldots,24\right\}}\left(\underline{\underline{x}}\right) = \frac{1}{\aleph}\sum_{j=1}^{\aleph}\prod_{k=1}^{|\mathfrak{I}|\times 24}\phi_{\mathcal{N}(\underline{\underline{v}}_k^{(j)},\Sigma^{(j)}_{(k,k)})}(\underline{\underline{x}}_k). \tag{2.2}$$

Note that $\Sigma^{(j)}_{(k,k)}$ is the kth diagonal element of the covariance matrix of multivariate Gaussian distribution j. As such, $\Sigma^{(j)}_{(k,k)}$ is the variance of the kth component of the normally distributed random variable centered on historical

[3] The dimensionality of the multivariate Gaussian distribution is necessarily the same as the number of *r.v.*s in $\left\{\underline{\underline{\widehat{V}}}[h] : h = 1, \ldots, 24\right\}$.

s.p. j. We note that such variance controls the "spread" of the probability density over the surrounding sample space along the dimension of component k. The choice of such variances, whose corresponding standard deviations are called *smoothing parameters* [32], p.3, is still a subject of ongoing research. Several methods are proposed in [32], p. 31, and [30], p. 72. Most are based on the minimization of the Approximated Mean Integrated Squared Error (*AMISE*) of the Kernel density estimator (see [30], p 50 for the definition of the *AMISE*). If all smoothing parameters are chosen equal – as is generally the practice [32], p. 7 – and we denote by $\sigma^{\bullet}$ the smoothing parameter value that minimizes the *AMISE*, it can be shown that $\sigma^{\bullet} \sim \aleph^{-1/(4+\eth)}$, where $\eth$ is the dimension of the multivariate Kernel function [30], p. 72. In the modeling of the buyer demands or multi-site wind speeds, this formula suggests the use of $\sigma^{\bullet} = 1$, owing to $\eth$ being relatively large ($24 \times |\mathfrak{I}|$ for the multi-site wind speeds, $168 \times |\mathcal{B}|$ for the buyer demands). Intuitively, the choice of $\sigma^{\bullet} = 1$ appears to be rather conservative, causing the probability densities of the multivariate Gaussian distributions to remain concentrated around the historical *s.p.*s. For illustration purpose, we provide in Fig. 2.2 the plot of historical wind speeds at two Midwestern wind farms in a given hour h (such graph can be seen as a crude visualization of their estimated *j.p.m.f.*) as well as the resulting approximated *j.p.d.f.* obtained via Kernel density estimation conducted with Gaussian Kernel functions and $\sigma^{\bullet} = 1$.

A shortcoming of estimating the density with a Gaussian Kernel function is that Gaussian multivariate distributions have their support defined all over the hyperspace $\mathbb{R}^{|\mathcal{S}^w| \times 24}$, which goes against the fact that the multi-site wind speeds are clearly *positive*. Thus, we redefine the probability distribution of $\left\{\underline{\widehat{V}}[h] : h = 1, \ldots, 24\right\}$ so that, wherever $\left\{\underline{\widehat{V}}[h] : h = 1, \ldots, 24\right\}$ components take negative values, the probability density is set to zero, and

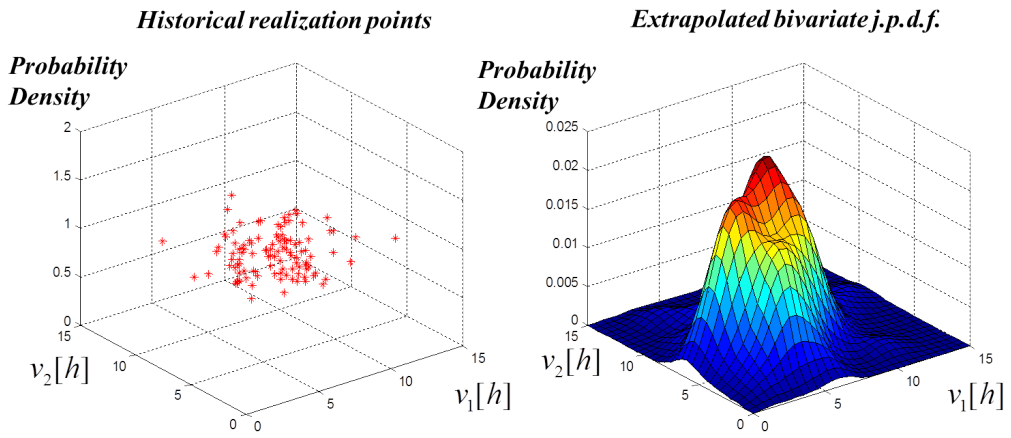

Figure 2.2: Historical wind speeds at two Midwestern sites in the same hour h and the resulting Kernel density estimation (Gaussian Kernel functions and smoothing parameters equal to 1)

the weight of such probability density is made to contribute to the probability density of the corresponding component being 0. In practice however, we do not need to explicitly compute the expression of the *j.p.d.f.* of $\left\{\underset{\sim}{\widehat{V}}[h] : h = 1, \ldots, 24\right\}$. We simply deal with it when sampling its distribution: if a component of the *s.p.* turns out to be negative, we simply set it to 0.

We sample $\left\{\underset{\sim}{\widehat{V}}[h] : h = 1, \ldots, 24\right\}$ by using the so-called composition method [33], p. 448. We first make use of the Inverse Transform [33], p. 440, method to choose the multivariate Gaussian to be sampled among all those that make up the multivariate Gaussian mixture. Such process is straightforward since the probability distribution to be sampled is a simple probability mass function with equiprobable realizations, each realization having the probability $\frac{1}{\aleph}$. Then we sample the selected multivariate Gaussian under the assumption that the latter can be written as a product of univariate Gaussians, as seen in (2.2). Each univariate Gaussian distribution is then sampled independently from one another by making use of well-known technique such as

the Box-Muller transform for example [33], p.465. The end result is a *s.p.* of the multi-site wind speed *r.p.* $\left\{\underline{\widehat{V}}[h] : h = 1, \ldots, 24\right\}$.

We further provide in Appendix B a study that compares the Kernel density estimation of the multi-site wind speeds to a Markov chain model in terms of predicting future trends in the aggregated wind power output. Results suggest that the Kernel density estimation of the aggregated wind power output performs as well as raw historical data in being representative of the wind power output data in a later year, and generally produces better results than a Markov chain model.

2.1.4 Conventional Generator Available Capacities

We introduce a simplifying assumption for the set $\mathcal{S}^c$ of market participants who sell the outputs of the conventional generation resources: similarly as for the buyer demands, seller $s \in \mathcal{S}^c$ offers the output of only one conventional resource. As such, we shall index each conventional generation resource by $s \in \mathcal{S}^c$. We model each conventional resource as a multi-state unit with two or more states - outaged, various partially derated capacities and full capacity. We assume that each conventional resource is statistically independent of any other generation resource. As such, if $\underset{\sim}{A}^s[t]$ designates the available capacity of seller s unit at time t, then $\underset{\sim}{A}^s[t]$ and $\underset{\sim}{A}^{s'}[t]$, with $s \neq s'$, $s, s' \in \mathcal{S}^c$, are statistically independent. We use a discrete-event driven Markov process model with the appropriate set of states and stochastic event-time distributions to represent the underlying *r.p.* governing the available capacity of each conventional resource. We assume statistically independent exponentially-distributed *r.v.*s. to represent the transition times between the states. Such model allows us to explicitly represent the periods

during which a conventional unit might be up, down, or running at derated capacities in the simulation.

In light of the statistical independence assumption, we construct individual *s.p.*s for each conventional resource. The methodology for simulating the available capacity of a conventional resource over time is well documented in the literature, and can be found under the names of *next-event method*, *state duration sampling*, or simply *sequential simulation* [34]. The procedure consists of simulating the sequence of available capacity states through which the conventional resource passes over time. We do so by sampling the appropriate transition-time exponential distribution as the conventional resource transitions from a state of the discrete-event driven Markov process to another [35], p. 59. We adapt the procedure to obtain the sample path of the unit available capacity over the span of a simulation period. One issue concerns the initial state of seller s unit in hour $h = 1$ of the simulated week. We want the system to be in steady-state from hour $h = 1$, so in order to avoid any transient behavior due to pre-specified starting conditions, we determine $a^s[1]$ by sampling the steady-state probability distribution of seller s unit available capacity. Suppose the unit has a total of J possible states, including $J - 2$ states with derated capacities denoted by $\mathfrak{d}_j^s$ and associated probability $\mathfrak{p}_j^s$, $j = 1, \ldots, J-2$. We characterize the steady-state probability distribution of seller s unit available capacity $\hat{\underset{\sim}{A}}^s$ as follows:

$$\begin{cases} \hat{\mathcal{A}}^s = (\kappa^s)^M & \text{with probability } (1 - \sum_{j=1}^{J-2} \mathfrak{p}_j^s - \mathfrak{q}^s) \\ \hat{\mathcal{A}}^s = \mathfrak{d}_1^s & \text{with probability } \mathfrak{p}_1^s \\ \vdots & \\ \hat{\mathcal{A}}^s = \mathfrak{d}_{J-2}^s & \text{with probability } \mathfrak{p}_{J-2}^s \\ \hat{\mathcal{A}}^s = 0 & \text{with probability } \mathfrak{q}^s \end{cases} \tag{2.3}$$

We make use of the inverse transform method [33], p. 440, to sample the probability mass function (*p.m.f.*) in (2.3). Another aspect of the initial state of seller s unit in hour $h = 1$ concerns the time that has yet to elapse before the unit transitions into another state. Since we do not simulate the past history of the unit, we do not know when exactly in the past, prior to hour 1, the unit went from one state to another. We make the reasonable assumption that the fraction of time that has already elapsed since the last transition of the unit is uniformly distributed. So, to determine the unit time-to-transition from its state in hour 1 (as determined via the sampling of the steady-state probability distribution in (2.3)) to the next, we sample the appropriate exponential distribution and multiply the time-to-transition obtained by a random number drawn from the uniform distribution in $(0, 1)$. At this stage, the "initial state" of seller s unit is fully defined, and its sample path over the considered simulation period may be obtained by simulating the sequence of its transitions between states. We describe the general procedure in the algorithm that follows. Note that in the algorithm, a state (of the underlying Markov process) is one of the possible values that may take the available capacity of the considered unit. Also, time is expressed in hours.

1. Set $h = 1$ and sample seller s unit initial state. To do so, sample the unit availability steady-state probability distribu-

tion (2.3) via inverse transform method. Draw random number $r' \in (0,1)$ to determine the proportion of time that has yet to elapse before the unit transitions into another state.

2. Identify all possible transitions from current state i to other states $\{j : j \in \Xi_i^s\}$ where Ξ_i^s is the set of eligible states to which the unit in state i may transition.

3. Sample - via inverse transform method - the *p.m.f.* of the distribution characterizing the probabilities of transition from state i to any other eligible states in Ξ_i^s. The realization determines the state into which the unit is going to transition next. Let us call such a state $\breve{j}$.

4. Sample - via inverse transform method - the *c.d.f.* of the exponential distribution characterizing the time to transition from state i to state $\breve{j}$. We denote by $\vartheta_{i\to\breve{j}}$ the sampled time to transition from state i to state $\breve{j}$. With such notation, and letting r be a random number uniformly distributed in $(0,1)$, $\vartheta_{i\to\breve{j}} = -\dfrac{\ln(r)}{(1/\tau_{i\to\breve{j}})}$ where $\tau_{i\to\breve{j}}$ is the average duration of stay in state i; round-up $\vartheta_{i\to\breve{j}}$ to the nearest hour.

5. If $h > 1$, then seller s unit switches to state $\breve{j}$ at time $h + \vartheta_{i\to\breve{j}}$. If $h = 1$, then seller s unit switches to state $\breve{j}$ at time $h + r'\vartheta_{i\to\breve{j}}$.

6. Advance the clock to time $h = h + \vartheta_{i\to\breve{j}}$ (or $h = h + r'\vartheta_{i\to\breve{j}}$ if h was equal to 1 in the previous step) and go back to step 2. Stop the algorithm when $h > 168$.

We briefly comment on the fact that the algorithm calls for rounding up the time-to-transitions in step 4. As a matter of fact, the underlying stochas-

tic process governing the available capacity of a conventional unit is that of a *continuous-time* Markov process. When using discretized time-axis, it is necessary to round up the sampled time-to-transitions to the nearest hour. Such a rounding results in a truncation error that is acceptable so long as the mean time-to-transitions of the unit are greater than the maximum truncation error of half a subperiod, i.e., half an hour. The resolution of the discretized time-axis must be fine enough to meet such a requirement for the simulation to be meaningful.

In terms of our approach, the state of seller s resource, i.e., its available capacity, is hence determined for each hour h of the week. The collection of hourly realizations $\{a^s[1], a^s[2], \ldots, a^s[168]\}$ constitutes a week-long *s.p.* of seller s resource available capacity.

2.1.5 The Role of the Statistical Independence Assumption

We note that the random process-based models for the buyer demands, multi-site wind speeds (power outputs) and conventional generation resource available capacities are built and sampled independently from one another. [4] By doing so, we implicitly assume that the *r.v.* $\underset{\sim}{V}_i[h]$ that represents the wind speed at site i in hour h, the *r.v.* $\underset{\sim}{D}^b[h']$ that represents the buyer b demand in hour h' and the *r.v.* $\underset{\sim}{A}^s[h'']$ that represents the available capacity of seller s conventional resource in hour h'', are statistically independent of one another, with $h, h', h'' \in \{1, \ldots, 168\}$. In other words, we assume that the behavior of buyer b demand in hour h has no impact on the behavior of the wind speed (power output) at site i (or the available capacity of any

[4] For the purpose of the following discussion, any statement on the wind speed random process and its time-indexed random variables applies equally well to a statement on its associated wind power output random process and its time-indexed random variables, since the wind power output is a function of the wind speed.

conventional resource s) in any hour and vice-versa. We note that such statistical independence assumptions result from the same lines of reasoning as the widely-deployed assumption that the demand and available capacities of conventional resources are statistically independent.

2.2 *ESR* Modeling and *SOP* Formulation

We devote this section to describe the modeling of the utility-scale *ESR*s and the formulation of the mathematical statement of the *SOP* that is solved to determine the hourly *ESR* operations. We discretize the time axis so as to adopt the granularity used in most North American *DAM*s, i.e., we adopt an hour as the shortest indecomposable period of time. As such, all the variables/parameters in the *ESR* models are indexed by the hour, and the *ESR* operations are scheduled on an hourly basis. We denote by $x[h]$ the variable x in hour h.

We consider the set $\mathcal{E} = \{e : e = 1, \ldots, E\}$ of *ESR*s. Each *ESR* $e \in \mathcal{E}$ acts either as a load in hours during which it charges, or as a generation resource in hours during which it discharges. In other hours, it remains idle with no impact on the side-by-side power system and market operations. We assume that the operational state – discharge, charge or idle – of *ESR* e, together with its associated *MW* discharge output $g^e[h]$ (charging load $\ell^e[h]$), remains unchanged over the duration of a particular hour h. We introduce the binary variables $u_g^e[h]$, $u_\ell^e[h] \in \{0, 1\}$ to specify the operational state of *ESR* e in hour h. Binary variable $u_g^e[h]$ ($u_\ell^e[h]$) takes value 1 if *ESR* e discharges (charges) during hour h, 0 otherwise. We enforce the physical fact that an *ESR* cannot both charge and discharge at the same time, that is, $u_g^e[h]$ and $u_\ell^e[h]$ cannot be both equal to 1, by requiring that for each hour

h, $u_g^e[h] + u_\ell^e[h] \leq 1$. *ESR* e is said to be idle when it neither discharges nor charges, i.e., $u_g^e[h] = u_\ell^e[h] = 0$. We also denote by $(\kappa_g^e)^M$ $\left((\kappa_\ell^e)^M\right)$ the maximum discharge (charge) capacity of *ESR* e and by $(\kappa_g^e)^m$ $((\kappa_\ell^e)^m)$ the minimum discharge (charge) capacity. We refer to $(\kappa_g^e)^m.u_g^e[h]$ $((\kappa_\ell^e)^m.u_\ell^e[h])$ and $(\kappa_g^e)^M.u_g^e[h]$ $((\kappa_\ell^e)^M.u_\ell^e[h])$ as the *effective* lower and upper limits on the output (load) of *ESR* e such that, in any hour h, for any *ESR* $e \in \mathcal{E}$, $(\kappa_g^e)^m.u_g^e[h] \leq g^e[h] \leq (\kappa_g^e)^M.u_g^e[h]$ and $(\kappa_\ell^e)^m.u_\ell^e[h] \leq \ell^e[h] \leq (\kappa_\ell^e)^M.u_\ell^e[h]$.

Let $\epsilon^e[h]$ be the stored energy in resource $e \in \mathcal{E}$ at the *close* of hour h, or, equivalently, at the *start* of hour $[h+1]$. This energy must satisfy the specified minimum and maximum stored energy *MWh* limits, $(\epsilon^e)^m$ and $(\epsilon^e)^M$, respectively, of *ESR* e. We also represent the discharge (charge) efficiency of *ESR* e by the factor $\eta_g^e \in (0,1]$ $(\eta_\ell^e \in (0,1])$. For each hour h that *ESR* e supplies $g^e[h]$ *MW* (charges $\ell^e[h]$ *MW*) to (from) the grid at its node, its stored energy level decreases (increases) by $\dfrac{1}{\eta_g^e} g^e[h]$ *MWh* $(\eta_\ell^e \ell^e[h])$.

The economic deployment of utility-scale *ESR*s aims to take advantage of arbitrage opportunities by charging the resources when electricity market prices are low and discharging their stored energy to displace electricity generated by higher-priced and, typically, polluting resources, with the overall efficiencies of the charge-discharge cycle explicitly taken into account. In this paper, we assume that each integrated *ESR* is controlled by the Independent System Operator (*ISO*), whose objective is to maximize the total system social surplus over all the hours. The *ISO*, therefore, ensures that the *ESR*s are deployed as system resources so as to enhance the economic performance of the side-by-side power system and *DAM* operations. A direct consequence of such *ESR* deployment policy is that the *ESR*s also contribute to avert uneconomical scarcity events, thereby improving the system reliability. The maximization of the system social surplus must be performed over multiple

hours so as to fully take advantage of the *ESR*s' ability to shift significant amounts of energy over time. We formulate the *scheduling optimization problem* (*SOP*) to determine the most economic operational trajectory for the *ESR*s considering the variations in the demands and the outputs of the renewable resources and the available capacity of each conventional resource over the time horizon of interest. The solution of this optimization problem determines the optimal load and supply-resource dispatch, including that of the *ESR*s, for each hour of the optimization period $\overline{\mathcal{H}} = \{h : h = 1, \ldots, \overline{H}\}$. The *SOP* is formulated as a multi-period *OPF* with the explicit representation of the inter-hour constraints in storage operations, demands and supply-resource outputs, as well as the topology of the transmission network in each hour $h \in \overline{\mathcal{H}}$. In the formulation of the *SOP*, we make explicit use of the lossslessness assumption typically deployed in the linearized power flow model, which is the practice in today's *ISO*-run markets [36], p. 534.

In view of presenting the mathematical statement of the *SOP*, we introduce the following additional notation: let $\mathcal{N} = \{n : n = 0, 1, \ldots, N\}$ be the set of network buses with bus 0 being the slack bus, and $\mathcal{L} = \{l = 1, \ldots, L\}$ the set of transmission lines. Let matrices $\underline{A}$, $\underline{B}_d$ and $\underline{B}$ designate the reduced branch to node incidence, the branch susceptance and the reduced nodal susceptance matrices, respectively. We denote by $\underline{b}_0$ the column vector of the augmented susceptance matrix corresponding to the slack node and by $\underline{\theta}$ the vector of voltage phase angles at the $|\mathcal{N}|-1$ buses other than the slack bus. We denote by $\underline{f} = \underline{B}_d \, \underline{A} \, \underline{\theta}$ the vector of line flows, $\underline{f}^M$ and $\underline{f}^m$ the vectors of transmission line ratings in each flow direction. We specify $(\kappa^s)^m$ to be the minimum capacity of seller $s \in \mathcal{S}^c$ conventional resource. We also define the conventional generation (wind farm generation) power injection at node n in hour h as $p_n^c[h] = \sum_{s \in \mathcal{S}^c \text{ at node } n} g^s[h]$ ($p_n^w = \sum_{s \in \mathcal{S}^w \text{ at node } n} g^s[h]$),

where $g^s[h]$ is the output of seller s generation resource in hour h. The power consumption due to loads at node n in hour h is similarly denoted by $p_n^d[h] = \sum_{b \in \mathcal{B} \, at \, node \, n} \ell^b[h]$, where $\ell^b[h]$ is the cleared demand of buyer b in hour h. We use $\lambda_n[h]$ to denote the dual variable associated with the power balance equation at bus n in hour h.

The decision variables of the *SOP* are the withdrawals $\ell^b[h]$ due to each demand $b \in \mathcal{B}$, the outputs $g^s[h]$ of the various supply resources $s \in \mathcal{S}$, the operational state binary variables $u_g^e[h]$ and $u_\ell^e[h]$, the withdrawals $\ell^e[h]$, the outputs $g^e[h]$ and the stored energy level $\epsilon^e[h]$ of each *ESR* in $e \in \mathcal{E}$, as well as the phase angles $\theta_n[h]$, $\forall n \in \mathcal{N} \setminus \{0\}$, $\forall h \in \overline{\mathcal{H}}$. The *SOP* co-optimizes the withdrawal/output of each load/resource – including those of the *ESR*s – over each hour $h \in \overline{\mathcal{H}}$ with the objective to maximize the total system social surplus:

$$\max_{\substack{\ell^b[h], g^s[h], \\ \ell^e[h], g^e[h], \\ u_g^e[h], u_\ell^e[h], \\ \epsilon^e[h], \theta_n[h]}} \sum_{h \in \overline{\mathcal{H}}} \left[\sum_{b \in \mathcal{B}} \beta^b[h](\ell^b[h]) - \sum_{s \in \mathcal{S}^c} \gamma^s[h](g^s[h]) - \sum_{s \in \mathcal{S}^w} \gamma^s[h](g^s[h]) \right]. \tag{2.4}$$

The hour h social surplus is expressed as the difference between the total social benefits $\sum_{b \in \mathcal{B}} \beta^b[h](\ell^b[h])$ and the total supply costs of the conventional and wind resources, $\sum_{s \in \mathcal{S}^c} \gamma^s[h](g^s[h]) + \sum_{s \in \mathcal{S}^w} \gamma^s[h](g^s[h])$. We further assume that the cost (benefit) functions $\gamma^s(\cdot)$, $\forall s \in \mathcal{S} = \mathcal{S}^c \bigcup \mathcal{S}^w$ ($\beta^b(\cdot)$, $\forall b \in \mathcal{B}$) are piecewise linear, as is the case in the *OPF*-based market clearing mechanisms, typically, used by the *ISO*s. We explicitly exclude the benefits/costs for the storage resources in the objective function (2.4) as those are indirectly accounted for in terms of the *ESR* impacts on the system supply-resource dispatch costs. Indeed, in the expression for the nodal power

balance equations, the term $p_n^e[h] = \sum_{e \in \mathcal{E} \text{ at node } n} (g^e[h] - \ell^e[h])$ explicitly represents the net power injection of the storage resources connected at node n in hour $h \in \overline{\mathcal{H}}$ ($g^e[h]$ and $\ell^e[h]$ cannot be both strictly positive in the same hour h, as per their effective lower and upper limits and the requirement that $u_g^e[h] + u_\ell^e[h] \leq 1$):

$$\left(\underline{p}^c[h] + \underline{p}^w[h]\right) - \underline{p}^d[h] + \underline{p}^e[h] = \underline{B}\,\underline{\theta}[h], \quad \forall h \in \overline{\mathcal{H}} \tag{2.5}$$

$$(p_0^c[h] + p_0^w[h]) - p_0^d[h] + p_0^e[h] = \underline{b}_0^\dagger\,\underline{\theta}[h], \quad \forall h \in \overline{\mathcal{H}}. \tag{2.6}$$

Each *ESR* $e \in \mathcal{E}$, whose stored energy $\epsilon^e[h-1]$ at the end of hour $[h-1]$ exceeds its minimum capability $(\epsilon^e)^m$, may act as a generation resource and displace higher-priced supply resources in hour h. In such cases, the output $g^s[h]$ of each displaced supply resource is reduced commensurately, as are their associated costs $\gamma^s[h](g^s[h])$ in the objective function (2.4), resulting in a corresponding increase in the social surplus (2.4) for that hour. For an optimal trajectory, the storage resources discharge, typically, in the peak hours so as to displace the outputs of the higher-priced supply resources and maximize the resulting increases in the objective function (2.4). On the other hand, when an *ESR* acts as a load to charge energy in hour h, it makes use of energy generated by both conventional and renewable resources, resulting in additional generation costs for that hour. The solution of the *SOP* takes advantage of arbitrage opportunities so that the charging hours for the storage resources are in the periods of low prices – typically, the low-load hours. The optimal solution that maximizes the total social surplus over all the hours in $\overline{\mathcal{H}}$ ensures that the *ESR*s are utilized only when the value of the energy they displace exceeds the costs incurred in their charging, with

the efficiencies of the charge/discharge cycle fully taken into account. Furthermore, the optimization scheme takes advantage of the potential synergy between storage and wind resources. In the absence of storage resources, the *ISO* may be forced to "spill" wind energy due to the insufficiency of the load demand in the low-load hours. The charging of the *ESR*s may be scheduled to be carried out in such hours of high supply and low demand, when the generation costs are, typically, low. The additional demand created by *ESR* charging may be supplied, in some cases, by the wind energy that would have otherwise been "spilled". In that sense, the storage resources provide the ability to shift the wind energy produced during the low load hours to the peak load hours, when it can be used to displace the outputs of polluting and more expensive conventional resources.

The *SOP* formulation explicitly incorporates transmission constraints to ensure that the line flows do not violate the thermal limits of the transmission lines:

$$-\underline{f}^m \leq \underline{B}_d \, \underline{A} \, \underline{\theta}[h] \leq \underline{f}^M, \quad \forall h \in \overline{\mathcal{H}}. \tag{2.7}$$

We represent of the *ESR* intertemporal operational constraints that relate the charge/discharge decisions to the stored energy in an *ESR*, with the discharge/charge efficiencies explicitly considered:

$$\epsilon^e[h] = \epsilon^e[h-1] - \frac{1}{\eta_g^e} g^e[h] + \eta_\ell^e \ell^e[h], \; \forall h \in \overline{\mathcal{H}}, \; \forall e \in \mathcal{E}. \tag{2.8}$$

The stored energy in each hour is a critically important decision variable, even though it is not explicitly represented in (2.4). The presence of the constraints in (2.8) introduces an intertemporal coupling in the multi-hour optimization, resulting in a system of interdependent *OPF*s. These equalities serve to

ensure that the storage resources accumulate energy during the lower-priced hours so as to discharge energy in subsequent, higher-priced hours. The discharge (charge) efficiency coefficient η_g^e (η_ℓ^e) $\in (0, 1]$ strongly influence the storage resource operations. The more efficient the *ESR*s, the higher their utilization since the optimization tries to minimize the energy losses incurred with each charge/discharge cycle so as to lower the overall supply costs.

We also include the constraints to specify the capacity ranges within which an *ESR* may discharge or charge, respectively.

$$(\kappa_g^e)^m.u_g^e[h] \leq g^e[h] \leq (\kappa_g^e)^M.u_g^e[h], \quad \forall h \in \overline{\mathcal{H}}, \quad \forall e \in \mathcal{E} \tag{2.9}$$

$$(\kappa_\ell^e)^m.u_\ell^e[h] \leq \ell^e[h] \leq (\kappa_\ell^e)^M.u_\ell^e[h], \quad \forall h \in \overline{\mathcal{H}}, \quad \forall e \in \mathcal{E}. \tag{2.10}$$

We note that the minimum and maximum discharge (charge) capacities are both multiplied by the operational state status variable $u_g^e[h]$ ($u_\ell^e[h]$). So, whenever *ESR* e discharges (charges) in hour h, the associated status variable $u_g^e[h]$ ($u_\ell^e[h]$) is 0, resulting in the discharge output $g^e[h]$ (charge withdrawal $\ell^e[h]$) being 0. This formulation preserves the linearity of the constraints, which helps with the computational tractability.

Further, we represent constraints to ensure that an *ESR* may not both discharge and charge in the same hour h since

$$0 \leq u_g^e[h] + u_\ell^e[h] \leq 1, \quad \forall h \in \overline{\mathcal{H}}, \quad \forall e \in \mathcal{E}. \tag{2.11}$$

$$u_g^e[h] \in \{0, 1\}, \quad u_\ell^e[h] \in \{0, 1\}, \quad \forall h \in \overline{\mathcal{H}}, \quad \forall e \in \mathcal{E}. \tag{2.12}$$

Also, we represent the constraints on the physical limits on the energy that

can be stored in *ESR* e by:

$$(\epsilon^e)^m \leq \epsilon^e[h] \leq (\epsilon^e)^M, \quad \forall h \in \overline{\mathcal{H}}, \quad \forall e \in \mathcal{E}, \tag{2.13}$$

with the initial stored energy ϵ_0^e is given by

$$\epsilon^e[0] = \epsilon_0^e, \quad \forall e \in \mathcal{E}. \tag{2.14}$$

The consideration of the limits on the demand/output of all each load and each supply resource results in the constraints:

$$0 \leq \ell^b[h] \leq d^b[h], \quad \forall h \in \overline{\mathcal{H}}, \quad \forall b \in \mathcal{B} \tag{2.15}$$

$$(\kappa^s)^m \leq g^s[h] \leq a^s[h], \quad \forall h \in \overline{\mathcal{H}}, \quad \forall s \in \mathcal{S}^c \tag{2.16}$$

$$0 \leq g^s[h] \leq w^s[h], \quad \forall h \in \overline{\mathcal{H}}, \quad \forall s \in \mathcal{S}^w. \tag{2.17}$$

The resulting *SOP* in (2.4)-(2.17) is a large-scale mixed-integer linear program (*MILP*). We use the superscript * to denote the optimal value of the decision variables that solve the *SOP*. For example, the $(g^e)^*[h]$ $((\ell^e)^*[h])$ values provide the *ESR* dispatch results $\forall e \in \mathcal{E}$, $\forall h \in \overline{\mathcal{H}}$. We note that the solution to the *SOP* determines not only the operations of the *ESR*s, but also the load and resource dispatch for each hour in the optimization period. Similarly, at the optimum, the dual variables (shadow prices) of the power balance constraints (2.5) and (2.6) are interpreted as the locational marginal prices (*LMP*s) for each hour $h \in \overline{\mathcal{H}}$. As such, we view the dispatch and shadow prices determined by the *SOP* solution to be those of a *DAM* with the explicit representation of the impacts of the *ESR*s on the nodal net power injections, and consequently, on the *DAM* outcomes. We make use of

this fact to represent the impacts of the utility-scale storage resources on the side-by-side power system and market operations. We also note that, absent the representation of the *ESR*s and their associated intertemporal coupling constraints (2.8), the *SOP* consists of H separate *OPF* problems that may then be independently solved. Each such *OPF* reduces to an hourly *DAM* clearing model. Thus, the *SOP* can be seen as a generalized statement of the *DAM* clearing problem, one with the ability to represent "time-coupled" phenomena over multiple hours. In terms of the simulation approach, the *SOP* is deployed to determine not only the schedule but to also emulate the clearing of the *DAM*s for power systems with integrated *ESR*s.

2.3 Explicit Representation of the Ramping Requirements on Conventional Generators

In this section, we extend the capabilities of our approach to effectively account for the additional costs of providing the power system with sufficient ramping capability to perform its load following task smoothly, even as the deepening penetration of renewable resources tends to exacerbate the ramping requirements [9]. More precisely, our goal is to assess the economic impact of specifying ramping requirements for the conventional generation resources at the *DAM* clearing level. We define the ramping requirements induced by the uncertain, time-varying demands and renewable generation outputs and modify the formulation of the *SOP* in eqs. (2.4)-(2.17) to explicitly represent ramping requirements on conventional generators. From the solution of the *SOP*, we can explicitly evaluate the value of providing an additional *MW/min* of ramping up (down) capability from the dual variables associated with the inequality constraints enforcing the ramping up (down) require-

ments. Moreover, the *LMPs* obtained from such solution are different from those obtained from a dispatch that ignores ramping requirements. Thus, by evaluating those metrics, we capture the most significant economic impacts in terms of explicitly representing the ramping requirements in systems with renewable resources.

We now show how to determine the ramping requirements on conventional generation resources in systems with integrated renewable resources. Recall that the controllable load [12] is defined as the total aggregated load to be served by controllable units (i.e., conventional generation resources), that is, the net difference between the total load and the total renewable resource generation output (including the net scheduled interchanges). It is convenient at this stage to particularize the notion of controllable load to that of nodal controllable load, which we define for every bus n as the nodal load netted by the renewable resource generation output at node n. We denote the controllable load at node n in hour $h \in \mathcal{T}_i$ by $\xi_n[h]$. To determine the system ramping requirements for hour h, the *ISO* has to estimate each nodal controllable load as well as their respective variability ranges. The controllable load point estimate at node n may be defined as $\xi_n[h] = \sum_{batnoden} \left[d^b[h] - w_n[h]\right]$, whereas its variability range may be given in the form of the interval $\left[(\xi_n[h])^m, (\xi_n[h])^M\right]$ (necessarily, point estimate $\xi_n[h]$ must belong to this interval). For example, we may assume the simultaneous deviations of the nodal controllable loads (worst-case scenario) and compute the sum of the maximum positive (negative) controllable load deviations over the nodes to obtain a conservative assessment of the system ramping up (down) requirement in hour h: $\sum_{n=0}^{N} \left[(\xi_n[h])^M - \xi_n[h]\right]$ $\left(\sum_{n=0}^{N} \left[(\xi_n[h])^m - \xi_n[h]\right]\right)$. The system contribution to raise generation action is determined by the sum of the contributions to raise generation action

of the conventional resources participating into the market and must exceed the system ramping up requirement. Similar reasoning may be applied to the determination of the system contribution to lower generation action. Seller $s \in \mathcal{S}^c$ unit contribution to raise (lower) generation action may be defined as the minimum (maximum) between its ramping capability over Δ *minutes* $\kappa_+^s \Delta$ ($\kappa_-^s \Delta$) and seller s unit available margins (note that κ_-^s is a negative quantity in *MW/min*). We may thus write the ramping up (down) requirement constraints for a given hour h as:

$$\sum_{s \in \mathcal{S}^c} \min \left\{ \kappa_+^s \Delta, a^s[h] - g^s[h] \right\} \geq \sum_{n=0}^{N} \left[(\xi_n[h])^M - \xi_n[h] \right] \tag{2.18}$$

$$\sum_{s \in \mathcal{S}^c} \max \left\{ \kappa_-^s \Delta, (\kappa^s)^m - g^s[h] \right\} \leq \sum_{n=0}^{N} \left[(\xi_n[h])^m - \xi_n[h] \right]. \tag{2.19}$$

We note that Δ can represent any duration of 60 *min* or less. As such, it is possible to define the ramping requirements over intra-hourly time scales so as to ensure that the set of conventional resources is potentially capable to ramp up (down) its aggregated output over a few minute duration. [5]

We also introduce intertemporal constraints to ensure that each conventional resource in $\mathcal{S}^c$ has sufficient ramping capability to transition from its cleared output $g^s[h-1]$ in hour $h-1$ to its cleared output in hour h. Assuming each conventional resource in $\mathcal{S}^c$ can have up to $\Delta = 60$ *min* to complete

[5] In case the *SOP* were to become infeasible due to the incorporation of the ramping up (down) requirement constraints, one may elect to "soften" said constraints so the solver can still find a feasible solution. To do so, one may simply substract (add) from (to) the right hand side of eq. (2.18) (eq. (2.19)) a positive decision variable meant to measure the quantity by which the constraint is, potentially, violated. Then, one must associate – in the objective function (2.4) – penalty costs to said decision variables (one for each of the ramping requirement) in order to penalize any violation of the corresponding constraint. By way of these penalty costs, the user can effectively specify the economic value that is placed upon the provision of sufficient ramping capability to meet the ramping requirements.

the transition, we have:

$$60 \cdot \kappa_{-}^{s} \leq g^{s}[h] - g^{s}[h-1] \leq 60 \cdot \kappa_{+}^{s}. \tag{2.20}$$

By enforcing these constraints for each hour of the *SOP* optimization period $\overline{\mathcal{H}}$, we effectively enable the system conventional resources to prepare for and respond to larger ramp requirements without violation and ensure the smooth ramping of each conventional resource from an hour to the next. We now reformulate the *SOP* with these constraints as follows:

$$\max_{\substack{\ell^{b}[h], g^{s}[h], \\ \ell^{e}[h], g^{e}[h], \\ u_{g}^{e}[h], u_{\ell}^{e}[h], \\ \epsilon^{e}[h], \theta_{n}[h]}} \sum_{h \in \overline{\mathcal{H}}} \left[\sum_{b \in \mathcal{B}} \beta^{b}[h](\ell^{b}[h]) - \sum_{s \in \mathcal{S}^{c}} \gamma^{s}[h](g^{s}[h]) - \sum_{s \in \mathcal{S}^{w}} \gamma^{s}[h](g^{s}[h]) \right],$$

subject to

$$\left(\underline{p}^{c}[h] + \underline{p}^{w}[h]\right) - \underline{p}^{d}[h] + \underline{p}^{e}[h] = \underline{B}\,\underline{\theta}[h], \quad \forall h \in \overline{\mathcal{H}} \tag{2.21a}$$

$$(p_{0}^{c}[h] + p_{0}^{w}[h]) - p_{0}^{d}[h] + p_{0}^{e}[h] = \underline{b}_{0}^{\dagger}\,\underline{\theta}[h], \quad \forall h \in \overline{\mathcal{H}} \tag{2.21b}$$

$$\sum_{s \in \mathcal{S}^{c}} \min\left\{\kappa_{+}^{s}\Delta, a^{s}[h] - g^{s}[h]\right\}$$
$$\geq \sum_{n=0}^{N} \left[(\xi_{n}[h])^{M} - \xi_{n}[h]\right], \ \forall h \in \overline{\mathcal{H}}, \ \forall s \in \mathcal{S}^{c} \tag{2.21c}$$

$$\sum_{s \in \mathcal{S}^{c}} \max\left\{\kappa_{-}^{s}\Delta, (\kappa^{s})^{m} - g^{s}[h]\right\}$$
$$\leq \sum_{n=0}^{N} \left[(\xi_{n}[h])^{m} - \xi_{n}[h]\right], \ \forall h \in \overline{\mathcal{H}}, \ \forall s \in \mathcal{S}^{c} \tag{2.21d}$$

$$\kappa_{-}^{s}.60 \leq g^{s}[h] - g^{s}[h-1] \leq \kappa_{+}^{s}.60 \tag{2.21e}$$

$$-\underline{f}^{m} \leq \underline{B}_{d}\,\underline{A}\,\underline{\theta}[h] \leq \underline{f}^{M}, \quad \forall h \in \overline{\mathcal{H}} \tag{2.21f}$$

$$\epsilon^{e}[h] = \epsilon^{e}[h-1] - \frac{1}{\eta_{g}^{e}} g^{e}[h] + \eta_{\ell}^{e}\ell^{e}[h], \ \forall h \in \overline{\mathcal{H}}, \ \forall e \in \mathcal{E} \tag{2.21g}$$

$$(\kappa_g^e)^m.u_g^e[h] \leq g^e[h] \leq (\kappa_g^e)^M.u_g^e[h], \quad \forall h \in \overline{\mathcal{H}}, \quad \forall e \in \mathcal{E} \tag{2.21h}$$

$$(\kappa_\ell^e)^m.u_\ell^e[h] \leq \ell^e[h] \leq (\kappa_\ell^e)^M.u_\ell^e[h], \quad \forall h \in \overline{\mathcal{H}}, \quad \forall e \in \mathcal{E} \tag{2.21i}$$

$$0 \leq u_g^e[h] + u_\ell^e[h] \leq 1, \quad \forall h \in \overline{\mathcal{H}}, \quad \forall e \in \mathcal{E} \tag{2.21j}$$

$$u_g^e[h] \in \{0,1\}, \quad u_\ell^e[h] \in \{0,1\}, \quad \forall h \in \overline{\mathcal{H}}, \quad \forall e \in \mathcal{E} \tag{2.21k}$$

$$(\epsilon^e)^m \leq \epsilon^e[h] \leq (\epsilon^e)^M, \quad \forall h \in \overline{\mathcal{H}}, \quad \forall e \in \mathcal{E}, \tag{2.21l}$$

$$\epsilon^e[0] = \epsilon_0^e, \quad \forall e \in \mathcal{E} \tag{2.21m}$$

$$0 \leq \ell^b[h] \leq d^b[h], \quad \forall h \in \overline{\mathcal{H}}, \quad \forall b \in \mathcal{B} \tag{2.21n}$$

$$(\kappa^s)^m \leq g^s[h] \leq a^s[h], \quad \forall h \in \overline{\mathcal{H}}, \quad \forall s \in \mathcal{S}^c \tag{2.21o}$$

$$0 \leq g^s[h] \leq w^s[h], \quad \forall h \in \overline{\mathcal{H}}, \quad \forall s \in \mathcal{S}^w. \tag{2.21p}$$

We remark that the extended *SOP* may be reduced to a *MILP*. Each "min" involved in non-linear constraint (2.18) can be replaced by a decision variable for which we enforce two constraints: to be less or equal than each argument in the corresponding "min". A similar device holds for non-linear constraint (2.19). We note that the dual variables $\rho^+[h]$ ($\rho^-[h]$) associated with the ramping up (down) requirement constraints (2.18) and (2.19) are of particular interest here, since they correspond to the sensitivities of the social surplus (2.4) with respect to an infinitesimal variation in the ramping up (down) requirement. They provide valuable information as to the worth of the ramp capability service. Also, the incorporation of constraints (2.18), (2.19) into the *SOP* has contributed to shrink the feasibility region of the original problem. As such, we may expect the dispatch produced by the extended *SOP* to be less economical than that without the explicit ramp requirements. Such consequences are investigated in chapter 4, section 4.5.

2.4 Summary

The models developed in this chapter form the basis of the simulation analytical framework. The random process-based models for the simulation inputs are meant to be sampled so as to provide hourly realizations of the buyer demands, multi-site wind speeds and conventional generator available capacities that can then be used to formulate the offers and bids in the hourly DAMs we aim to emulate by solving a SOP-type of problem. We note that the ESRs, which are deployed to maximize the economic performance of the DAMs, are inherently represented in the SOP and so their scheduling is coordinated with the dispatch of the loads and other supply resources. The next chapter highlights the role of each model as part of the overall simulation methodology.

CHAPTER 3

SIMULATION METHODOLOGY

We devote this chapter to discussing the fundamentals of the simulation approach. We start by laying out the basic time frame of the simulation in section 3.1 and proceed to providing an overview of the Monte Carlo simulation we perform to emulate the side-by-side power system operations and transmission-constrained DAMs in section 3.2. We continue with the detailed description of the mechanics involved in the execution of a so-called *simulation run* in section 3.3, wherein we also indicate how to compute the various market outcomes of interest from the simulation outputs. We conclude the chapter in section 3.4 by discussing various implementational aspects aimed at ensuring the computational tractability of the stochastic simulation approach.

3.1 Time Frame of the Stochastic Simulation

The simulation is carried out for a study period $\mathcal{T}$ that ranges, typically, from a few weeks to multiple years. We decompose $\mathcal{T}$ into non-overlapping simulation periods $\mathcal{T}_i$'s such that $\mathcal{T} = \bigcup_{i=1}^{T} \mathcal{T}_i$. We define each simulation period $\mathcal{T}_i$ in such a way that the system resource mix and unit commitment, the transmission grid, the operating policies, the market structure and the seasonality effects remain unchanged over its duration. While there are many possible choices for a simulation period, we specify each simulation period

to be of one-week duration. This choice captures the load patterns over the week and week-end days, and is able to incorporate the maintenance schedules. We further decompose each simulation period into subperiods, where a subperiod is the smallest indecomposable unit of time represented in the simulation. We assume that each variable is constant over the entire duration of a subperiod. The simulation, as such, ignores any phenomenon whose time scale is smaller than a subperiod. We choose to use subperiods of one hour duration as an acceptable compromise between the level of detail needed for a realistic representation of the power system and market operations and the computational tractability of the simulation. The subperiod selection is particularly appropriate as many existing DAMs are cleared on an hourly basis. We denote by h the index of the subperiods in a simulation period $\mathcal{T}_i$ such that $\mathcal{T}_i = \{h : h = 1, \ldots, 168\}$. A breakdown of the simulation approach time frame [1] is depicted in Fig. 3.1.

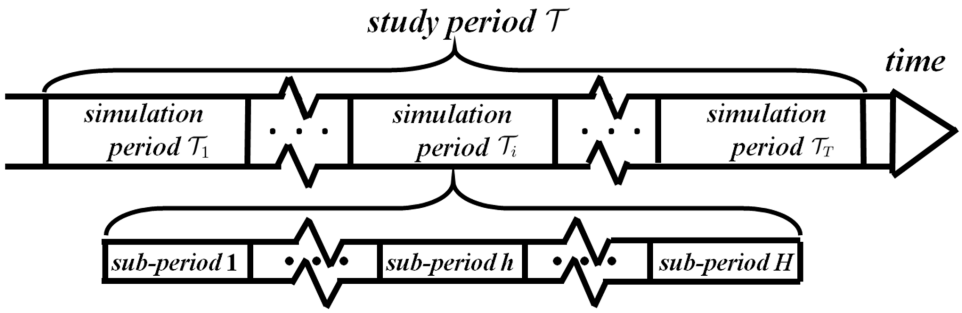

Figure 3.1: The time dimension in the simulation approach

We note that we perform one Monte Carlo simulation for each simulation period $\mathcal{T}_i$. We assume that the outcomes of the Monte Carlo simulation of a given simulation period has no bearing on the Monte Carlo simulation of any other simulation period [2] and so, each simulation period may be simulated

[1] We point out that the proposed approach is sufficiently general to be applicable to other time scales.

[2] While, as mentioned previously, the power system operational conditions may differ

independently from one another. Such fact has an important consequence in terms of implementation (see 3.4), since it allows the parallelization of the Monte Carlo simulation of each simulation period. As such, in what follows, we shall focus on the Monte Carlo simulation of an arbitrary simulation period $\mathcal{T}_i$, such that any conclusion we draw for such simulation period is applicable to all other simulation periods in $\mathcal{T}$. In the next section, we discuss the Monte Carlo simulation of a given simulation period.

3.2 The Proposed Monte Carlo Simulation Procedure

The simulation emulates the side-by-side power system operations and transmission-constrained day-ahead market. Specifically, in each simulation period, we emulate the clearings of the 168 hourly DAMs where the market outcomes determine the contributions to the performance metrics of interest. The modeling of the highly variable demands, multi-site renewable power outputs and conventional generator available capacities, all of which are uncertain and participate in the hourly DAMs, is in terms of discrete-time $r.p.$s which are collections of $r.v.$s (random vectors in the case of the buyer demands and multi-site wind speeds) indexed by the 168 hours of the simulation period, as seen in chapter 2. These $r.p.$s constitute the inputs to the simulation, in the sense that their multi-period realizations, the so-called sample paths $s.p.$s, determine the bids and offers made into the 168 DAMs of the simulation period. For convenience in the rest of the thesis, we shall refer to these $r.p.$s as *input* $r.p.$s, in light of their role in driving the clearing of the DAMs, thus the simulation. We note that, in this work, the utility-scale

from one simulation period to another, we effectively assume that those changes are exogenous to the simulation procedure itself, and so the Monte Carlo simulation of a given simulation period has, indeed, no impact on that of another.

energy storage resources are deployed as a *system resource* by the Independent System Operator (*ISO*). As such, they are neither bid nor offered in the *DAM*s; rather, they are at the disposal of the operator to bring maximum economic benefits to the side-by-side power system and *DAM* operations. From this perspective, the *ESR*s are therefore scheduled as part of the *DAM* clearing mechanism, in such a way that the *ESR*s operations are coordinated with the demands and other supply-side resources over multiple subperiods. [3] We make use of the *SOP* developed in sections 2.2 and 2.3 to emulate the clearings of the hourly *DAM*s and schedule, concurrently, the operations of the *ESR*s. Over the course of a simulation period, we actually require – for reasons that are made clear in section 3.3 – the solution to a sequence of 7 *SOP*s to map the input *r.p.*s into the *output* discrete-time *r.p.*s, also indexed by the 168 hours of the simulation period, that represent the market outcomes and the scheduled *ESR* operations. We provide a conceptual representation of such a mapping in Fig. 3.2.

We make use of Monte Carlo simulation techniques in the simulation approach to effectively evaluate various performance metrics that reflect the statistical properties of the market outcome (output) *r.p.*s. We point out that the Monte Carlo simulation represents, in itself, the means through which we can perform such an assessment, which is otherwise impossible to perform analytically (or at least, not without considerable simplifying assumptions) due to the lack of a closed-form expression linking the output

[3] We point out that our framework is sufficiently flexible to also represent privately owned, for-profit storage resources that would be bid/offered in the *DAM*s. In such a case, however, the scheduling of the storage resources is not determined as part of the *DAM* clearing, but rather as part of a commercial strategy that would seek to take advantage of arbitrage opportunities (differences in the electricity prices) in order to maximize profit. The bids/offers of such storage resources reflect said commercial strategy, and so their representation in our simulation framework is akin to that of a demand (upon storage charge) or a conventional generation resources (upon storage discharge)

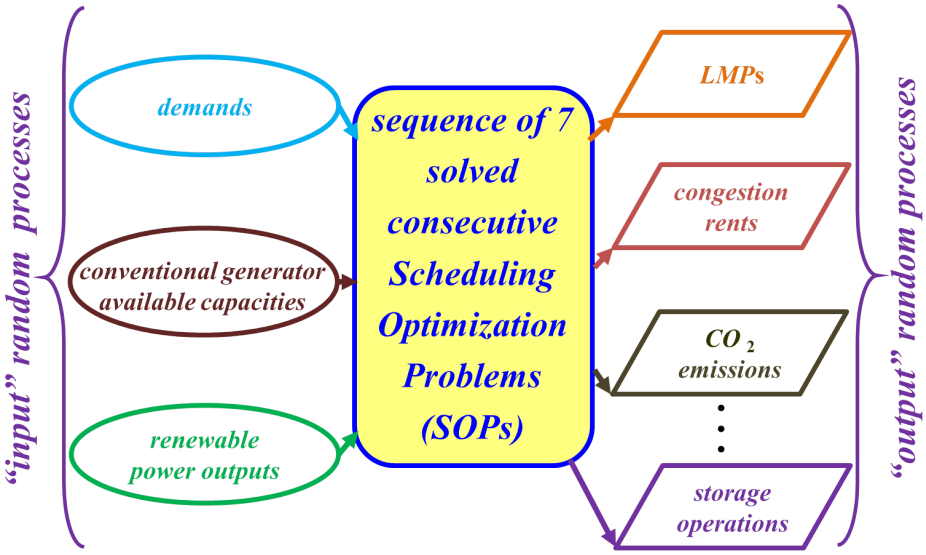

Figure 3.2: Conceptual structure of the stochastic simulation approach

*r.p.*s to the input *r.p.*s. We provide in Fig. 3.3 a conceptual flow-chart of the overall Monte Carlo simulation procedure and proceed to formally describe it in what follows.

The simulation approach makes use of the so-called *independent Monte Carlo* [37], p.10, and requires the construction of multiple *independent and identically distributed* (*i.i.d.*) *s.p.*s for each output *r.p.* to evaluate the performance metrics. Note that in this context, the phrase "*i.i.d. s.p.*s" has the sense that the *s.p.*s constitute the realizations of independent identically distributed *r.p.*s. A simulation run is the basic process through which we construct a *s.p.* for each of the output *r.p.*s. It consists of sampling each one of the input *r.p. j.c.d.f.s* – or joint probability mass functions (*j.p.m.f.*s) depending on the *r.p.* model – in order to generate the *s.p.*s whose hourly realizations are used as inputs in the sequence of 7 *SOP*s. [4] The *s.p.*s of the input *r.p.*s are mapped into *s.p.*s of the output *r.p.*s via the solution to the

[4]We recall that the construction and sampling procedure for each input *r.p.* was thoroughly described in chapter 2.

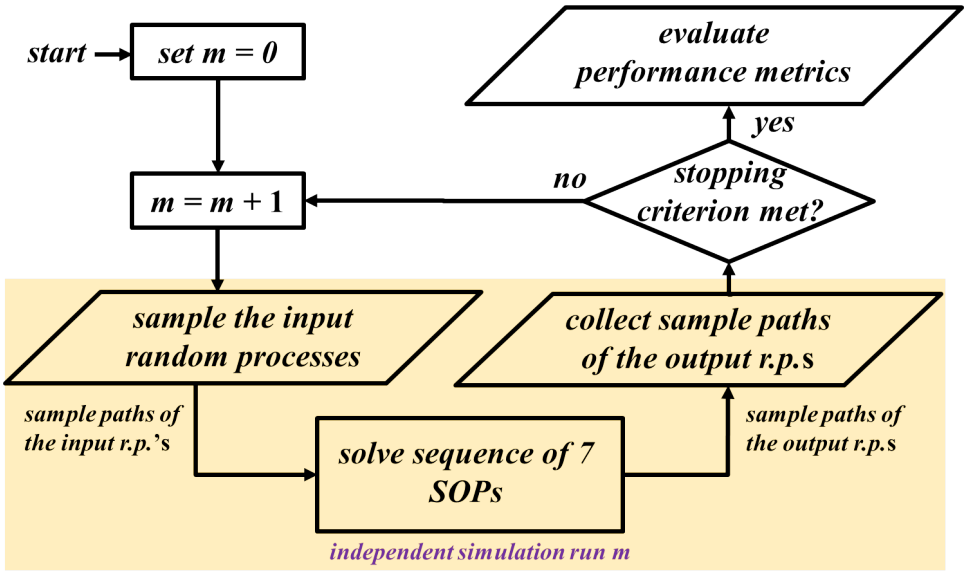

Figure 3.3: Monte Carlo simulation: conceptual flow chart

sequence of 7 *SOP*s. Thus, a *s.p.* for each output *r.p.* is obtained from the execution of a simulation run.

We carry out multiple simulation runs in order to create the output *s.p.*s from which we estimate the performance metrics for each market outcome of interest. We select our performance metrics to be the expected values of the time-indexed *r.v.*s making up the output *r.p.*s of interest. [5] Let M be the number of simulation runs; we estimate, for an output *r.p.* $\{\underset{\sim}{Y}[h] : h = 1, \ldots, 168\}$, the hourly sample mean point estimate $\overline{y}[h]$ of each *r.v.* $\underset{\sim}{Y}[h]$, $h = 1, \ldots, 168$:

$$\overline{y}[h] = \frac{1}{M} \sum_{j=1}^{M} y^{(j)}[h] \tag{3.1}$$

where $y^{(m)}[h]$ is the realization of *r.v.* $\underset{\sim}{Y}^{(m)}[h]$ in simulation run m (note that the $\underset{\sim}{Y}^{(m)}[h]$'s are *i.i.d.*). We refer the reader to section 3.3 for more

[5] Other metrics may be defined along similar lines. It is also possible to approximate the output *r.p. j.p.m.f.*s.

information about obtaining such realizations for several market outcomes of interest. The number of simulation runs M depends on the statistical reliability requirements specified for the estimation of the desired expected values. We define the statistical reliability of the hourly sample mean estimator $\overline{\underset{\sim}{Y}}[h] = \frac{1}{M}\sum_{m=1}^{M} \underset{\sim}{Y}^{(m)}[h]$ to be the length of the $100(1-\alpha)\,\%$ confidence interval with $0 < \alpha < 1$ for the true mean $\mu_{\underset{\sim}{Y}[h]}$ of *r.v.* $\underset{\sim}{Y}[h]$ [38], p. 82, p. 451. According to the Central Limit Theorem, the sample mean estimator $\overline{\underset{\sim}{Y}}[h]$ is approximately normally distributed for large M [31], p. 78. Thus, we can establish that $\mu_{\underset{\sim}{Y}[h]}$ lies in the interval $\left[\overline{\underset{\sim}{Y}}[h] - z_{(1-\alpha/2)}\frac{\sigma_{\underset{\sim}{Y}[h]}}{\sqrt{M}}, \overline{\underset{\sim}{Y}}[h] + z_{(1-\alpha/2)}\frac{\sigma_{\underset{\sim}{Y}[h]}}{\sqrt{M}}\right]$ with a $100(1-\alpha)\%$ probability, where $\sigma_{\underset{\sim}{Y}[h]}$ is the standard deviation of *r.v.* $\underset{\sim}{Y}[h]$, and $z_{1-\alpha/2} = \Phi^{-1}(1-\alpha)$, with Φ^{-1} the inverse of the cumulative distribution function (*c.d.f.*) of the standard normal distribution $\mathcal{N}(0,1)$. Note that the length of the confidence interval is a function in $\sqrt{M}^{-1}$. While it is possible to select M so as to set the confidence interval length and achieve the desired statistical reliability, in practice, a function in $\sqrt{M}^{-1}$ decays very slowly for large M; beyond a certain value of M, the improvement in statistical reliability is generally too small to warrant the extra computing-time needed to perform additional simulation runs.

In the next section, we delve into the mechanics of a simulation run by detailing its execution.

3.3 Simulation Run Mechanics

We recall that a simulation run essentially consists of sampling each one of the input *r.p. j.c.d.f.s* – or joint probability mass functions (*j.p.m.f.*s) depending on the *r.p.* model – in order to generate the *s.p.*s whose hourly realizations are used as inputs in the sequence of 7 *SOP*s. In this section, we

clarify our choice of solving a sequence of 7 *SOP*s, and detail the use of the input *s.p.*s in the parametrization of the 7 *SOP*s. Then, we indicate how to compute the various market outcomes of interest from the solutions to the sequence of 7 *SOP*s.

The emulation of the *DAM* clearings – complete with the coordinated scheduling of *ESR* operations – over the course of a simulation period entails solving a sequence of 7 *SOP*s, one for each day of the week. In such a context, each solved *SOP* serves two purposes: to emulate, for a given day in the simulation period $\mathcal{T}_i$, the clearing of its 24 hourly *DAM*s, and to schedule the *ESR* operations over a week-long period whose first day is the day whose *DAM* clearing results are obtained. For clarity in the presentation, we will refer to such a day as day j in the simulation period $\mathcal{T}_i$, with $j \in \{1, \ldots, 7\}$. We regard the solutions of the *SOP* for the 24 hours of day j to be the outcomes of the corresponding hourly *DAM*. These day j outcomes serve to construct the output *s.p.*s whose values we use to quantify the performance metrics of interest. The *SOP* optimization period $\overline{\mathcal{H}} = \left\{h : h = 1, \ldots, \overline{H}\right\}$ must also include additional hours that immediately follow the 24 hours of day j to ensure that the *ESR*s are scheduled in such a way as to reflect their continued operations beyond the simulated day j. Such additional period is required so that the *ESR*s are not discharged by the last hour of day j, an unrealistic outcome as the *ESR*s are operated on a broader horizon than a day. To avoid complications with a limited scheduling horizon, we solve each *SOP* over a week-period and so $\overline{H} = 168$ for a given simulation period $\mathcal{T}_i$. The solution of each *SOP* for the hours beyond those of the simulated day j are *not* used in the construction of the output *s.p.*s; they serve simply to represent the continued operations of the *ESR*s beyond day j. The stored energy of each *ESR* at the end of the last hour of day j is recorded to be

used as the initial stored energy of each *ESR* in the formulation of the *SOP* for the day $(j+1)$. For the purposes of this discussion, we assume that the initial stored energy level ϵ_0^e of each *ESR* $e \in \mathcal{E}$ in the first hour of day 1 is given.

For each hour h in day j, the so-called cost (benefit) functions $\gamma^s(\cdot)$, $\forall s \in \mathcal{S} = \mathcal{S}^c \bigcup \mathcal{S}^w$ ($\beta^b(\cdot)$, $\forall b \in \mathcal{B}$) in the *SOP* objective (2.4) are the offer (bid) functions submitted by each seller (buyer) for the 24 *DAM*s of day j. The upper bounds on the demands in (2.15) and the supply-resource outputs in (2.16) and (2.17) are set by the hourly realizations of the *s.p.*s of the corresponding input *r.p.*s. More specifically:

- the sampled realization $d^b[h]$ of $\underset{\sim}{D}^b[h]$ determines the maximum demand quantity bid by buyer $b \in \mathcal{B}$ in hour $h \in \mathcal{T}_i$;
- the sampled realization $w^s[h]$ of $\underset{\sim}{W}^s[h]$ determines the maximum wind capacity offered by seller $s \in \mathcal{S}^w$ in hour $h \in \mathcal{T}_i$; and
- the sampled realization $a^s[h]$ of $\underset{\sim}{A}^s[h]$ determines the maximum power output offered by seller $s \in \mathcal{S}^c$ in hour $h \in \mathcal{T}_i$.

In this way, the sampled realizations serve to parametrize the *SOP* in the first 24 hours of its optimization period $\overline{\mathcal{H}}$ (recall: these first 24 hours correspond to day j).

For each hour h beyond the 24 hours of day j, the offer (bid) functions, as well as the upper bounds on the demands and supply-resource outputs are obtained differently to reflect the fact that, in the real world, the market players only submit their bids and offers for the "current" day j and any supplementary information about the hours following day j must be estimated

by the *ISO*. Thus, we assume that the demands are fixed and the sellers offer at a predetermined price in all hours following day j; furthermore, we make use of the expected values for the loads and wind power outputs, coupled with the assumption that a conventional generation resource keeps running at full capacity (potentially after recovering from a forced outage state) to determine the upper bounds on the demands and supply-resource outputs in these hours. We illustrate in Fig. 3.4 the overall procedure for the execution of a given simulation run. We also show in Fig. 3.5 the detailed utilization of the input *s.p.*s elements in the parametrization of the *SOP* for a given day j.

We use the solutions of the *SOP* for the 24 hours of day j to be the outcomes of the corresponding hourly *DAM*. We note that, at the optimum, the dual variables associated with the power balance equations (2.5) and (2.6) constitute the *LMP*s in the corresponding hour h in day j at each node of the transmission grid. The *LMP*s are used as the nodal prices of the *MWh* commodity in hour h in day j [6] and we denote by $(\lambda_n)^*[h]$ the *LMP* in hour h at node n. The optimal solution to the *SOP* also yields, for each hour h in day j, the optimal resource dispatch, i.e., the power output $(g^s)^*[h]$ (consumption $(\ell^b)^*[h]$) of each generation resource $s \in \mathcal{S}$ (demand $b \in \mathcal{B}$), the scheduled discharge $(g^e)^*[h]$ (charge $(\ell^e)^*[h]$) of each *ESR* $e \in \mathcal{E}$, as well as the vector of power flows $(\underline{f})^*[h] = \underline{B}_d\, \underline{A}\, (\underline{\theta})^*[h]$ on the grid lines. We use these optimal values to compute the hourly realizations of the output *r.p.*s of interest.

The total wholesale purchase payments $\varsigma^{\mathcal{B}}[h]$ in hour h are computed as (having that $p_n^d = \sum_{b \text{ at node } n} \ell^b$):

[6] In the simulation, if the fixed demand at node n cannot entirely be met (loss of load event), we set the *LMP* at the regulatorily specified cap price, typically, the marginal price of the most expensive conventional resource.

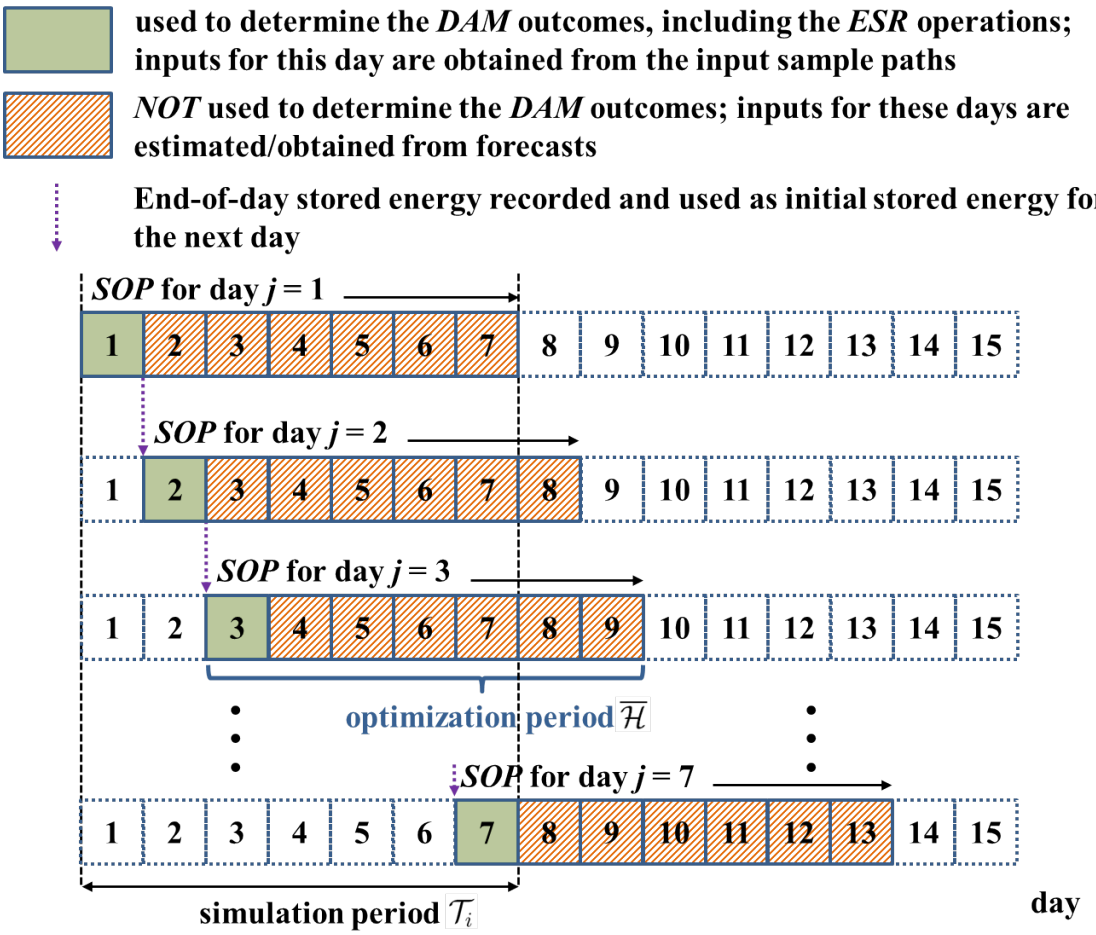

Figure 3.4: Role of the *SOP* in the emulation of the *DAM*s of a simulation period

$$\varsigma^{\mathcal{B}}[h] = \sum_{n \in \mathcal{N}} (\lambda_n)^*[h] \,.\, (p_n^d)^*[h]. \tag{3.2}$$

The total payments to the supply side $\varsigma^{\mathcal{S}}[h]$ in hour h are computed similarly (having that $p_n^c = \sum_{s \in \mathcal{S}^c \text{ at node } n} g^s$ and $p_n^w = \sum_{s \in \mathcal{S}^w \text{ at node } n} g^s$):

$$\varsigma^{\mathcal{S}}[h] = \sum_{n \in \mathcal{N}} (\lambda_n)^*[h] \,.\, \left[(p_n^c)^*[h] + (p_n^w)^*[h]\right]. \tag{3.3}$$

Consequently, the total congestion rents $k[h]$ are:

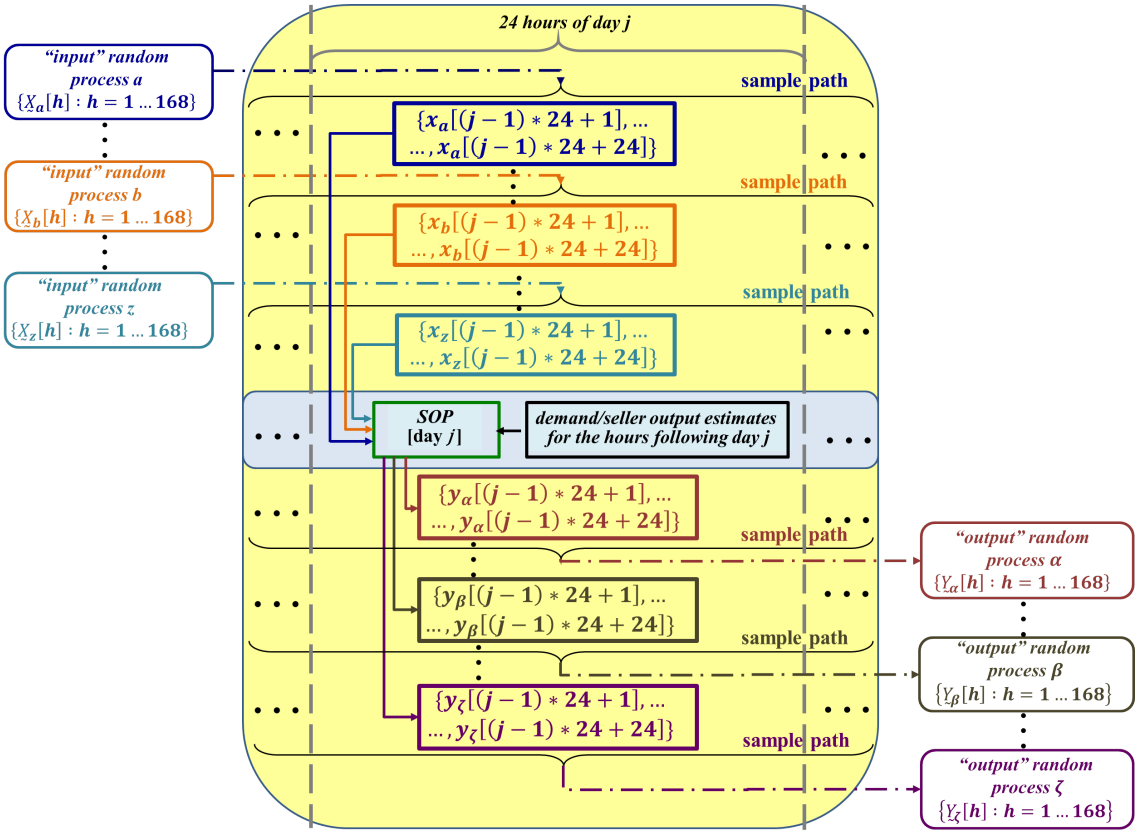

Figure 3.5: Simulation of a day as part of a simulation run

$$k[h] = \varsigma^{\mathcal{B}}[h] - \varsigma^{\mathcal{S}}[h]. \tag{3.4}$$

Let χ^s be the quantity in kg/MWh of CO_2 emissions released by the conventional unit of seller $s \in \mathcal{S}^c$. Then, the total CO_2 emissions are given by:

$$\nu[h] = \sum_{s \in \mathcal{S}^c} \chi^s \cdot (g^s)^*[h]. \tag{3.5}$$

In the case of the reliability metrics, we note that a loss of load event occurs only in case the *fixed* demand is not met. Therefore, the evaluation of the *LOLP* and *EUE* reliability metrics refers purely to the fixed demand and is

not meaningful for price responsive demands. In the simulation, we represent the fixed demands as price-sensitive demands with their willingness-to-pay set at the outage cost figures used in the evaluation of the *VOLL* [39]. In this way, the *SOP* gives highest priority to serve the fixed demand in light of its higher willingness-to-pay. We note that a loss of load event may be due to a supply shortfall or lack of transmission transfer capability, and that the reliability metrics we compute reflect that fact. At a node with loss of load, the unserved energy in hour h is the shortfall in supply that results in not meeting the total *fixed* demand at that node in that hour. Let $u_n[h]$ be the unserved energy at node n in hour h. Its value is computed as:

$$u_n[h] = \sum_{\substack{b \in \mathcal{B} \\ b \text{ at node } n \\ \text{fixed demand}}} d^b[h] - (\ell^b)^*[h]. \tag{3.6}$$

We use the indicator function $i_{(0,+\infty)}(\cdot)$ to compute the system *LOLP* contribution in hour h. The function takes for argument the system unserved energy (i.e. the sum of all the nodal unserved energies) and returns 1 whenever the system unserved energy is strictly positive, 0 otherwise. Then, the system *LOLP* contribution in hour h is given by $i_{(0,+\infty)}(\sum_{n \in \mathcal{N}} u_n[h])$.

To conclude this section, we stress again that all the hourly realizations obtained as above, together with the hourly realizations of the other subperiods $h' \neq h$, $h' \in \mathcal{T}_i$, constitute *s.p.*s of their associated output *r.p.*s. With each simulation run, new *s.p.*s for the market outcome output *r.p.*s are collected and used to estimate the performance metrics of interest via equation (3.1).

At this stage of the exposé, it should be apparent that the whole simulation process can be rather time-consuming. In the next section, we discuss implementational aspects aimed at improving the computational tractability

of the simulation approach.

3.4 Implementational Aspects of the Simulation Approach

The proposed simulation approach is primarily intended for longer-term studies to examine the economics, reliability performance and the environmental impacts of various integrated resource mixes under specified scenarios. For multiple year duration study periods, such an endeavor can prove computationally intensive, particularly for large-scale systems. Although it is always possible to exploit the generality of the approach and select a coarser time resolution, i.e., longer subperiods, to cut on computation time at the expense of a more detailed representation, we discuss a few steps that can be taken to ensure the computational tractability of the simulation approach without modifying the time resolution.

First and foremost, we discuss the use of a relaxed version of the *SOP* for improved tractability in the Monte Carlo simulations. We relax the highly-computationally-intensive *MILP* into the more tractable linear program (*LP*) we next describe. The proposed relaxation involves the modification of constraints (2.9) and (2.10): we assume that the *ESR* minimum charge $(\kappa_{\ell}^{e})^{m}$ and discharge $(\kappa_{g}^{e})^{m}$ capacities are 0, with all the binary variables u_{g}^{e} and u_{ℓ}^{e} equal to 1. The relaxed *SOP* is then formulated as follows:

$$\max_{\substack{\ell^{b}[h],g^{s}[h],\\ \ell^{e}[h],g^{e}[h],\\ u_{g}^{e}[h],u_{\ell}^{e}[h],\\ \epsilon^{e}[h],\theta_{n}[h]}} \sum_{h\in\overline{\mathcal{H}}}\left[\sum_{b\in\mathcal{B}}\beta^{b}[h](\ell^{b}[h]) - \sum_{s\in\mathcal{S}^{c}}\gamma^{s}[h](g^{s}[h]) - \sum_{s\in\mathcal{S}^{w}}\gamma^{s}[h](g^{s}[h])\right], \tag{3.7a}$$

subject to

$$\left(\underline{p}^{c}[h] + \underline{p}^{w}[h]\right) - \underline{p}^{d}[h] + \underline{p}^{e}[h] = \underline{B}\,\underline{\theta}[h], \quad \forall h \in \overline{\mathcal{H}} \tag{3.7b}$$

$$(p_0^{c}[h] + p_0^{w}[h]) - p_0^{d}[h] + p_0^{e}[h] = \underline{b}_0^{\dagger}\,\underline{\theta}[h], \quad \forall h \in \overline{\mathcal{H}} \tag{3.7c}$$

$$\sum_{s \in \mathcal{S}^c} \min\left\{\kappa_+^s \Delta, a^s[h] - g^s[h]\right\}$$
$$\geq \sum_{n=0}^{N} \left[(\xi_n[h])^M - \xi_n[h]\right], \; \forall h \in \overline{\mathcal{H}}, \; \forall s \in \mathcal{S}^c \tag{3.7d}$$

$$\sum_{s \in \mathcal{S}^c} \max\left\{\kappa_-^s \Delta, (\kappa^s)^m - g^s[h]\right\}$$
$$\leq \sum_{n=0}^{N} \left[(\xi_n[h])^m - \xi_n[h]\right], \; \forall h \in \overline{\mathcal{H}}, \; \forall s \in \mathcal{S}^c \tag{3.7e}$$

$$\kappa_-^s .60 \leq g^s[h] - g^s[h-1] \leq \kappa_+^s .60 \tag{3.7f}$$

$$-\underline{f}^m \leq \underline{B}_d\,\underline{A}\,\underline{\theta}[h] \leq \underline{f}^M, \quad \forall h \in \overline{\mathcal{H}} \tag{3.7g}$$

$$\epsilon^e[h] = \epsilon^e[h-1] - \frac{1}{\eta_g^e} g^e[h] + \eta_\ell^e \ell^e[h], \; \forall h \in \overline{\mathcal{H}}, \; \forall e \in \mathcal{E} \tag{3.7h}$$

$$0 \leq g^e[h] \leq (\kappa_g^e)^M, \quad \forall h \in \overline{\mathcal{H}}, \quad \forall e \in \mathcal{E} \tag{3.7i}$$

$$0 \leq \ell^e[h] \leq (\kappa_\ell^e)^M, \quad \forall h \in \overline{\mathcal{H}}, \quad \forall e \in \mathcal{E} \tag{3.7j}$$

$$(\epsilon^e)^m \leq \epsilon^e[h] \leq (\epsilon^e)^M, \quad \forall h \in \overline{\mathcal{H}}, \quad \forall e \in \mathcal{E}, \tag{3.7k}$$

$$\epsilon^e[0] = \epsilon_0^e, \quad \forall e \in \mathcal{E} \tag{3.7l}$$

$$0 \leq \ell^b[h] \leq d^b[h], \quad \forall h \in \overline{\mathcal{H}}, \quad \forall b \in \mathcal{B} \tag{3.7m}$$

$$(\kappa^s)^m \leq g^s[h] \leq a^s[h], \quad \forall h \in \overline{\mathcal{H}}, \quad \forall s \in \mathcal{S}^c \tag{3.7n}$$

$$0 \leq g^s[h] \leq w^s[h], \quad \forall h \in \overline{\mathcal{H}}, \quad \forall s \in \mathcal{S}^w. \tag{3.7o}$$

We note that the outcomes of the resulting *LP* cannot reflect the impacts of the *ESR* minimum discharge/charge capacities. In actual simulations, the discharge outputs (charge loads) that fall below the minimum charge $(\kappa_\ell^e)^m$ (discharge $(\kappa_g^e)^m$) capacities can be approximated by simply rounding them to either 0 (in which case, such *ESR*s would be considered idle) or said

minimum discharge (charge) capacities, whichever is closer. We found that the proposed relaxation proved effective in the case studies reported in section 4, as there were very few hours for which such rounding was necessary. We also note that the use of the relaxed *SOP* is crucial in actual implementations of the stochastic simulation approach due to the sheer number of *SOP*s that need to be solved.

An associated procedure to reduce the computational burden is to systematically "warm-start" the relaxed *SOP*s [40]. The basic idea of a "warm start" is to provide the simplex algorithm used to solve the relaxed *SOP* with a "good" initial solution, i.e., a solution that is "close" to the desired optimal solution. The provision of such a "good" solution may reduce considerably the number of simplex pivots required to reach the optimal solution, thereby reducing the computational time requirements. In our approach, we make extensive use of our finding that the optimal solution to the relaxed *SOP* for a given day j is generally "close" to that of the relaxed *SOP* for day $(j-1)$, as the patterns of the demands, conventional generation available capacities, *ESR* operations and renewable resource outputs do not necessarily change much (or rather, do not change too much) when shifting the optimization period one day forward. Thus, to solve the relaxed *SOP* for day j, we provide our *LP* solver engine with an initial solution that is simply the solution to the relaxed *SOP* for day $(j-1)$. Our extensive testing shows that a reduction of 35% in simulation time is, typically, obtained with "warm start".

Another step in the improvement of the computational tractability is the judicious selection of the number of simulation periods to be simulated. We take advantage of the fact that several weeks in a season have similar load shapes and wind patterns, and that certain resources are scheduled for planned outages in view of maintenance operations. In such cases, we select

an appropriate representative week among them for simulation and weigh its results in the study period by the number of weeks it represents. In this way, we reduce the number of simulation periods to be run to cover the entire study period, thereby cutting down the computational efforts. Typically, for regions with four distinct seasons, 14-18 representative weeks suffice to cover the entire annual simulation, and so the overall simulation time is cut by about a third.

We also have studied the application of a wide range of *variance reduction techniques*. Our findings indicate that only the control variate technique [31], p. 57, is effective in bringing about significant variance reduction. The use of the hourly aggregated available generation capacity, i.e., the sum of conventional resource, *ESR* and wind available capacities, as a control variate in each hour h can reduce computing times significantly for some of the metrics, in particular, the economic measures. For example, we have seen a 50% reduction in the evaluation of the average hourly total wholesale payments in the extensive testing we performed. On the other hand, the control variate scheme performs poorly in the evaluation of the reliability indices due to the weak correlation observed in practice among the control variate and the hourly total unserved energy. Such a result follows from the rarity of loss of load events. Consequently, the random variable representing the hourly total unserved energy is, in an arbitrary hour, very much akin to a constant equal to 0, save for the few positive outcomes – each with very low probability of occurrence – that quantify the unserved energy in the rare loss of load event cases. To put things in perspective, if one computes the correlation coefficient between a *r.v.* such as the hourly aggregated available generation capacity and a *r.v.* that is essentially equal to 0 – such as the hourly total unserved energy – the correlation coefficient will be nearly 0.

Experimental results are in line with this intuition: computed correlation coefficients among the hourly aggregated available generation capacity (the control variate) and the hourly total unserved energy (the random variable of interest) are very close to 0 in all hours, which is not practical for the control variate scheme that requires that the control variate and the random variable of interest be strongly correlated. We also make use of the Latin Hypercube Sampling (LHS) technique in the systematic generation of the random numbers needed to sample the multivariate probability distributions of our input *r.p.*s. The application of the technique is along the lines of [41]. Our experience indicates, however, that the LHS technique does not significantly contribute to the variance reduction of our estimates and, consequently, to savings in the overall simulation time.

We obtain a significant improvement of the method's computational tractability with the parallelization of the simulation of each representative week on dedicated cores/computers. In this way, the overall simulation time is dramatically reduced; indeed, the time reduction to essentially a single simulated week becomes possible whenever there are as many computers/cores as the number of representative weeks. We can take further advantage of parallelization from the fact that the simulation runs are statistically independent of one another. As such, we also parallelize the construction of the *s.p.*s. Such parallelization can additionally reduce the overall computation times, with the reduction depending on the number of dedicated cores available. As a result, the parallelization of the simulation runs associated with each representative week on a machine with X cores will divide the simulation time by X.

3.5 Summary

The simulation approach developed in this chapter incorporates the random processes introduced in chapter 2 into the framework of an independent Monte Carlo simulation. The core idea is to create, for each simulation run, statistically independent sample paths of the input random processes for use in the emulation of the hourly DAMs. While a sample path itself is representative of the spatial and temporal correlations characterizing the random variables of its input random process, the statistical independence of such a sample path – with respect to those drawn for other simulation runs – ensures that each output random process sample path is statistically independent from those constructed via other simulation runs. It is then possible to evaluate the statistical reliability of the hourly sample means of any given output random process in order to test the Monte Carlo simulation convergence of such a particular output on an hourly basis.

The chapter also presents various techniques aimed at lessening/dividing the computational burden associated with the execution of the multiple simulation runs necessary to ensure the simulation convergence or, as is the case with variance reduction techniques, reducing the necessary number of such simulation runs. Effective methods for improving the tractability of the simulation approach notably include the parallelization of each independent simulation run, the warm-start of the linear program used as a relaxation to the SOP problem, the use of representative weeks and – albeit more delicate to implement – the deployment of the control variate technique.

In the next chapter, we illustrate the broad capabilities of the stochastic simulation approach with a variety of case studies aimed at investigating the economic, reliability and emission variable effects of power systems with

integrated wind resources and *ESR*s.

CHAPTER 4

ILLUSTRATIVE CASE STUDIES

4.1 Overview of the Test Systems and Case Studies

We performed extensive testing of the simulation approach on various test systems to study a broad range of applications, including resource planning, production costing issues, transmission planning, environmental assessments, reliability and policy analysis. We illustrate the application of the approach with four representative sets of studies performed on modified *IEEE* 118-[42] and *WECC* 240-bus systems [43]. The first study assesses the impacts of deepening wind penetration on the economic, reliability and emission variable effects of the modified *WECC* 240-bus system with/without integrated *ESR*s; the second investigates the ability of a combination of wind and storage resources to replace - from purely a system reliability perpective - conventional resources in the modified *WECC* 240-bus system; the third examines the impacts of *ESR* siting on transmission utilization and the economics of a load center in the modified *IEEE* 118-bus test system; and the fourth evaluates the economic impacts of the explicit representation of ramping requirement under various wind penetrations in the modified *IEEE* 118-bus test system.

The studies performed on the *WECC* 240-bus system use scaled load data for the year 2004, offer data based on marginal cost information [43] and 3 years of historical wind data from the *WECC* geographic footprint [1]. In

these case studies, we scale the load data so that the annual peak load is 81,731 *MW*. The 902 conventional generation units of the test system have a total nameplate capacity of 96,443 *MW*. Each conventional resource is modeled as a 2-state unit with its own failure/recovery rate. The system further incorporates 4 wind farms at distinct Californian locations. The total wind nameplate capacity amounts to 13,600 *MW* (unless otherwise specified), about 16% of the annual peak load, and is equally distributed among the 4 wind farms. We use for these farms the wind turbine characteristics, including power curves, described in the *NREL* wind integration studies [1]. The storage resources are specified on a case-by-case basis in each study.

For the *IEEE* 118-bus test system, we use scaled *ISO* load data for the year 2007 [44] and historical wind data from the *ISO* geographic footprint [1]. We scale the load data so that the annual peak load is 8,300 *MW*. The 99 conventional generation units of the test system have a total nameplate capacity of 9,914 *MW*. Each conventional resource is again modeled as a 2-state unit with its own failure/recovery rate. The system also incorporates 4 wind farms, whose wind turbine characteristics, including power curves, are collected from *NREL* wind integration studies [1]. The aggregated nameplate capacity of wind power amounts to 2,720 *MW* (unless otherwise specified), about 30% of the annual peak load, and is equally distributed among the 4 wind farms. The storage resources are also specified on a case-by-case basis in each study.

In all case studies, we assume that each buyer bids his load as a *fixed* demand in each hourly *DAM*. Owing to the fact that wind power has no fuel cost, we assume that wind power is offered at 0 *$/MWh* in each hourly *DAM* throughout the simulation period. For each study, we limit our analysis to a single year in order to focus on the insights into the nature of the

results obtained. Taking into account the seasonality effects, as well as the maintenance schedules for the conventional generation units, we select 16 representative weeks for the simulation periods to quantify the variable effects over the 52 weeks of the year. We perform a unit commitment for every one of the 16 representative weeks so as to maintain the desired reserve margins (i.e., conventional and – if applicable – storage capacity in excess of the weekly peak load in percentage). We also note that, for synthesis, all chronological plots are done over the "average week of the year", for which the hourly values are averaged over all the representative weeks of the year, with weights equal to the number of actual weeks represented by each represented week.

For the test system, our extensive numerical studies indicate that beyond 100 simulation runs, there is too little improvement in the statistical reliability of the economic and emission metrics to warrant the extra computing time required for the execution of additional simulation runs. On the other hand, the computation of the reliability metrics required about 500 simulation runs, owing to the fact that our test system is relatively reliable and the loss of load events constitute rare occurrences. In terms of computational tractability, our test results indicate that the computational time requirements of running our case studies on the modified *WECC* 240-bus system are about 4 times higher than those of running analogous case studies on the *IEEE* 118-bus test system. These results must be analyzed in light of the fact that our modified *WECC* 240-bus has twice as many buses, 2.4 times as many transmission lines and about 10 times more conventional generation units whose cycles of failures/recoveries we simulate than the *IEEE* 118-bus system.

4.2 The Economic, Reliability and Emission Impacts of Deepening Wind Penetration in Power Systems with/without Integrated *ESRs*

In the first case study, we examine the impacts of integrated *ESR*s on the modified *WECC* 240-bus system under deepening wind penetration: from 0 *MW* total wind nameplate capacity in the base case to 13,600 *MW*, in 3,400 *MW* increments. The total wind nameplate capacity is allocated in equal quantities among 4 wind farms at distinct locations. To gain insights into the impacts of the integrated *ESR*s on the variable effects, we evaluate each wind penetration case with and without the *ESR*s. In the no storage cases, the supply-side resources consist of the system conventional generation units and the 4 wind farms, while operations use a 15 % reserves margin provided solely by the conventional units. In the storage cases, the system sports, in addition to the resource mix of the no storage cases, 5 identical storage units, each with 400 *MW* capacity, 4,000 *MWh* storage capability and a round-trip efficiency of 0.9. The 15 % reserves margin is met by both the conventional units *and* the storage units. We provide in Fig. 4.1 a plot of the expected hourly storage charge load/discharge output for one of the *ESR*s, and in Fig. 4.2 plots of the expected hourly values of what we call, for convenience, the *system marginal prices* (*SMP*s) – the weighted averages of the *LMP*s over all the system nodes, with weights equal to the cleared demands.

The results indicate that the *ESR*s tend to charge (discharge) during the low-load (peak-load) hours when the electricity prices are low (high). The *SMP* plots further show that the *ESRs* not only favorably impact the peak-load hour prices, they also reinforce the benefits brought about by integrated wind resources. We note from the plots in Fig. 4.3 and Fig. 4.4 that, as

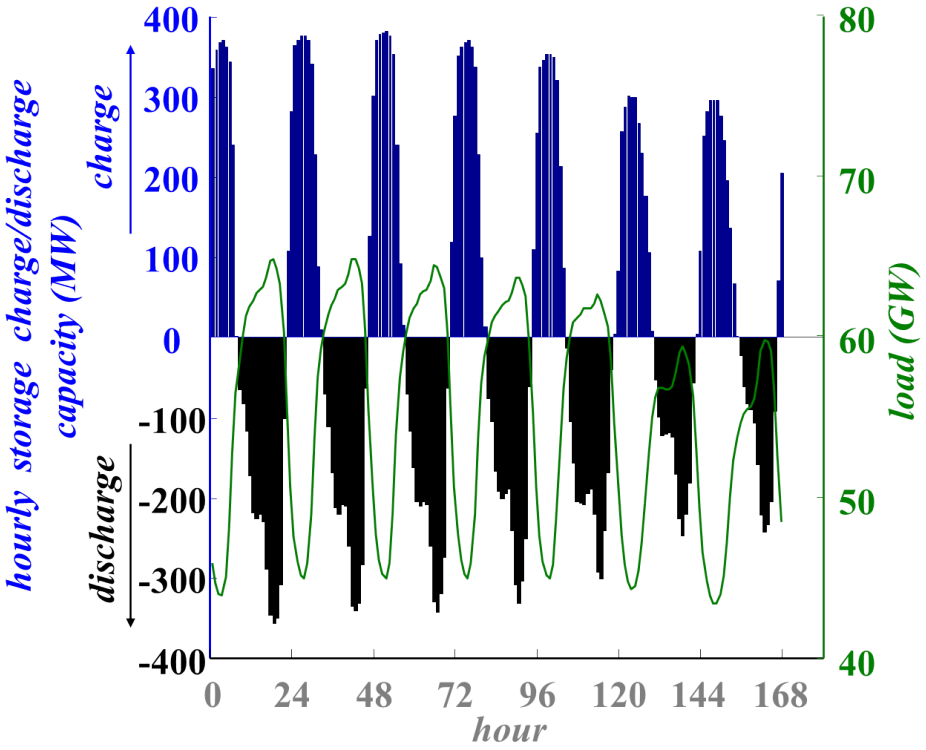

Figure 4.1: Expected hourly storage operations

the wind penetration deepens, the expected hourly total wholesale purchase payments and CO_2 emissions are reduced.

Significant improvements in the system reliability indices are shown in Fig. 4.5 and Fig. 4.6. These plots also make plainly clear that these reductions and improvements are characterized by diminishing returns as the wind penetration deepens. Such results are representative of the ability of the *ESR*s to attenuate, to some extent, such diminishing returns.

Overall, storage works in synergy with wind to drive down further wholesale purchase payments and improve system reliability. On the other hand, CO_2 emissions are insignificantly affected by the integration of a storage unit. We attribute this result to the fact that, in a system where the nameplate

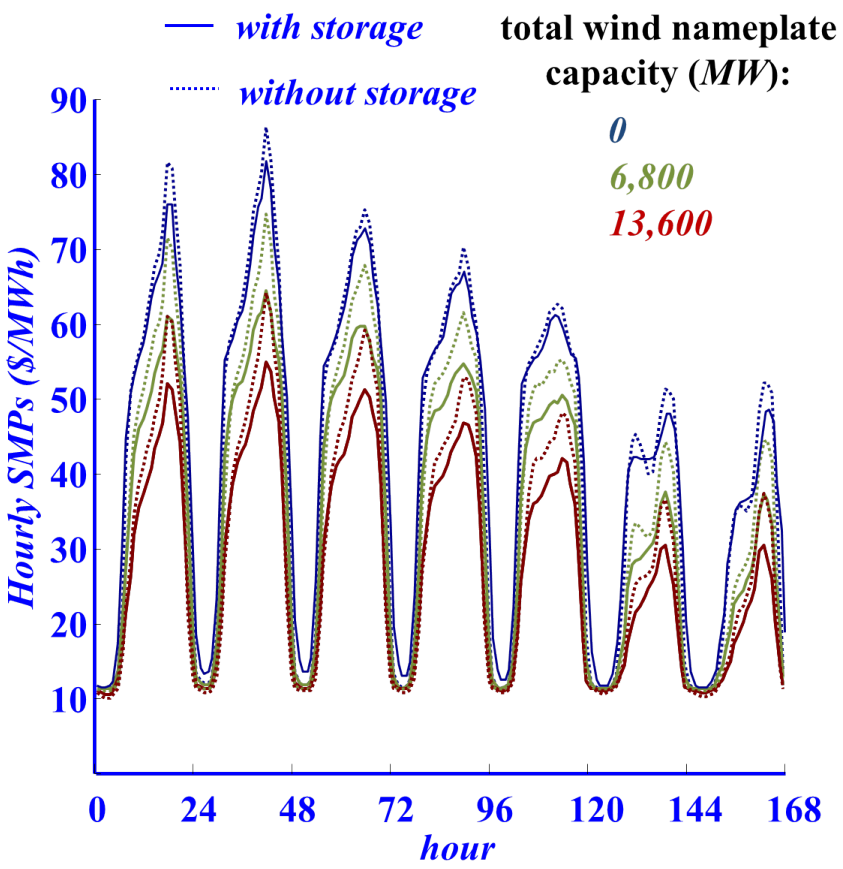

Figure 4.2: Expected hourly *SMP*s

wind capacity does not exceed the system base load, CO_2 emissions depend largely on the relative utilization of the various fossil-fuel fired units, as affected by the charge/discharge cycles of the *ESR*s. In this particular case, the reductions in CO_2 emissions caused by the *ESR* displacement of polluting conventional resources during the peak-load hours are about the same as the increases in CO_2 emissions due to *ESR* charging during the low-load hours.

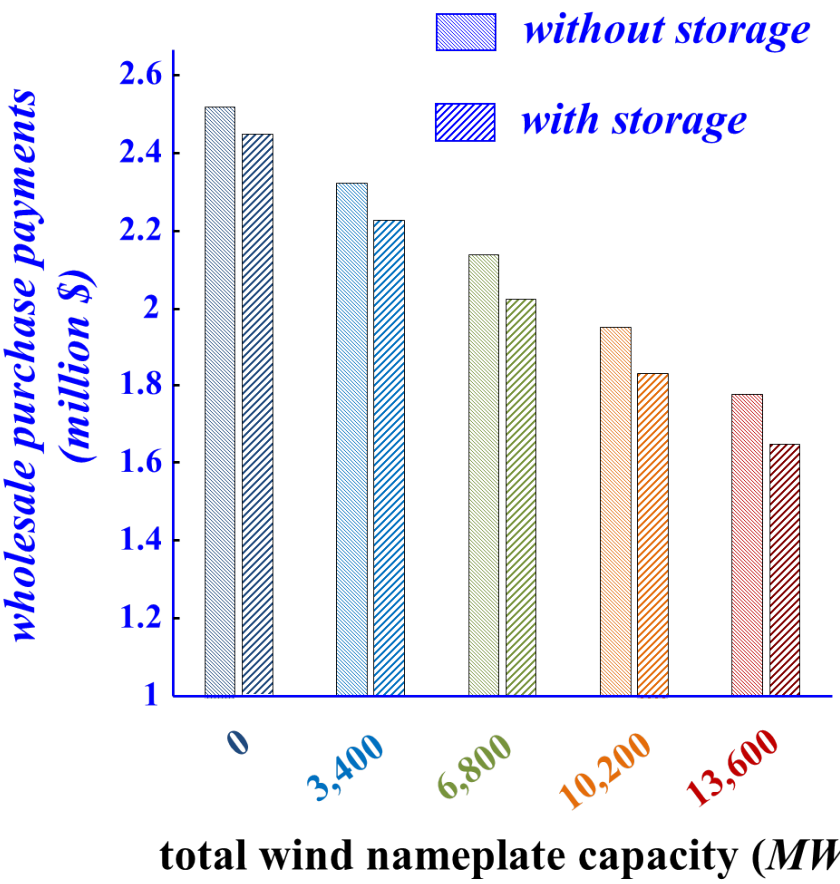

Figure 4.3: Average hourly total wholesale purchase payments; all values are averages over the hours of the year

4.3 Ability of a Combination of Wind and Storage Resources to Replace Conventional Resources from a Pure System Reliability Perspective

In the second case study, we investigate the extent to which a combination of wind and *ESR*s may replace conventional resources from a purely system reliability perspective in the *WECC* 240-bus system. For reference, we also provide the results of the same case study with no *ESR*s. The base case with no wind and no *ESR*s evaluates the system *LOLP* and *EUE* with a 15 % system reserves margin. In all the other cases, the conventional resource mix

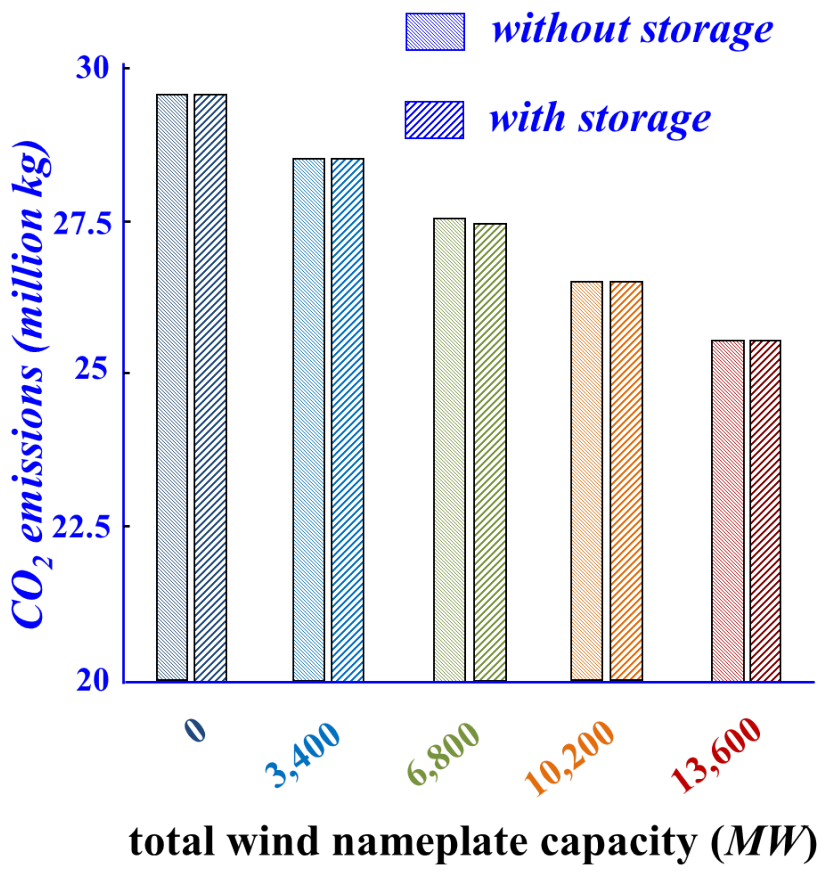

Figure 4.4: Expected hourly total CO_2 emissions; all values are averages over the hours of the year

is supplemented by 4 wind farms – with a total nameplate capacity of 13,600 MW, i.e., about 16 % of the annual 81,731 MW peak load – and 5 identical storage units as in the first study set. In these cases, the reserves are provided by the conventional *and* ESRs (where applicable) and we examine the impacts of progressively retiring some conventional resources, thus decreasing reserves margin levels. We provide in Fig. 4.7 and Fig. 4.8 the annual $LOLP$ and EUE values, respectively, as functions of the system reserves margin levels.

The sensitivity results without ESRs indicate that the 13,600 MW of installed wind capacity can replace roughly 4 % of the weekly peak loads, on

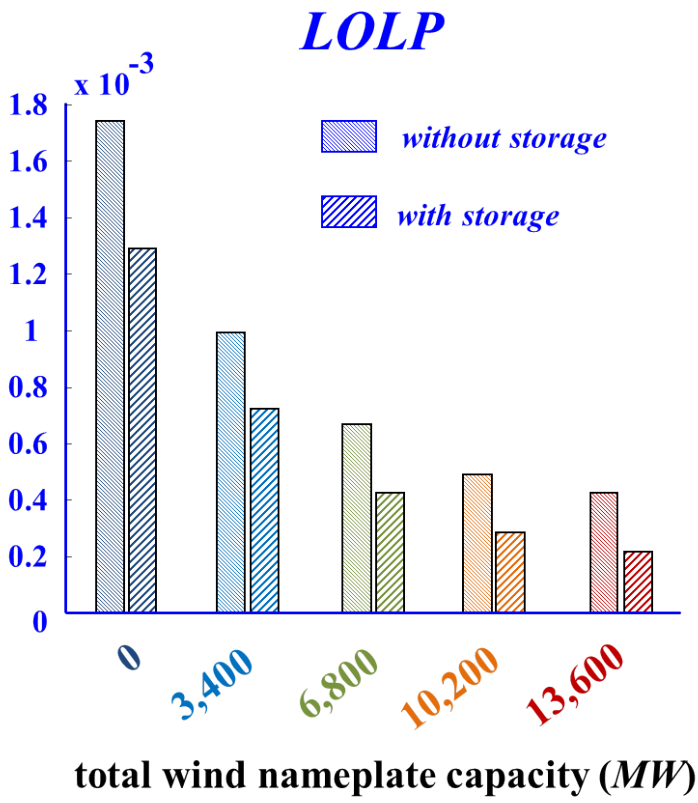

Figure 4.5: Annual LOLP

average over the year, in terms of retired conventional generation capacity, that is about 3,000 *MW*. With the integrated *ESR*s, and all other conditions unchanged, the *LOLP* results indicate that another half percent can be replaced, which corresponds to an additional 400 *MW* of retired conventional generation capacity. We note that, as the reserves are provided by the conventional *and ESR*s, these additional 400 *MW* represent the added benefits, from a purely reliability perspective, of combining wind and storage resources.

While the wind resources by themselves had a firm capacity of about 22 % of their total nameplate capacity, the integration of 2,000 *MW* of storage capacity raised the wind resource firm capacity by an additional 3 % of the total wind nameplate capacity. This result indicates that wind and *ESR*s

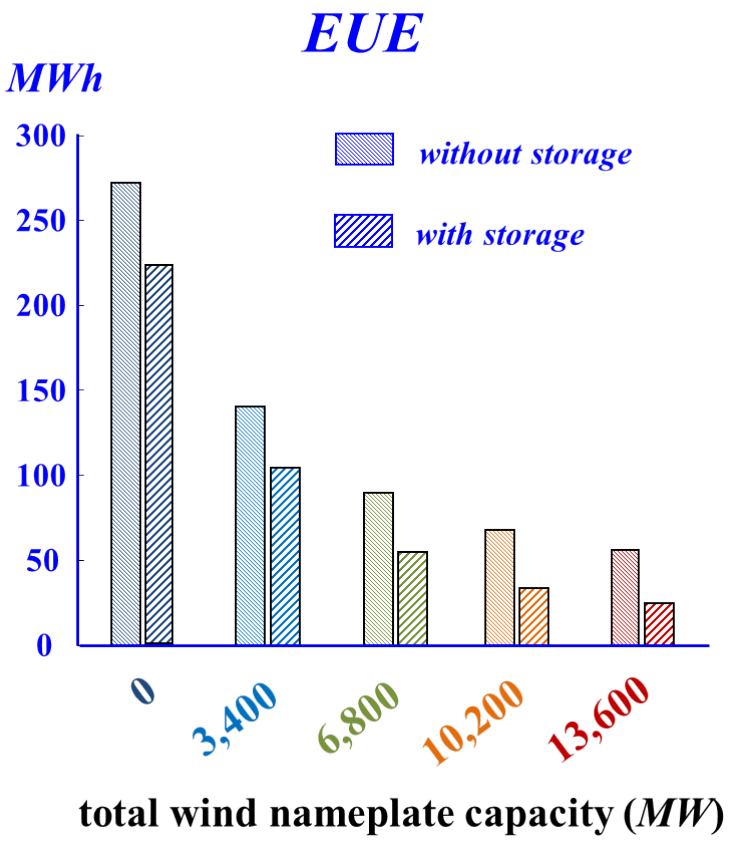

Figure 4.6: Annual EUE

can work synergistically to improve system reliability.

4.4 Impacts of *ESR* Siting on Transmission Utilization and Economics at a Load Center

The third case study pinpoints the ability of the simulation approach to study congestion impacts. We examine the impacts of *ESR* siting on transmission utilization and the economics of node 59, the most heavily loaded bus in our modified *IEEE* 118-bus test system. We present sensitivity cases that involve the siting of 4 identical *ESR*s – each with 200 *MW* capacity, 2,000 *MWh* storage capability and a round-trip efficiency of 0.9 – as the *ESR*s are successively further removed from bus 59. The total *ESR* capacity accounts

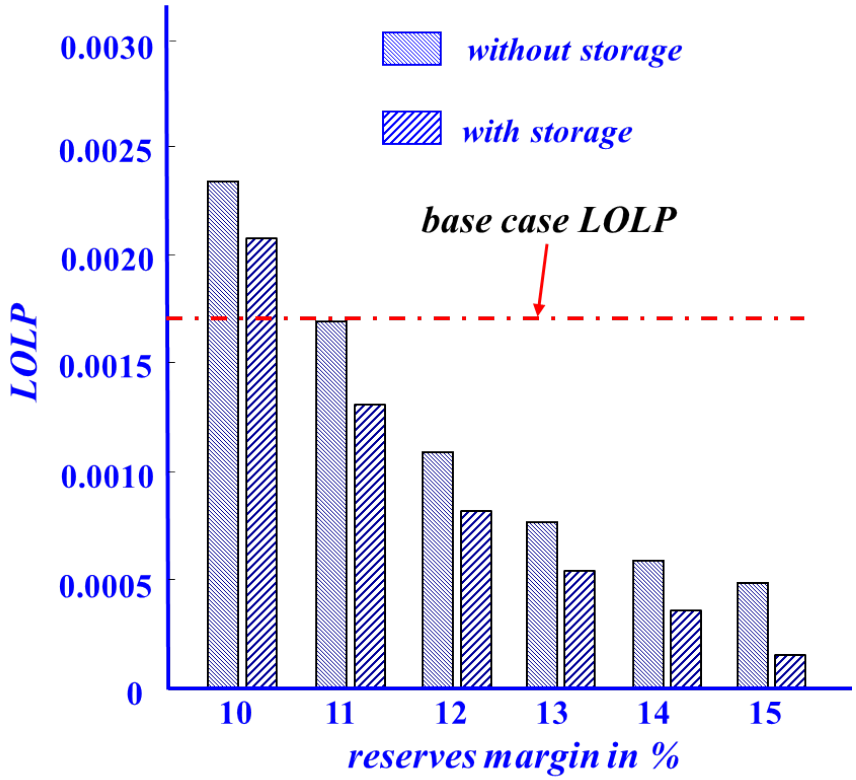

Figure 4.7: Annual $LOLP$ versus system reserves margins

for about 10 % of the annual peak load. For reference, we provide a base case with no integrated ESRs. In the first subcase, all the 4 ESRs are located at bus 59. In each subsequent subcase, the ESRs are sited one more node removed from bus 59, such that in the 4th subcase, all ESRs are 3 nodes away from bus 59. Figure 4.9 depicts the locations of the 4 ESRs in the $IEEE$ 118-bus test system network for each subcase.

We provide in Fig. 4.10 plots of the expected hourly total congestion rents along with the system load, while Fig. 4.11 highlights what we have identified to be a congested transmission path, from a major generation source node with 2 nuclear 400 MW units to the major load center at bus 59.

The congestion rent plots in Fig. 4.10 indicate that ESR operations cause congestion during the low-load hours, especially so the closer to bus 59 the

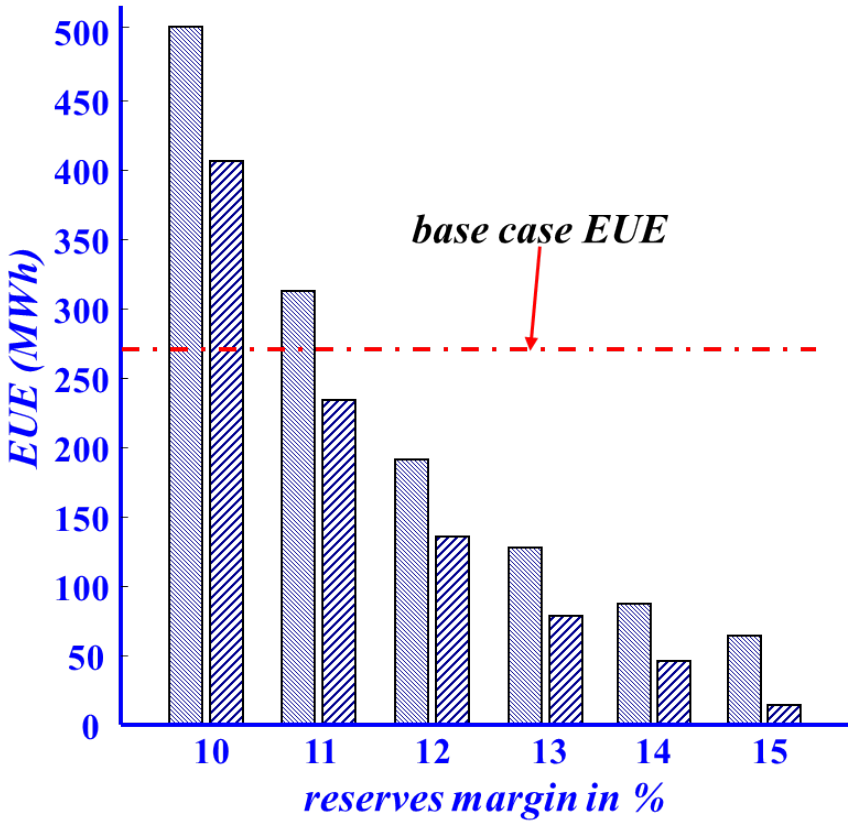

Figure 4.8: Annual *EUE* versus system reserves margins

*ESR*s are sited. We provide in Fig. 4.12 plots of the expected hourly *LMP*s at bus 59 that incorporate the impacts of such congestion.

For each siting subcase, the congestion rents are clearly reflected in the bus 59 *LMP* and particularly so during the low-load hours. These plots further indicate the influence of siting the *ESR*s on the decreases (increases) of bus 59 *LMP* during the high-load (low-load) hours due to *ESR* discharge to displace more expensive conventional resources (charge). The observed congestion leads to an examination of effective steps to reduce the congestion rents. For example, the increase of the total transmission capacity of the path (depicted in Fig. 4.11) by 100 % results in the elimination of the congestion and in virtually identical *LMP*s for each siting subcase, as shown in Fig. 4.13.

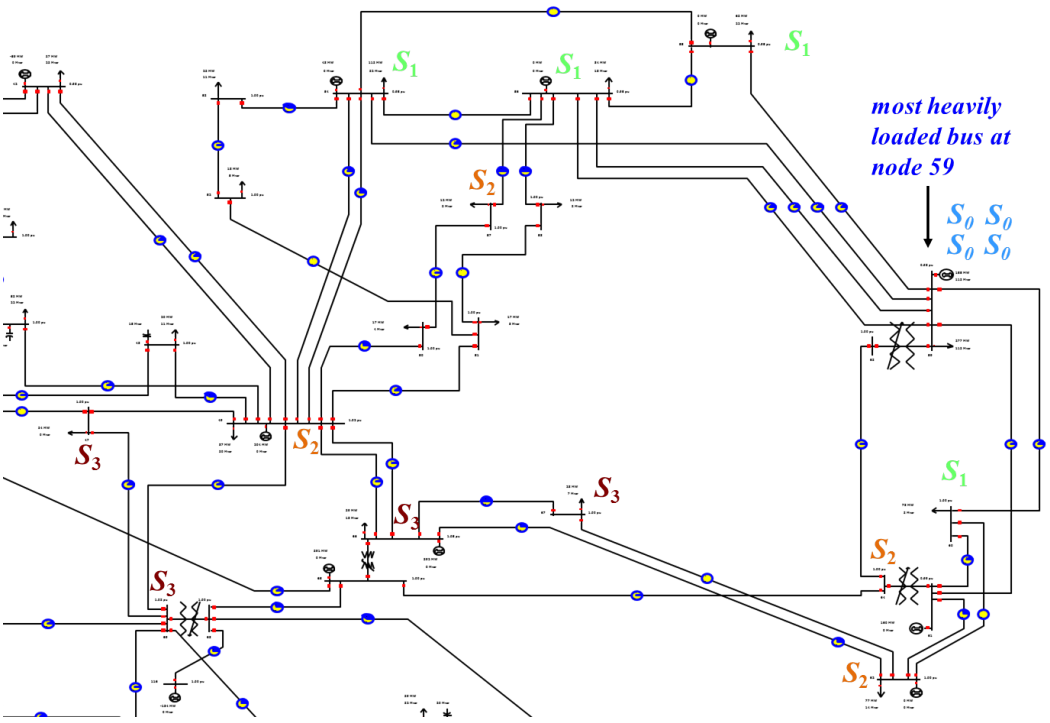

Figure 4.9: *ESR* locations in the *IEEE* 118-bus test system network for each subcase: each letter "S" represents an *ESR* while the sub-index denotes the remoteness in terms of nodes removed from bus 59

The results also indicate that, in this particular case study, it is best to locate the *ESR*s 3 nodes away from bus 59 in order to avert the transmission path congestion and the resulting raise in bus 59 *LMP*. Indeed, the curves in Fig. 4.13 are essentially the same as the curve in Fig. 4.12 representing the evolution of bus 59 *LMP* before the reinforcement of the transmission path and when the *ESR*s are 3 nodes removed from bus 59. Overall, this third case study suggests that the siting of *ESR* can have significant impact on the network congestion patterns and, consequently, on the *LMP*s.

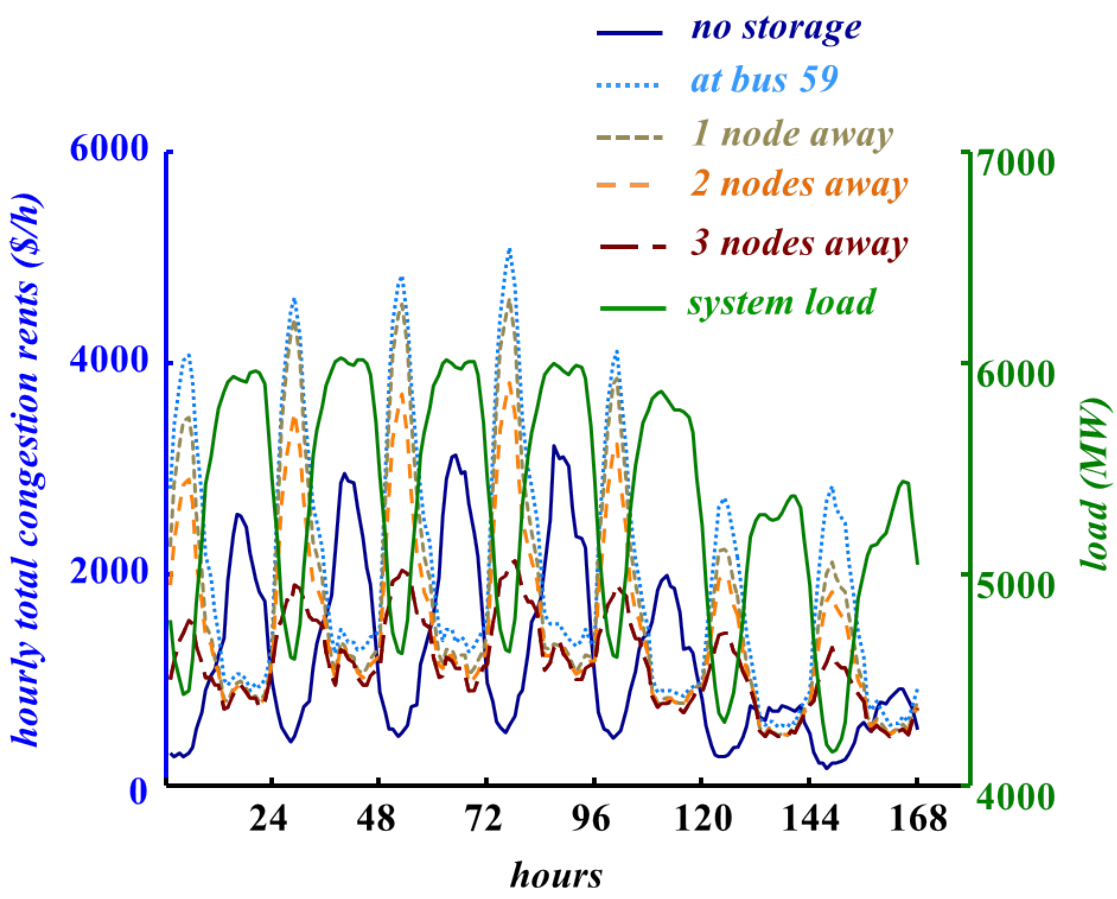

Figure 4.10: Expected hourly total congestion rents and system load

4.5 Explicit Ramping Requirements Impacts on Conventional Generation Resources

We perform sensitivity studies in the *IEEE* 118-bus test system to quantify the economic impacts of the explicit representation of ramping requirement at the *DAM* level under deepening wind penetrations: from 0 *MW* total wind nameplate capacity in the base case to 2,720 *MW*, in 680 *MW* increments. For each case, we run two simulations: one with the impacts of wind power output variability neglected for the estimation of ramping requirements and another with the ramping requirements for wind variability

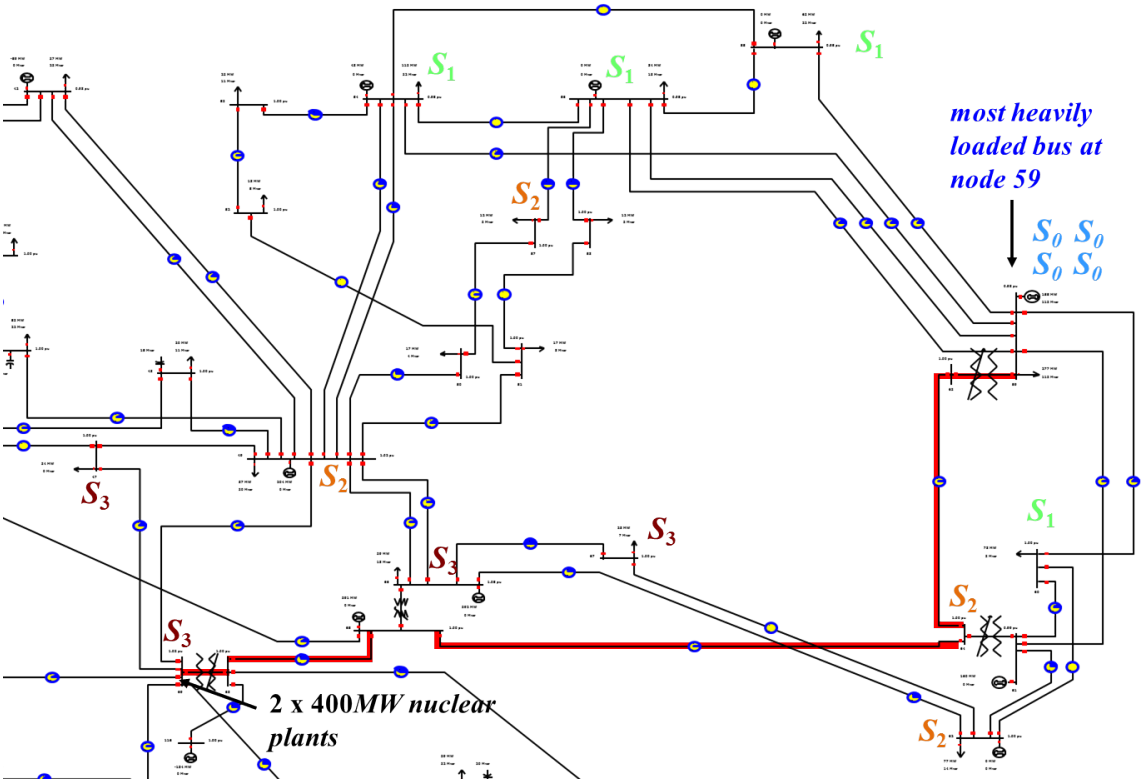

Figure 4.11: Section of the 118-bus system near the load center with the identified congested path in bold line

explicitly represented.

We use the average total wholesale purchase payments as a metric to evaluate the system-wide economic impacts of incorporating ramping requirements into the *DAM*s. Fig. 4.14 shows the duration curves of the expected hourly total wholesale purchase payments for the various cases investigated, while Fig. 4.15 exhibits the average values of each duration curve in order to provide a more global and concise assessment of the economic impacts.

Results indicate that the incorporation of ramping requirements in the *DAM*s results in higher total wholesale purchase payments, especially so during the peak load hours, when the market clearing process must rely on more expensive conventional units to achieve power balance while meeting

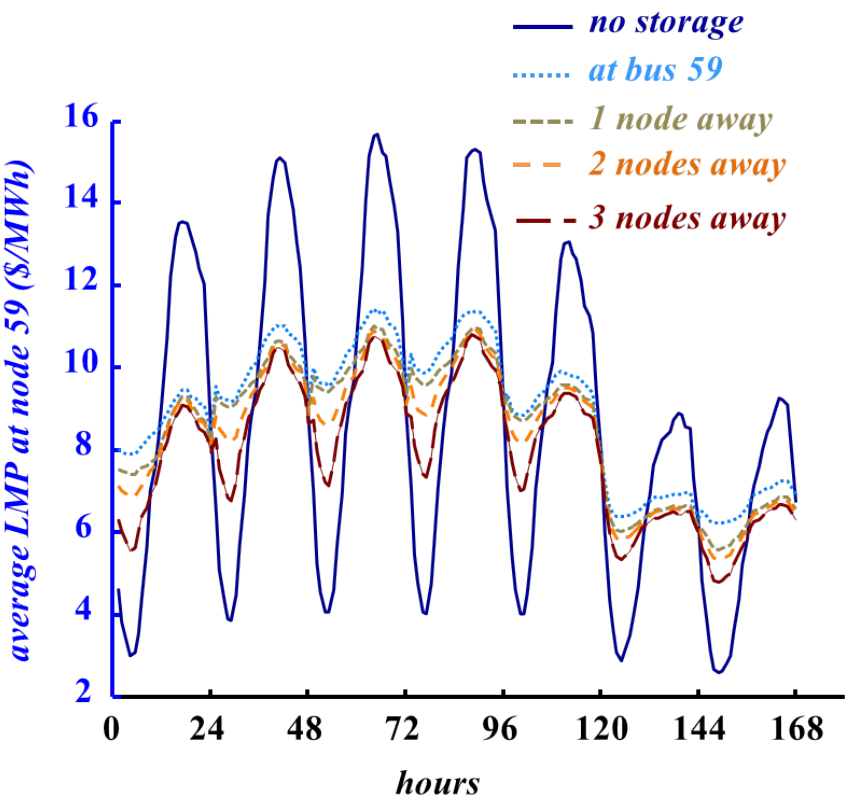

Figure 4.12: Expected hourly LMP at bus 59 before doubling the transmission capacity of the path

the ramping requirements. The stricter ramp requirements that arise as a result of deepening wind penetration are also shown to entail additional costs that reduce the benefits of wind integration. We also provide in Fig. 4.16 and Fig. 4.17 the duration curves for the expected hourly payments to generator 36 and the expected hourly LMP at its node, respectively. We note that generator 36 is a 155 MW coal/steam *base-loaded* unit. As such, its output is virtually unchanged throughout all the simulations and remains at its upper limit (unless in case of forced outage). Therefore, generator 36 cannot provide any up-ramp capability and the simulation results indicate (not shown here) that it is never called upon to provide down-ramp capability.

The plots show that the payments to generator 36 essentially follow the

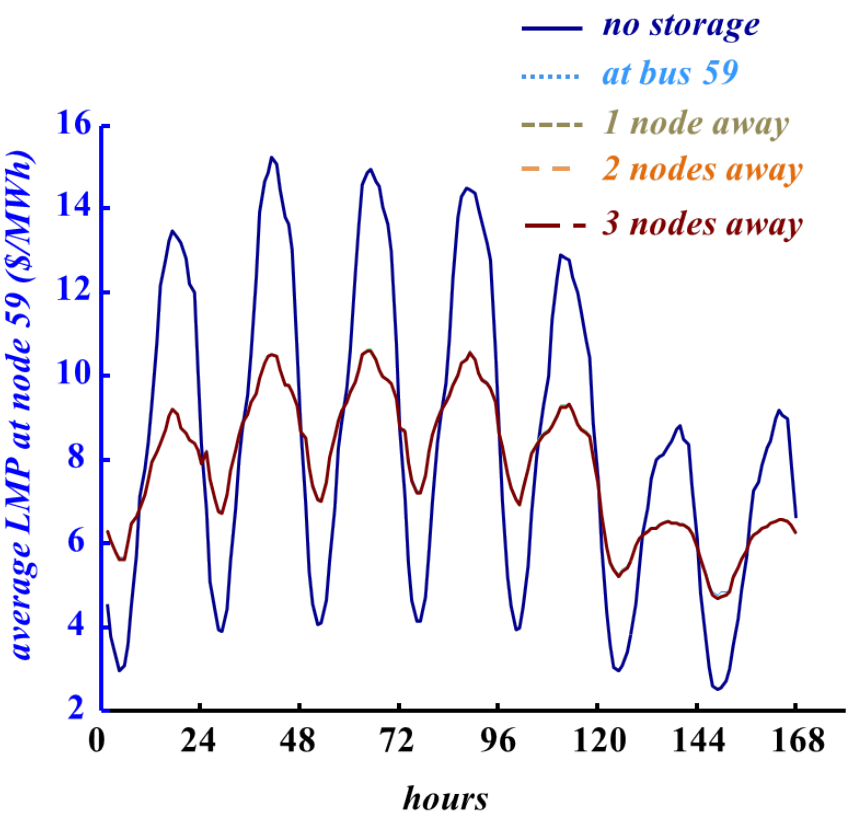

Figure 4.13: Expected hourly LMP at bus 59 after doubling the transmission capacity of the path

variations of the LMP at its node. We observe, again, that the explicit representation of stricter ramping requirements induced by the deepening penetrations of wind resources tend to limit the reductions in generator 36 LMP. However, the introduction of such stricter ramping requirements significantly drives up generator 36 LMP as compared to the case where the wind induced ramping requirements are not represented. As a result, generator 36 is paid a higher LMP for the MWh it sells in the energy DAM, even though it does not provide any ramp capability services. This study therefore suggests that the revenues of some generators may be significantly impacted by explicit ramping requirements, even if such generators do not

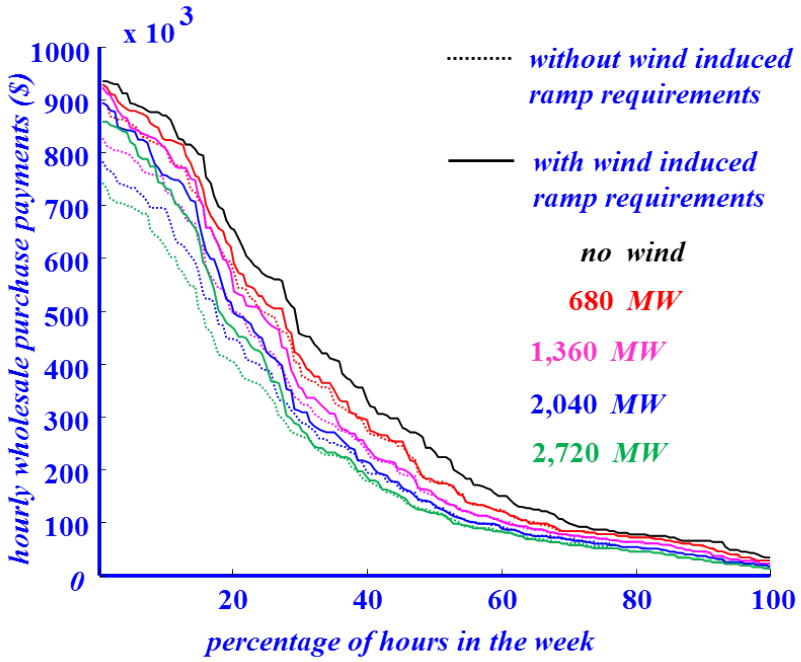

Figure 4.14: Expected hourly total wholesale purchase payment duration curves

provide any ramp capability services.

4.6 Summary

The chapter illustrates the simulation approach wide range of applications with four representative set of studies performed on the *IEEE* 118- and *WECC* 240-bus systems. The first study shows that the benefits of deepening wind penetration on the *WECC* 240-bus system economics, reliability and emissions can be further magnified by the operation of utility-scale *ESR*s deployed as system resources. The second study highlights the limited ability of wind resources to substitute – from purely a system reliability perpective – conventional resources in the *WECC* 240-bus system. It is shown, however, that *ESR*s can contribute to improving said ability when integrated into

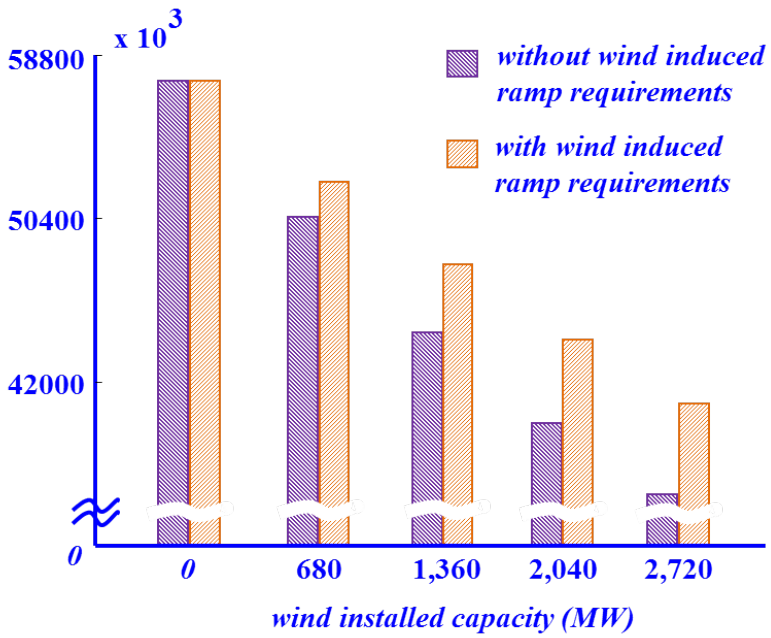

Figure 4.15: Expected total wholesale purchase payment

the system. The third study demonstrates that the siting of *ESR* in the *IEEE* 118-bus test system can have a significant impact on transmission utilization and on the electricity price at a load center. The fourth study demonstrates that the electricity prices can be significantly impacted by the enforcement of ramping requirement on conventional resources under various wind penetrations in the modified *IEEE* 118-bus test system.

These application studies point to the versatility of the simulation approach in estimating the impacts of various system conditions on the economic, reliability and emission variable effects.

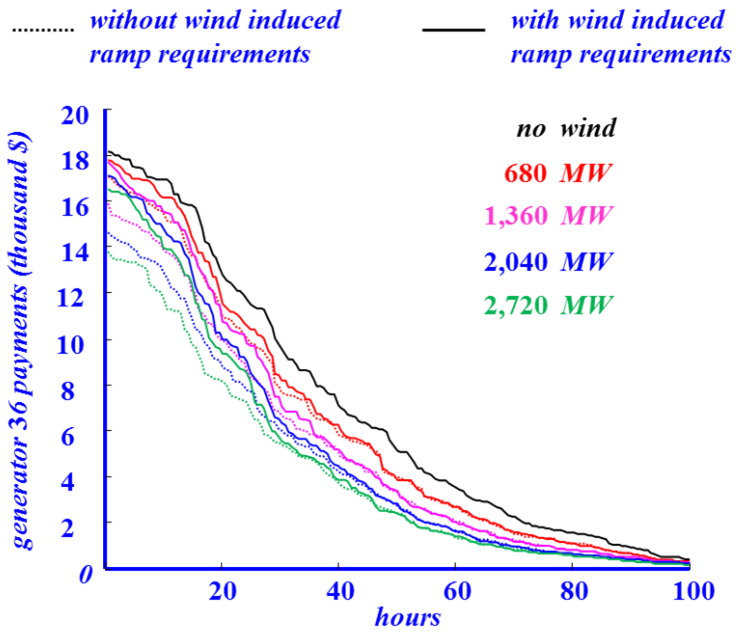

Figure 4.16: Expected hourly payments duration curve to generator 36

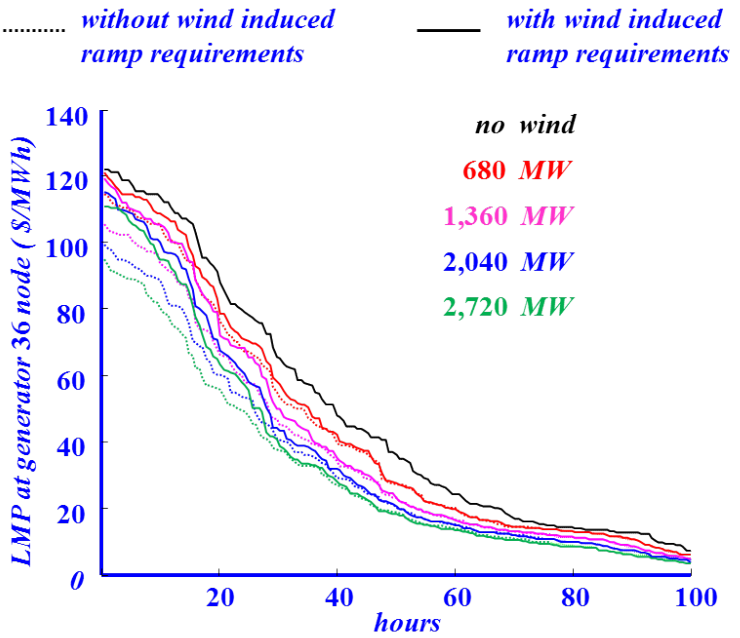

Figure 4.17: Expected hourly generator 36 *LMP* duration curve

CHAPTER 5

CONCLUDING REMARKS

In this chapter, we summarize the work presented in this dissertation and discuss some possible directions for future research.

5.1 Summary

In this work, we have introduced a comprehensive, practical stochastic simulation methodology for the quantification of the variable effects of power systems with a combination of variable energy resources, such as wind and solar, and utility-scale energy storage resources. Our approach also explicitly represents the ramping requirements on the conventional generation resources. Such requirements provide the system with the necessary flexibility to perform load following as increasing amounts of variable energy resources are being integrated into the grid. The attention to computational tractability allows the quantification of the power system variable effects to be performed over longer-term periods. The methodology can assess the impacts of integrated renewable and storage resources, as well as the influence of ramping requirements at the *DAM* level, on the variable economic, reliability and emission effects of the power system operating in a market environment, and with the full consideration of transmission constraints. The simulation approach explicitly represents the demands, renewable resource outputs and conventional generator available capacities with random

process-based models in order to capture the uncertain and time-varying behaviors of these sources of uncertainty, including the explicit consideration of the cross-correlations among the wind farms (buyers in the DAM) and the time correlations. An important aspect is that these models do not require any calibration or the use of complex transformations and thus are relatively straightforward to implement. We develop models for the energy storage resources and deploy the SOP solutions to optimally schedule their operations over multiple time periods, in coordination with the demands and the conventional/renewable resources. The SOP is specifically formulated to act as a DAM clearing mechanism capable of making coordinated dispatch decisions over multiple time periods and accounting for intertemporal constraints in the storage resource operations or the formulation of interhour ramping requirements. The ramping requirements are also adjusted based on the anticipated variations of the loads and renewable resource outputs. We make extensive use of Monte Carlo simulation techniques to systematically sample the random processes associated with the demands, renewable resource outputs and conventional generator available capacities and generate the corresponding sample paths. We use the realizations of these sample paths to formulate the offers and bids into each hourly market. We solve, in each day of a weekly simulation period, an SOP to emulate the clearing of the hourly transmission-constrained DAMs and schedule, concurrently, the ESR operations. We construct the market outcome sample paths from the SOP solutions and use them in the approximation of various metrics of interest. These metrics include the hourly expected locational marginal prices (LMPs), revenues of the generators, total payments made by buyers in the DAMs, congestion rents, the system-wide CO_2 emissions, ESR operations as well as the reliability indices $LOLP$ and EUE. The approach provides a

broad range of capabilities and is applicable to a wide array of planning, investment analysis and operational planning problems. Salient characteristics include the ability to allow the comparison of various resource mixes and network configurations and the ability to answer a broad spectrum of *what if* questions.

The representative results we present from the extensive studies performed demonstrate effectively the strong capabilities of the simulation approach. The results of these studies on modified *IEEE* 118- and *WECC* 240-bus systems clearly indicate that energy storage and wind resources tend to complement each other and this symbiosis reduces wholesale costs and improves system reliability. In addition, we observe that emission impacts with energy storage depend on the resource mix characteristics. An important finding is that storage seems to attenuate the "diminishing returns" associated with increased penetration of wind generation. The limited ability of integrated storage resources to enhance the wind resource capability to replace conventional resources from purely a system reliability perspective is evidenced in the studies presented. Some useful insights into the siting of storage resources are obtained and they indicate the potentially significant impacts of such decisions on the network congestion patterns and, consequently, on the *LMP*s. The explicit representation of ramping requirements on conventional resources at the *DAM* level contributes to drive the total wholesale purchase payments up. The increase is notably marked during the peak load hours, as the higher demand for energy makes it more difficult, hence costlier, to meet the ramping requirements. Higher levels of wind penetration result in increased ramping requirements, which in turn tend to reduce the benefits of wind integration. The stricter ramping requirements can potentially impact, often in a favorable way, the revenues of generators that do not even provide

any ramp capability services.

The development of the approach provides the first practical implement for the simulation of large-scale power systems with integrated renewable and storage resources. The importance of this tool becomes more pronounced as there is more attention given to energy storage resources as a result of the deepening penetration of renewable resources. Such developments create myriad opportunities for the effective deployment of the stochastic simulation methodology to provide the quantitative answers to a broad range of applications in planning, operational analysis, investment evaluation, policy formulation and analysis and to address various *what if* questions.

5.2 Possible Directions for Future Research

The analytical framework of the simulation approach is sufficiently general to allow the representation of various other resources, such as the active demand response resources, as well as the provision of different types of reserves products. In particular, the deepening penetration of intermittent, time-varying resources calls for the enforcement of more stringent ramping and reserve requirements in the day-ahead, hour-ahead and real-time markets, so as to secure enough capacity and ramping capability from the system conventional resources to effectively compensate for the fluctuations of time-varying resource outputs. The idea may be taken one step further, where flexibility markets would evaluate, from an economic standpoint and in order to meet the (net) load following and – at finer time scales – regulation requirements, the worth of flexibility services offered by fast-ramping generators or storage resources. Thus, future work may focus on extending the capabilities of the *SOP* so it can fully co-optimize energy and ancillary markets, including

those ancillary markets dedicated to the provision of system flexibility. The simulation approach could then be used to quantify the flexibility costs of mitigating the fluctuations of time-varying resource outputs. Ultimately, the *SOP* could be turned into a full unit commitment problem so the simulation approach can account for the conventional generator minimum up (down) times, as well as start-up and shutdown costs. Such enhancement, however, would come at the price of computational tractability, as mixed-integer programs are notoriously more difficult to solve than linear programs.

APPENDIX A

NOTATION

A.1 General Notation

For a generic real-valued variable r, we denote by:

$(r)^M$: the upper bound of variable r

$(r)^m$: the lower bound of variable r

r^* : the optimal value of decision variable r in the *SOP*

$\underline{r}^\dagger$: vector r transpose

$|\mathcal{R}|$: the cardinal of set $\mathcal{R}$

$i_{(r_1,r_2)}(.)$: indicator function of interval (r_1, r_2)

M : the number of simulation runs

A.2 Time in the Simulation

$[t]$: discrete time variable

$\mathcal{T} = \bigcup_i \mathcal{T}_i$: study period

$\mathcal{T}_i$: *ith* simulation period

$\mathcal{T}_i = \{h : h = 1, \ldots, H\}$: the set of subperiods h, i.e. smallest indecomposible unit of time, in a simulation period $\mathcal{T}_i$; in the proposed application of the approach, a subperiod is of duration one hour and $H = 168$

$\overline{\mathcal{H}} = \left\{h : h = 1 \ \ldots \ \overline{H}\right\}$: optimization period of the *SOP*

Δ : duration of a ramping event

A.3 Random Processes

Letter x (y) is used for demonstration purpose and refers to a generic stochastic process/random variable that could stand for any "input" ("output") random process/random variable. In terms of notation, what applies to x also applies to y.

$\underset{\sim}{X}$: random variable X

$\Omega_{\underset{\sim}{X}}$: sample space of $\underset{\sim}{X}$

x : a realization of random variable $\underset{\sim}{X}$

$x^{(j)}$: jth independent realization of random variable $\underset{\sim}{X}$ (i.e., the realizations are generated from *i.i.d.* $\underset{\sim}{X}$)

$\left\{\underset{\sim}{X}[h] : h \in \mathcal{T}_i\right\}$: discrete-time stochastic process defined for all subperiods $h \in \mathcal{T}_i$

$\{x[h] : h \in \mathcal{T}_i\}$: sample path of $\left\{\underset{\sim}{X}[h] : h \in \mathcal{T}_i\right\}$

$\Omega_{\left\{\underset{\sim}{X}[h]:h\in\mathcal{T}_i\right\}}$: sample space of $\left\{\underset{\sim}{X}[h] : h \in \mathcal{T}_i\right\}$

$\overline{\underset{\sim}{X}}$: sample mean estimator of $\underset{\sim}{X}$

$\overline{x}$: sample mean point estimate of $\underset{\sim}{X}$

$\mu_{\underset{\sim}{X}}$: expected (mean) value of random variable $\underset{\sim}{X}$

$\sigma_{\underset{\sim}{X}}$: standard deviation of random variable $\underset{\sim}{X}$

$\left\{\underset{\sim}{D}[h] : h = 1, \ldots, 168\right\}$: aggregated system load stochastic process

$\left\{\underset{\sim}{D}^b[h] : h = 1, \ldots, 168\right\}$: demand of buyer b stochastic process

δ^b : fraction of buyer b demand with respect to the aggregated system load $\forall h \in \mathcal{T}_i$.

$\left\{\underset{\sim}{\underline{V}}[h] \ : \ h = 1, \ldots, 24\right\}$: daily multi-site wind speed pattern stochastic process

$\left\{\underset{\sim}{\underline{W}}[h] \ : \ h = 1, \ldots, 24\right\}$: daily multi-site wind power output pattern stochastic process

$\mathfrak{I} = \{\iota : \iota = 1, \ldots, |\mathfrak{I}|\}$: the set of wind farm sites

$\underset{\sim}{V}^{\iota}[h]$ ($\underset{\sim}{W}^{s}[h]$): the random variable associated with the wind speed (power output) experienced (available) by (to) wind farm (seller) $\iota \in \mathfrak{I}$ ($s \in \mathcal{S}^{w}$) in hour $h = 1, \ldots, 24$

$\underline{\underset{\sim}{V}}[h] = \left[\underset{\sim}{V}^{1}[h], \ldots, \underset{\sim}{V}^{|\mathfrak{I}|}[h]\right]^{\dagger}$: the random vector of the multi-site wind speeds in hour $h = 1, \ldots, 24$

$\underline{v}[h]$: a realization of the multi-site wind speed random vector in hour $h = 1, \ldots, 24$

$\underline{\underset{\sim}{W}}[h] = \left[\underset{\sim}{W}^{1}[h], \ldots, \underset{\sim}{W}^{|\mathcal{S}^{w}|}[h]\right]^{\dagger}$: the random vector of the multi-site wind power outputs in hour $h = 1, \ldots, 24$

$\underline{w}[h]$: a realization of the multi-site wind power output random vector in hour $h = 1, \ldots, 24$

$\underline{\underline{v}}$: sample path of $\left\{\underline{\underset{\sim}{V}}[h] \ : \ h = 1, \ldots, 24\right\}$ rearranged into a supervector

$\underline{\underline{w}}$: sample path of $\left\{\underline{\underset{\sim}{W}}[h] \ : \ h = 1, \ldots, 24\right\}$ rearranged into a supervector

$\underset{\sim}{A}^{s}[t]$: available capacity of seller $s \in \mathcal{S}^{c}$ conventional generating unit at time t

$\hat{\underset{\sim}{A}}^{s}$: steady-state available capacity of seller $s \in \mathcal{S}^{c}$ conventional generating unit

$\mathfrak{d}_{j}^{s}$: jth derated capacity of seller $s \in \mathcal{S}^{c}$ conventional generating unit

$\mathfrak{p}_{j}^{s}$: probability of seller $s \in \mathcal{S}^{c}$ conventional generating unit to be in derated capacity state $\mathfrak{d}_{j}^{s}$

$\mathfrak{q}_{j}^{s}$: probability of seller $s \in \mathcal{S}^{c}$ conventional generating unit to be on forced outage

Ξ_{i}^{s} : the set of eligible states to which seller $s \in \mathcal{S}^{c}$ unit in state i may transition

$\breve{j}$: retained state to which the conventional unit is going to transition to

$\tau_{i \to \breve{j}}$: average duration of stay in state i

$\vartheta_{i \to \breve{j}}$: time-to-transition from state i to state j

$\underset{\sim}{U}$: system unserved energy random variable

A.4 Transmission Network (DC Power Flow Assumptions)

$\mathcal{N} = \{n : n = 0, 1, \ldots, N\}$: the set of network buses with bus 0 as the slack bus. We consider the network consists of $N + 1$ buses.

$\mathcal{L} = \{(i, j) : i \in \mathcal{N},\ j \in \mathcal{N},\ i \text{ and } j \text{ are connected}\}$: the set of transmission lines

$\underline{A}$: the reduced branch to node incidence matrix

$\underline{B}_d$: the branch susceptance matrix

$\underline{B}$: the reduced nodal susceptance matrix

$\underline{b}_n$: the column vector of the nodal susceptance matrix corresponding to bus n

$\underline{\theta} = [\theta_1, \theta_2, \ldots, \theta_N]$: the vector of power angle (excluding the slack bus power angle which is taken as 0)

$\underline{f} = \underline{B}_d\, \underline{A}\, \underline{\theta}$: vector of line flows

$\underline{f}^M$: the vector of transmission line thermal rating

$\underline{f}^m$: the vector of transmission line thermal rating in the opposite flow direction

$f^{(i,j)}$: the power flow on line (i, j)

A.5 *SOP*

$\mathcal{S}^w$: the set of wind farms that participate in the *DAM*

$\mathcal{S}^c$: the set of conventional generators that participate in the *DAM*

$\mathcal{S} = \mathcal{S}^w \bigcup \mathcal{S}^c$

γ^s : offering price of seller s

g^s : seller s unit output (decision variable)

$[\kappa^s]^M$: maximum capacity of seller s generating unit (wind farm)

$[\kappa^s]^m$: minimum capacity of seller s generating unit

$p_n^c = \sum_{s \in \mathcal{S}^c \text{ is at node } n} g^s$: the power injection at node n due to conventional unit generation

$p_n^w = \sum_{s \in \mathcal{S}^w \text{ is at node } n} g^s$: the power injection at node n due to wind farm generation

$\mathcal{B}$: the set of buyers in the DAM

β^b : buyer b willingness-to-buy

ℓ^b : buyer b demand (decision variable)

$p_n^d = \sum_{b \in \mathcal{B} \text{ is at node } n} \ell^b$: the power consumption at node n due to loads

$\mathcal{E}$: the set of storage units participating into the DAM

u_g^e : storage unit e discharge status variable (decision variable)

g^e : storage unit e output (decision variable)

$p_n^e = \sum_{e \in \mathcal{E} \text{ is at node } n} g^e - d^e$: the *net* power injection at node n due to storage unit e generation/consumption

$[\kappa_g^e]^M$: maximum discharge capacity of storage unit e

$[\kappa_g^e]^m$: minimum discharge capacity of storage unit e

η_g^e : discharge efficiency of storage unit e

$\epsilon^e[h]$: storage unit e stored energy level at the end of hour h

u_ℓ^e : storage unit e charge status variable (decision variable)

ℓ^e : storage unit e demand (decision variable)

$[\kappa_\ell^e]^M$: maximum charge capacity of storage unit e

$[\kappa_\ell^e]^m$: minimum charge capacity of storage unit e

η_ℓ^e : charge efficiency of storage unit e

$\eta^e = \eta^e_\ell . \eta^e_g$: round-trip efficiency of storage unit e

$\underline{\lambda}$: the vector of dual variables to the power balance constraints; interpreted as LMPs; the vector excludes λ_0 (LMP at the slack node)

The following market outcomes actually are hourly realizations of the associated random variables, which themselves are component of the associated stochastic process.

$\varsigma^{\mathcal{B}}[h]$: total wholesale purchase payments in subperiod h

$\varsigma^{\mathcal{S}}[h]$: total payments to the supply side in subperiod h

$k[h]$: congestion rents in subperiod h

$\nu[h]$: total CO_2 emissions in subperiod h

$u_n[h]$: unserved energy at node n in subperiod h

A.6 Ramping Requirements

ξ_n : the controllable load at node n

κ^s_+ : ramping up capability of seller $s \in \mathcal{S}^c$ unit

κ^s_- : ramping down capability of seller $s \in \mathcal{S}^c$ unit

APPENDIX B

A COMPARISON OF STOCHASTIC MODELING TECHNIQUES: THE KERNEL DENSITY ESTIMATION APPROACH VS. THE MARKOV CHAIN MODEL

In view of studying the impacts of wind integration in the long-run, many models for representing wind patterns have been proposed. Most models attempt to characterize the wind speed/power output as a stationary random process following a parametric distribution [16]. However, such models not only fail to represent wind as a pattern, or more precisely as a random process with memory, but also generally do not account for the correlations existing among multiple wind farms. In this study, we incorporate such considerations by assuming that the aggregated wind power output, that is, the instantaneous sum of the individual wind farm power outputs, is a random process with the Markov property [45], and we empirically build such a Markov chain based on the aforementioned assumption. We choose to model the aggregate wind power output for two reasons: on one hand, it constitutes the variable of interest in power system planning studies (as opposed to the wind speed which is only a precursor); on the other hand, by deriving the probability transition matrices from the time-series of the aggregated wind power output, we preserve the correlations existing among the multiple wind farm power outputs. However there is no guarantee that the aggregated power output as a random process actually possesses the Markovian property. To properly verify such hypothesis, we propose to assess how well a Markov chain built upon 2004 wind data will 'fit' the random process governing wind in year 2005. In essence, we aim at comparing two random processes, and that in

turn, entails the use of a metric dedicated to evaluating the closeness of two random processes. In this report we found out that one of the most adapted metrics for our problem was the Mahalanobis distance [46], which measures the distance of a sample path to a given distribution. We make use of such a metric to compare the performances of the Markov chain versus those of a Gaussian mixture model obtained by Kernel density estimation and the empirical probabilistic distribution of the aggregated wind power output in 2004. From there on, we derive results that allow us to conclude on the relative performance of the Markov chain with respect to the other models.

This study report contains four additional sections. In section B.1, we introduce the Markov chain model adopted for the representation of the aggregated wind power output over time. Section B.2 describes how the performance of the Markov chain and the other models are assessed via the use of Mahalanobis distance, and Section B.3 is devoted to the results of an application study aimed at assessing the capability of a Markov chain based on 2004 statistical data to fit year 2005 data. We conclude with a summary in section B.4.

B.1 The Markov Chain Model

In this section, we provide the general idea and assumptions behind the modeling of the aggregated wind power output as a Markov chain. Recall that the goal of the proposed modeling via Markov chain is the good representation of the aggregated wind power output as a random process. We start off by assuming that the aggregated wind power output (along with wind speeds) has daily patterns within each season of the year [47]. As such, we define for each season and any given day within it, a finite state-space Markov chain

that is non time-homogeneous over the subperiods of the day. In practice, we choose a time granularity commensurate with the available dataset and divide up the day into such subperiods. For each of those subperiods, we define as many discrete states of aggregated wind power output as desired. Such state definition must be able to cover the whole range of wind power output experienced in a given day over the whole dataset. Then, each day of data within a given season is considered to be a sample path for the random process just defined. By doing the statistics over each transition from a subperiod to the next, it is possible to establish the probability transition matrix between one of one subperiod to the next. As such, the Markov chain built upon such process is not time-homogeneous over the duration of one day, yet it is cyclostationary in the sense that statistically, all days within a season are the same and so is the random process – let us call it $\left\{\underset{\sim}{W}[h] \,:\, h = 1, \,\ldots\, , 24\right\}$ – hence defined.

We illustrate the concept by the example that follows: let us define a Markov chain for the aggregated wind power output for any day in a given season with a time resolution of one hour and eight discrete states. Figure B.1 displays how the seven states might be defined (given the sample path with highest aggregated wind power output), and Fig. B.2 provides a state diagram of the Markov chain.

Mathematically, the Kolmogorov equations yield the following state probability equations: let $A_{|h}$ be the probability transition matrix from states in hour h to states in hour $(h+1)$. More precisely $A_{|h} = \{a_{i,j|h}\}_{i,j=0\ldots7}$ where each entry of the matrix is to be read as $a_{i,j|h} = P\{\underset{\sim}{X}_{h+1} = x_j | \underset{\sim}{X}_h = x_i\}$. Also, let π_h be the state probability vector at hour h, then $\pi_h = [P\{\underset{\sim}{X}_h = x_0\}, P\{\underset{\sim}{X}_h = x_1\}, ..., P\{\underset{\sim}{X}_h = x_7\}]$. We then have the following relationship for all h such as h is an hour in the considered season:

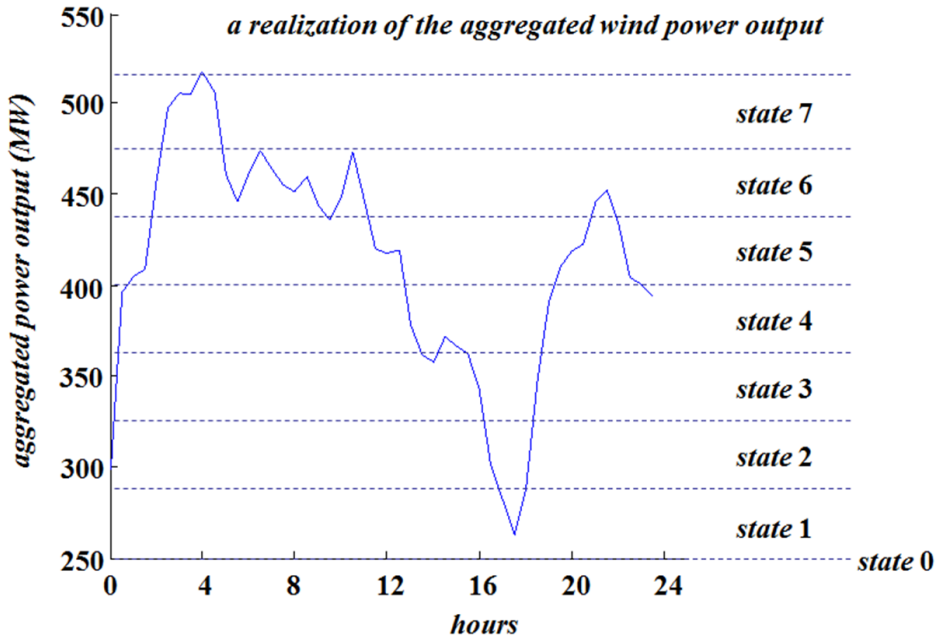

Figure B.1: Definition of the system state space

$$\pi_{h+1(\text{mod } 24)} = \pi_{h(\text{mod } 24)} A_{|h(\text{mod } 24)} \tag{B.1}$$

where the notation (mod 24) indicates modulo 24. As a matter of fact, since the Markov chain is assumed to be the same for every day in a given season, one may well initialize the chain at hour 1 of a given day and let the model runs for multiple days. For example, the state probability vector of hour 27, π_{27}, may be computed using (B.1) after initialization of the system in hour 1:

$$\pi_{27} = \pi_1 \left(\prod_{h=1}^{24} A_{|h} \right) A_{|1} A_{|2} A_{|3}. \tag{B.2}$$

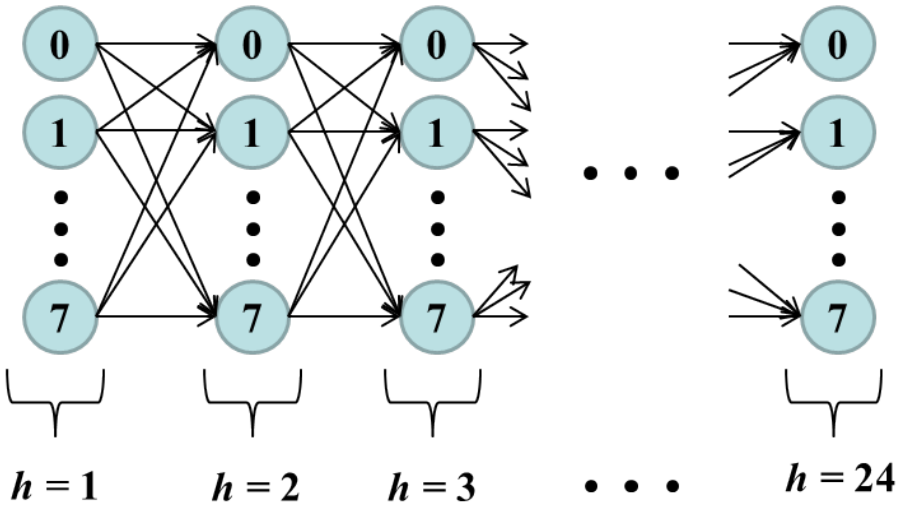

Figure B.2: An 8 state Markov chain with hourly subperiods

B.2 Assessing the Distance Between Two Random Processes

With the Markov chain model of the aggregated wind power output at hand, it is natural to assess whether such model constitutes a good approximation of the real (or say observable) random process governing the aggregated wind power output. Recall that in planning studies, our intent does not lie in predicting the wind ahead of time, but simply sketching its behavior years ahead of the future. For that reason, we need to study whether the statistical models built upon a present or past year are representative of statistical behaviors in future years. Having built our Markov chain model $\left\{\underset{\sim}{W}[h] \,:\, h = 1, \,\ldots\, , 24\right\}$ upon a given year data, the next step consists in assessing how well our model fits future year data.

The literature proposes many metrics aimed at assessing the distance between two probability distributions or random processes [48]. In our case, our Markov chain is a cyclostationary random process with discrete time steps (i.e., the subperiods) and so we may characterize it by its multivariate

probability distribution whose dimensionality is equal to the number of subperiods in a day. However, due to the empirical nature of our study and data, few metrics listed in the literature are actually applicable to our problem. It mostly has to do with the fact that most metrics assume that both distributions have the same support. However, this is hardly the case in our practice, unless one reduces the value of each state to a unique wind power output value and uses such method to similarly process the data of the future years against which one wants to assess his model. In practice, the sample paths that can be obtained from the Markov chain are highly dimensional (same dimension as the number of subperiods within a day) and thus are very unlikely – however close in reality – to coincide with any of the sample paths in the data of future years. As such, we need a more flexible notion of the distance between two distributions that can recognize whether a sample path from the Markov chain is representative of the future year data. The Mahalanobis distance (B.3) can be used for this purpose, as it provides for any sample path its distance with respect to a distribution characterized by its first and second order moments, i.e. its mean vector and covariance matrix. Suppose the total number of subperiods is 24, then let $\underline{w} = \{w[1], w[2], ..., w[24]\}^\dagger$ be a sample path of Markov chain $\left\{\underline{\overline{W}}[h] \ : \ h = 1, \ \ldots \ , 24\right\}$, $\underline{\mu} = (\mu[1], \mu[2], ..., \mu[24])^\dagger$ be the mean vector of the future year data and C its covariance matrix; then the Mahalanobis distance $D_M(w)$ may be written as:

$$D_M(\underline{w}) = \sqrt{\left(\underline{w} - \underline{\mu}\right)^\dagger \ C^{-1} \ \left(\underline{w} - \underline{\mu}\right)}. \tag{B.3}$$

Therefore, one may obtain an estimation of how well the Markov process $\left\{\underline{\overline{W}}[h] \ : \ h = 1, \ \ldots \ , 24\right\}$ fits the future year data by sampling a great many times – via Monte Carlo simulation [37] – the Markov chain process, comput-

ing the distance of its sample paths to the future year data distribution and, upon convergence of the Monte Carlo simulation, [1] evaluating the estimate of the average of Mahalanobis distances over all sample paths.

We next provide the essential steps of the algorithm used to compute the estimates of the average of Mahalanobis distances over all sample paths. The algorithm also briefly describes a method for obtaining sample paths from the Markov chain. Note that in such methodology, a state in itself has its own empirical probability distribution dependent upon time, and such distribution is sampled to generate a realization of the aggregate wind power output at the considered time.

Step 1 : Derive a sample path from the Markov chain: to do so, initialize the chain by sampling the distribution of states at subperiod 1. Use such realization as π_1 and compute the state probability distribution at subperiod 2 using (B.1). Then sample the state distribution at subperiod 2 and uses such realization as π_2. Compute the state probabilities at subperiod 3 and repeat the process until obtaining a sample path with realizations for the entire day.

Step 2 : Compute the Mahalanobis distance of the sample path with respect to the future year data using (B.3).

Step 3 : If the Monte Carlo simulation has converged, stop. If not, then go back to step 1 and generate another sample path.

Such algorithm is next put into practice in Section B.3 where the model is

[1] See 3.2 for such a convergence criterion

tested with real-world data.

B.3 Results of the Comparison

We apply the theoretical framework developed in Sections B.1 and B.2 to a case study in which the Markov chain is built from *NREL* 2004 wind data [49]. We then assess to what extent such model fits *NREL* 2005 wind data within each season. A Gaussian mixture based upon 2004 data and the sample paths from 2004 data are also put to the test in order to provide reference cases. To gain insight into the Mahalanobis distance, all models are also evaluated against 2004 data, with the raw 2004 data generally providing the best fit possible and serving as a benchmark for the two other models. Note that per Mahalanobis distance definition, the mean distance of 2004 raw data with respect to itself is not 0; only the mean vector of the distribution would result in a distance of zero. The study is run multiple times for different numbers of Markov chain states as well as for two different time resolutions, namely half-an-hour and one hour. The Gaussian mixture model, which essentially consists in a weighted sum of multivariate Gaussian distributions with modes centered on the historical data (that is the sample paths of the raw data) [30], p. 39, has unit variance in all components where all components are assumed to be independent from each other (i.e., the multivariate Gaussian is in fact the product of its univariate distributions). Note that such model is easily sampled via the composition method described in 2.1.3.

The results for each case study are summarized in the tables B.1-B.4:

Table B.1: Averages of the Mahalanobis distances over the sample paths. Half-an-hour resolution. 2004 → 2004

Half-hourly resolution						
2004 → 2005	Markov 6 states	Markov 16 states	Markov 26 states	Markov 36 states	Gaussian mixture	Raw 2004 data
winter	55.57	23.47	17.58	15.28	6.73	6.77
spring	89.14	36.31	28.14	23.07	6.95	6.83
summer	30.38	15.75	13.06	12.27	6.73	6.75
fall	38.13	17.97	14.25	13.55	6.78	6.79

Table B.2: Averages of the Mahalanobis distances over the sample paths. Half-an-hour resolution. 2004 → 2005

Half-hourly resolution						
2004 → 2005	Markov 6 states	Markov 16 states	Markov 26 states	Markov 36 states	Gaussian mixture	Raw 2004 data
winter	51.72	21.59	16.02	13.82	8.85	8.59
spring	82.40	35.19	28.13	25.47	19.46	19.38
summer	34.83	17.86	15.25	14.29	11.57	11.53
fall	41.19	20.13	16.75	15.36	11.89	12.20

Table B.3: Averages of the Mahalanobis distances over the sample paths. An hour resolution. 2004 → 2004

Hourly resolution						
2004 → 2005	Markov 6 states	Markov 16 states	Markov 26 states	Markov 36 states	Gaussian mixture	Raw 2004 data
winter	18.54	9.15	7.50	7.02	4.59	4.75
spring	18.68	9.16	7.92	7.43	4.77	4.75
summer	11.15	6.87	6.08	5.90	4.50	4.70
fall	13.70	7.62	6.88	6.27	4.74	4.72

Table B.4: Averages of the Mahalanobis distances over the sample paths. An hour resolution. 2004 → 2005

Hourly resolution						
2004 → 2005	Markov 6 states	Markov 16 states	Markov 26 states	Markov 36 states	Gaussian mixture	Raw 2004 data
winter	16.96	8.55	7.03	6.49	5.06	4.99
spring	18.68	9.97	8.68	8.14	6.42	6.83
summer	12.00	7.28	6.56	6.32	5.82	5.77
fall	13.37	7.65	6.85	6.22	5.82	5.77

The Mahalanobis distances are always consistently smaller in the one hour resolution case because the sample paths contain half the information (their

dimensions are half) of their half-an-hour counterparts and therefore have less possibility to be "distant" from the 2004 and 2005 distributions. Interestingly, 2004 raw data produces similar results when measured against itself and measured against 2005 data in the one hour resolution case. Such result suggests that, at this resolution, history seems to repeat itself. The Gaussian mixture significantly outperforms any type of Markov chain due to the fact that it is a very conservative extrapolation of 2004 raw data. The unit variance on all components does not allow for much deviation with respect to the original historical 2004 sample paths. Markov chains are found to perform better with a greater number of states – seemingly approaching the results given by the other two models – partly for the same reason that unit-variance Gaussian mixtures perform well: they constitute a rather conservative extrapolation of the 2004 data. Also note that the Gaussian mixture slightly outperforms the 2004 raw data in some cases, and one might conclude that extrapolating the data can potentially lead to better statistical models.

B.4 Concluding Remarks

This study reports on the suitability of a Markov chain model for representing well the statistical behavior of the aggregated wind power output. An approach for building the Markov chain model is given and tested against future year data using the Mahalanobis distance as a metric to assess whether the Markov chain model based upon one year data is representative of future year data. The performance of the Markov chain model is also compared to that of a Gaussian mixture model and of sample paths directly taken from 2004 data. Results suggest that Markov chains are outperformed by the

Gaussian mixture model and the 2004 raw data. They can, however, perform relatively well, that is, close to the performance of the Gaussian mixture model and 2004 raw data, if constructed with a high number of states. The Gaussian mixture model performs equally as well as the 2004 raw data in fitting the 2005 data.

REFERENCES

[1] GE Energy, "Western wind and solar integration study," NREL, Tech. Rep., 2010. [Online]. Available: http://www.nrel.gov/docs/fy10osti/47434.pdf

[2] F. Van Hulle et al., "Integrating wind - developing Europe's power market for the large-scale integration of wind power," Trade Wind, Tech. Rep., 2009.

[3] U. of Hawaii, "Oahu wind integration study - final report," U.S. Department of Energy, Office of Electricity Delivery and Energy Reliability, Tech. Rep., 2011.

[4] P. Denholm, E. Ela, B. Kirby, and M. Milligan, "The role of energy storage with electricity renewable generation," NREL, Tech. Rep., 2010. [Online]. Available: http://www.nrel.gov/docs/fy10osti/47187.pdf

[5] D. Rastler, "Electricity energy storage technology options – a white paper primer on applications, costs and benefits," EPRI, Tech. Rep., 2010. [Online]. Available: http://large.stanford.edu/courses/2012/ph240/doshay1/docs/EPRI.pdf

[6] Electricity Advisory Committee, "Bottling electricity: storage as a strategic tool for managing variability and capacity concerns in the modern grid," DOE, Tech. Rep., 2008. [Online]. Available: http://energy.gov/sites/prod/files/oeprod/DocumentsandMedia/final-energy-storage_12-16-08.pdf

[7] I. Gyuk et al., "Grid energy storage," U.S. Department of Energy, Tech. Rep., 2013. [Online]. Available: http://energy.gov/sites/prod/files/2013/12/f5/Grid%20Energy%20Storage%20December%202013.pdf

[8] EnerNex Corporation, Wind Logics, "Wind integration study - final report," Xcel Energy and the Minnesota Department of Commerce, Tech. Rep., 2004.

[9] N. Navid, G. Rosenwald and D. Chatterjee, "Ramp capability for load following in the MISO markets -

white paper," Midwest ISO, Tech. Rep., 2011. [Online]. Available: https://www.misoenergy.org/Library/Repository/CommunicationMaterial/KeyPresentationsandWhitepapers/RampCapabilityforLoadFollowinginMISOMarketsWhitePaper.pdf

[10] H. Balériaux, E. Jamoulle, and F. Linard De Guertechin, "Simulation de l'exploitation d'un parc de machines thermiques de production d'electricite couples a des stations de pompage," *RevueE (edition SRBE)*, vol. 5, no. 7, pp. 3 –24, 1967.

[11] Y. Zhang and A. Chowdhury, "Reliability assessment of wind integration in operating and planning of generation systems," in Proceedings of the *IEEE PES General Meeting*, Calgary, July 26-30 2009, pp. 1–7.

[12] N. Maisonneuve and G. Gross, "A production simulation tool for systems with integrated wind energy resources," *IEEE Transactions on Power Systems*, vol. 26, no. 4, pp. 2285 –2292, Nov. 2011.

[13] J. Morales and J. Perez-Ruiz, "Point estimate schemes to solve the probabilistic power flow," *IEEE Transactions on Power Systems*, vol. 22, no. 4, pp. 1594–1601, 2007.

[14] J. Morales, A. Conejo, and J. Perez-Ruiz, "Simulating the impact of wind production on locational marginal prices," *IEEE Transactions on Power Systems*, vol. 26, no. 2, pp. 820–828, 2011.

[15] C. Anderson and J. Cardell, "The impact of wind energy on generator dispatch profiles and carbon dioxide production," in *45th Hawaii International Conference on System Science (HICSS)*, Maui, Jan 04-07 2012, pp. 2020–2026.

[16] F. Vallee, J. Lobry, and O. Deblecker, "System reliability assessment method for wind power integration," *IEEE Transactions on Power Systems*, vol. 23, no. 3, pp. 1288 –1297, Aug. 2008.

[17] J. Himelic and F. Novachek, "Sodium sulfur battery energy storage and its potential to enable further integration of wind (wind-to-battery project)," Xcel Energy, Tech. Rep., 2011. [Online]. Available: http://www.xcelenergy.com/staticfiles/xe/Corporate/RenewableEnergyGrants/Milestone6FinalReportPUBLIC.pdf

[18] Y. Yuan, X. Zhang, P. Ju, K. Qian, and Z. Fu, "Applications of battery energy storage system for wind power dispatchability purpose," *Electric Power Systems Research*, vol. 93, no. 0, pp. 54 – 60, 2012. [Online]. Available: http://www.sciencedirect.com/science/article/pii/S0378779612002088

[19] B. Hartmann and A. Dan, "Cooperation of a grid-connected wind farm and an energy storage unit – demonstration of a simulation tool," *IEEE Transactions on Sustainable Energy*, vol. 3, no. 1, pp. 49–56, Jan 2012.

[20] M.-S. Lu, C.-L. Chang, W.-J. Lee, and L. Wang, "Combining the wind power generation system with energy storage equipment," *IEEE Transactions on Industry Applications*, vol. 45, no. 6, pp. 2109–2115, Nov 2009.

[21] S. Tewari and N. Mohan, "Value of NaS energy storage toward integrating wind: Results from the wind to battery project," *IEEE Transactions on Power Systems*, vol. 28, no. 1, pp. 532–541, 2013.

[22] R. Walawalkar and J. Apt, "Market analysis of emerging electric energy storage systems," DOE/NETL, Tech. Rep., 2008.

[23] S. Gill, E. Barbour, I. Wilson, and D. Infield, "Maximising revenue for non-firm distributed wind generation with energy storage in an active management scheme," *Renewable Power Generation, IET*, vol. 7, no. 5, pp. 421–430, Sept 2013.

[24] H. Haghi, M. Bina, and M. Golkar, "Nonlinear modeling of temporal wind power variations," *IEEE Transactions on Sustainable Energy*, vol. 4, no. 4, pp. 838–848, 2013.

[25] D. Burke and M. O'Malley, "A study of principal component analysis applied to spatially distributed wind power," *IEEE Transactions on Power Systems*, vol. 26, no. 4, pp. 2084–2092, 2011.

[26] J. Morales, R. Mínguez, and A. Conejo, "A methodology to generate statistically dependent wind speed scenarios," *Applied Energy*, vol. 87, no. 3, pp. 843–855, 2010.

[27] P. Pinson and G. Kariniotakis, "Conditional prediction intervals of wind power generation," *IEEE Transactions on Power Systems*, vol. 25, no. 4, pp. 1845–1856, 2010.

[28] N. Chen, Z. Qian, I. Nabney, and X. Meng, "Wind power forecasts using Gaussian processes and numerical weather prediction," *IEEE Transactions on Power Systems*, vol. PP, no. 99, pp. 1–10, 2013.

[29] B. Rajagopalan, U. Lall, D. Tarboton, and D. Bowles, "Multivariate nonparametric resampling scheme for generation of daily weather variables," *Stochastic Hydrology and Hydraulics*, vol. 11, pp. 65–93, 1997.

[30] W. Härdle, M. M., S. S., and W. A., *Nonparametric and semiparametric models*. Springer-Verlag Berlin Heidelberg, 2004.

[31] P. Bratley, B.L. Fox and L.E. Schrage, *A guide to simulation.* Springer-Verlag New York, 1983.

[32] A. Bowman and A. Azzalini, *Applied smoothing techniques for data analysis.* Oxford, Clarendon Press, 1997.

[33] W. K. A.M. Law, *Simulation modeling and analysis.* McGraw-Hill, 2000.

[34] J. Ubeda and R. Allan, "Sequential simulation applied to composite system reliability evaluation," *IEE Proceedings Part C: Generation, Transmission and Distribution*, vol. 139, no. 2, pp. 81 –86, Mar. 1992.

[35] S. Asmussen and P. Glynn, *Stochastic simulation: algorithms and analysis.* Springer, 2007.

[36] A. Wood and B. Wollenberg, *Power generation, operation and control.* NY: John Wiley and Sons, Inc., 1996.

[37] G. Fishman, *A first course in Monte Carlo.* Duxbury, 2006.

[38] J. Kleijnen, *Statistical techniques in simulation - Part 1 and 2.* Marcel Dekker, Inc. New York, 1974.

[39] V. Silva, "Value of flexibility in systems with large wind penetration," Ph.D. dissertation, Imperial College London, 2010. [Online]. Available: http://tel.archives-ouvertes.fr/docs/00/72/43/58/PDF/VSilva_PhDAllChapters_v9_-_unlinked_-_test.pdf

[40] B. Stott and E. Hobson, "Power system security control calculations using linear programming," *IEEE Transactions on Power Apparatus and Systems*, vol. PAS-97, no. 5, pp. 1713 –1731, sept. 1978.

[41] A. Kowli and G. Gross, "Quantifying the variable effects of systems with demand response resources," in Proceedings of the *IREP Symposium - Bulk Power System Dynamics and Control*, Buzios, Aug 01-06 2010.

[42] "118-bus Power Flow Test Case," http://www.ee.washington.edu/research/pstca/pf118/pg_tca118bus.htmD.

[43] J. Price and J. Goodin, "Reduced network modeling of *WECC* as a market design prototype," in Proceedings of the *IEEE PES General Meeting*, Detroit, July 24-28 2011, pp. 1–6.

[44] "LCG consulting energy online - Midwest ISO load data," http://www.energyonline.com/Data/GenericData.aspx?DataId=6&MISO___Cleared_Load.

[45] B. Hajek, *Notes for ECE 534 - An exploration of random processes for engineers*. Univ. of Illinois at Urbana-Champaign, 2009.

[46] P. Mahalanobis, "On the generalised distance in statistics," *Proceedings of the National Institute of Sciences of India*, Retrieved in 2008.

[47] N. Maisonneuve, "A production simulation tool for systems with wind energy resources," Master's thesis, Dept. of Electrical Engineering, University of Illinois at Urbana Champaign, 2009, http://energy.ece.uiuc.edu/gross/papers/Dissertations/Maisonneuve.pdf.

[48] G. J McLachlan, *Discriminant Analysis and Statistical Pattern Recognition*. Wiley Interscience, 1992, ISBN 0471691151.

[49] "Eastern wind integration and transmission study - NREL data," http://www.nrel.gov/wind/systemsintegration/ewits.html.